Utrecht University

groendus

Utrecht University

Faculty of Geosciences

-

Copernicus Institute for Sustainable Development

Master's Thesis

Combining Predictive and Heuristic Control Strategies for Optimal Deployment of Distributed Energy Storage Systems

Author:
Robert Peeters

Student number: 4021053
r.r.peeters1@students.uu.nl

Supervisor:
Prof. Dr. Madeleine Gibescu

Second Reader
Dr. Ibtihal Abdelmotteleb

Company Supervisor:
Ir. Roland de Wit

In partial fulfillment of the degree of

MSc Sustainable Development (Track: Energy & Materials)

March 10, 2021

Abstract

The continued integration of variable renewable energy (VRE) sources in the energy system is essential for the mitigation of climate change. However, the intermittent, unpredictable, and distributed nature of mainly solar and wind energy will substantially increase the need for grid flexibility. Currently, flexibility in the power system is mainly provided by (thermal) generation capacity on the supply side. Consequently, continued and economically feasible decarbonisation of the energy system will require more flexibility on the demand side. Demand side management (DSM) in short time frames can consist of demand response (DR) and distributed energy storage systems, and relies on smart grids in which energy management systems may shift loads to dynamically match supply and demand.

This thesis proposes a two-step DSM program which manages distributed battery energy storage systems (BESS) within a portfolio of solar energy producers and prosumers. The first step uses model predictive control (MPC) to continuously readjust the aggregate (dis)charging schedule of the BESSs, based on new solar irradiance and temperature forecasts, in order to minimize the imbalances between expected and actual energy generation. The second step comprises a heuristic control program, which is executed within each time step of the MPC program and allows for additional (dis)charging in order to (passively) contribute to grid balance when price peaks are expected in the imbalance market. Both optimization steps also take into account battery degradation.

In contrast with what is common in the literature, the DSM program is based on actual market and weather forecasts, as opposed to (model-adjusted) historical data. Perfect foresight is only assumed with respect to portfolio demand. Solar irradiance forecasts are recursively improved using a Kalman Filter. An auxiliary optimization program is used to determine the optimal size of the BESSs. To accurately gauge the potential of the DSM program, a number of representative days are selected from two sets of weather forecasts using hierarchical clustering.

The results suggest that MPC is a feasible framework for DSM in an real world environment were new weather forecasts come available on a rolling basis. However, while the Kalman Filter successfully improves the accuracy of the forecasts, the remaining mismatch between actual and forecasted VRE supply more often than not results in an increase of total imbalance. This is the case for both forecast data sets, and is also a result of the 24-hour optimization horizon combined with a constraint on the final SoC of the BESS. Moreover, the net potential economic gain from the Lithium Iron Phosphate batteries examined is minimal, indicating the necessity of DSM deploying both BESSs and DR.

Acknowledgements

I owe a debt of gratitude to several people, without whom I would not have been able to complete this thesis. I would like to thank Madeleine Gibescu for her continued support and encouragement. Her guidance was essential in shaping a research approach on a topic I was only somewhat familiar with initially. In addition, I would like to thank her for introducing me to a host organization in the field, which has allowed me to add relevance to the research. I would like to thank Ibtihal Abdelmotteleb for her efforts in the pre-processing phase of essential data, and for her useful insights on some practical challenges I encountered. Last but not least, I would like to thank CT Energy (now Groendus) for giving me the chance to carry out my thesis research at an innovative company at the forefront of the energy transition. Naturally, a special thanks goes out to Roland de Wit and Quirien Schouten, for welcoming me to their office. Specifically, I would like to thank Roland for his constructive feedback, and Quirien for his continued and flexible assistance with the data gathering.

Contents

List of Figures

List of Tables

Nomenclature

Symbols

Δ	Absolute day-ahead/actual portfolio imbalance	kWh
Δ^+	Portfolio imbalance surplus	kWh
ζ	multi optimization weight	–
E^{BESS}	battery output	kWh
P^{ch}	battery charging power	kW
P^{dis}	battery discharging power	kW
β	binary charging/discharging variable	–
η	battery charging/discharging efficiency	%
Q_{loss}	battery capacity loss	%
β_{lowT}	low temperature degradation coefficient	h
k_{lowT}	cycle degradation stress factor	$Ah^{-0.5}$
$I_{Ch,ref}$	reference/maximum charging current	A
I_{Ch}	charging current	A
Δ^-	Portfolio imbalance shortage	kWh
C_{nom}	nominal battery cell capacity	Ah
D	daily degradation rate	%
Q_{BESS}	battery capacity	kWh
P^{pc}	Passive contribution power	kW
λ	binary regulation state variable	–
π	imbalance price	$/kW$
E^{pc}	Passive contribution Energy	kWh
FEC	Full Equivalent Cycles	–
DoD	Depth of Discharge	%
SoC	State of Charge	%

Δ^{pre}	Total imbalance before Demand Side Management	kWh
N_0	maximum number of battery cycles per day	–
$\mathbf{Z}^{BESS}$	Vector of all Battery Parameters	–
Δ^{post}	Total imbalance after Demand Side Management	kWh
δ	time interval	kWh
τ	time	$minutes$
t, k	time period (Program Time Unit)	–
E^{DA}	net portfolio result (day ahead forecast)	kWh
E^{ACT}	net portfolio result (actual)	kWh

Abbreviations

ACF	Autocorrelation Function
ACT	actual
$aFRR$	Automatic Frequency Restoration Reserves
AIC	Aikaike Information Criterion
$ARMA$	auto-regressive moving-average
ASM	Ancillary Services Market
BAU	Business as Usual
$BESS$	Battery Energy Storage Systems
BRP	Balance Responsible Party
BSP	Balancing Service Providers
$C\&I$	Commercial Industrial
$CAPEX$	capital expenditure
CPP	Critical Peak Pricing
DA	day-ahead
DAM	Day-Ahead Market
DLC	Direct Load Control
DR	Demand Response
DSM	Demand Side Management
DSO	Distribution System Operator
EMS	Energy Management System

$ENDEX$	European Energy Derivatives Exchange
$EPEX$	European Power EXchange
$ESCO$	Energy Service Company
ESS	Energy Storage Systems
EV	Electric Vehicles
FCR	Frequency Containment Reserves
GHI	Global Horizontal Irradiance
$HEMS$	(Home) Energy Management System
$HVAC$	Heating, Ventilation and Air Conditioning
IDM	Intra-day Market
$IGCC$	International Grid Control Cooperation
ISP	Imbalance Settlement Period
KF	Kalman Filter
LP	Linear Programming
LR	Logistic Regression
$mFRR$	Manual Frequency Restoration Reserves
$MILP$	Mixed Integer Linear Programming
MPC	Model Predictive Control
$OPEX$	operational expenditure
$PACF$	Partial Autocorrelation Function
PTU	Program Time Unit
PV	Photo-voltaic
RES	Renewable Energy Sources
RR	Replacement Reserve
RTP	Real Time Pricing
TCL	Thermostatically Controlled Loads
TES	Thermal Energy Storage
TOU	Time-of-Use (Pricing)
TSO	Transmission System Operator
UPS	Uninterrupted Power Supply

$V2G$	Vehicle-to-Grid
VPP	Virtual Power Plant
VRE	Variable Renewable Energy
$VRES$	Variable Renewable Energy Sources

Chapter 1

Introduction

1.1 Background

1.1.1 The Energy Transition

In 2019, the Netherlands adopted its national Climate Agreement in fulfillment of the European Union-wide commitment to Paris Agreement, which targets a 40% reduction of greenhouse gas emissions by 2030 compared to 1990. Notwithstanding the remaining gap between its estimated effects and the national target to reduce emissions by 49% by 2030 compared to 1990, as well as the persistent emissions gap between current global policies and the abatement required to limit global warming to 1.5 °C, this national climate policy framework envisages an ambitious economic, technological, and societal transition (Hekkenberg, 2019; Olhoff & Christensen, 2019). A major part of this effort comprises the decarbonization of electricity generation and the electrification of transportation and heating. By 2030, offshore wind energy should generate 49 TWh and onshore renewable energy should generate 35 Twh, about 70% of the total energy mix. By 2050, the share of non-renewables should be negligible (EZK, 2019). This substantial shift towards variable renewable energy (VRE) sources will increase the variability and uncertainty of electricity generation, due to the intermittency and unpredictability of solar and wind energy (Huber et al., 2014). The electrification of heating and transportation is likely to exacerbate (inter-temporal) mismatches between supply and demand, since peak demand from these sources coincides with current peak load hours (Boßmann & Staffell, 2015). Moreover, the distributed nature of VRE sources, and higher peak loads due electrification, may result in increasing incidence of local congestion (Siano, 2014; Vardakas et al., 2014). This is unlikely to be mitigated by enhanced energy efficiency, which has a differently distributed

impact on the load curve (Baruah et al., 2014).

Consequently, both the technological infrastructure and the market mechanisms of the electricity system will become increasingly strained (Lund et al., 2015). Beyond a 30% share of variable renewable energy (VRE) in annual electricity consumption, the flexibility requirement of the power systems will increase dramatically. More frequent and larger up and down ramping of operating reserves will be needed to counteract voltage fluctuations and ensure local power quality[1]. This will not only increase wear and tear, and reduce efficiency, reliance on dispatchable thermal generation capacity to balance temporal (and spatial) mismatches between supply and demand will eventually impede the continued decarbonization of the energy system (Huber et al., 2014; Kondziella & Bruckner, 2016; Notton et al., 2018).

Increasing reliance on reserve capacity will also drive up costs during peak demand hours, while the nearly zero marginal cost of VRE supply will drive down electricity prices on wholesale spot markets. Higher fluctuations and unpredictability of residual loads - i.e. electricity demand that cannot be met by renewable electricity generation - will increase price volatility, intraday trading volume, and demand for peak load capacity and balancing services (Lund et al., 2015; Nicolosi & Fürsch, 2009). On the supply side, curtailment of VRE production results in higher Levelised Costs of Electricity, that are often not taken into account by feasibility studies (Groppi et al., 2020).

1.1.2 Demand Side Flexibility

Context & Concepts

Although strengthening the power grid and expanding international interconnections will temper the impact of VRE generation, the growing need for flexibility in electricity system is inevitable (Lund et al., 2015). Put differently, the system's ability to *"cope with uncertainty and variability in demand and generation to maintain systems reliability at reasonable costs"* (Ma et al., 2013) must increase. Huber et al. (2014) estimate that a VRE-share in annual electricity consumption above 30% dramatically increases flexibility requirements in Europe. While an integrated European balancing area will require a maximum hourly net load ramp of 11% of peak load, compared to 30% at the regional level, this is just the case for a VRE-penetration of 50%. In an European super grid with 100%

[1] In addition to the location-constraints of VRE-supply its non-synchronous nature and relatively small installation size further erodes power quality (Sinsel et al., 2020).

VRE supply, 20% of total annual demand would have to be stored. Twice that capacity would be required in a non-integrated energy system (Kondziella & Bruckner, 2016). Such figures underline the substantial effort of integrating VRES into today's energy system (Lund et al., 2015; Mier & Weissbart, 2020).

Consequently, the quest for greater flexibility has turned to *demand side management* (DSM) in recent years. DSM can be defined as *"the planning and implementation of those electric utility activities designed to influence customer uses of electricity in ways that will produce desired changes in the utility's load shape"* (Gellings, 1985). Specifically, *"DSM optimizes the power flows in the network, regulates the voltage profiles [...] minimizes the energy losses, reconfigures the network, [and] exploits storage devices and responsive loads in an integrated way"* (Pilo et al., 2009). DSM encompasses, inter alia, load conservation (i.e. energy efficiency), strategic load growth, demand response (DR), and demand side energy storage. These measures can be driven by economic/market-, environmental- and network reliability-considerations, and increase in economic value and risk to consumer comfort with shorter time scales (see figure 1.1, where Spinning Reserve is included as the capacity safeguarding the stability of the system at the smallest timescale)(Aghaei & Alizadeh, 2013; Chiu et al., 2012; Lampropoulos et al., 2013)). A comprehensive review of the DR taxonomy is provided in section 2.2.1

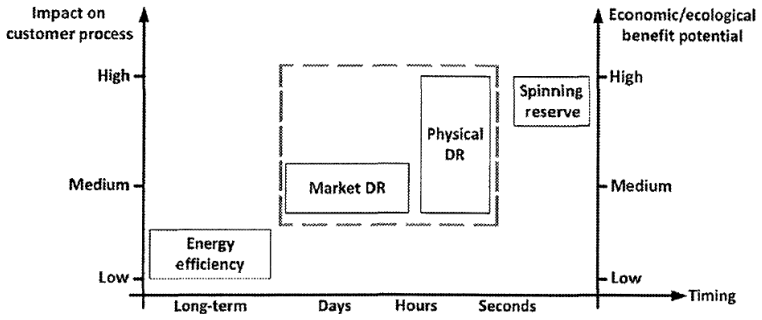

Figure 1.1: DSM categories (Diekerhof et al., 2018)

DR refers to those DSM-approaches *"designed to incentivize end-users to alter their short-term electricity consumption patterns by scheduling in time and leveling the instantaneous power demand."* These control actions may be effectuated by different signals. Traditionally, *frequency-based* or *direct load control (DLC)* mechanisms were only activated in case of system stress. However, since the 1973 oil crisis and the liberalization of the electricity system, a range of economic incentive schemes have emerged, which are concisely presented in section 3.1 (Lampropoulos et al., 2013).

Figure 1.2 visualizes possible DSM-strategies. all of which exploit *flexible loads* on the demand side, which have an adjustable consumption pattern (Rajabi et al., 2017). These adjustments may mitigate transmission and distribution losses, reliance on expensive operating reserves and the need for grid reinforcement and large scale centralized energy storage systems (ESS). Hence, DR is considered a cost-effective option to meet the flexibility requirements of power systems with high shares of VRES (Carreiro et al., 2017). Flexible loads can be roughly divided in *deferrable loads* and *curtailable loads* (Diekerhof et al., 2018). The former can be adjusted through *basic shifting* of the time of use, if loads need a constant power supply for a specific period of time or through *interruptable shifting* if it is possible to disrupt the load run in addition to shifting its time of use. The latter is eligible for *continuous switching*, since the load duration is determined by external upper and lower set points (Rajabi et al., 2017).

However, a substantial part of power demand is not suitable for these strategies. These *critical loads* must be serviced, even during (economically or environmentally) sub-optimal moments. In this case, distributed energy storage can enable peak shaving and valley filling instead (Chiu et al., 2012). Especially when combined with *battery* energy storage, non-dispatchable photovoltaic (PV) solar installations can become de facto dispatchable, thus improving the utilization ratio of distributed energy sources and reducing electricity consumption costs (Han et al., 2015). At the power system level, distributed energy storage offers advantages over grid-scale installations. For instance, the complexity, and therefore the cost of battery energy storage, increases with size (Faisal et al., 2018), and centralized ESS are not able to benefit from the geographical smoothing of VRE supply fluctuations that occurs in distribution grids (Lund et al., 2015).

Demand Side Management Implementation

Smart Grids are integral to the implementation of DSM, allowing *(Home) Energy Management Systems (H)EMS)* to optimally control flexible loads and energy storage systems (ESS). Through smart metering and (two-way) information and communications technologies, these control systems are able to respond to supply-side signals, thus improving efficiency and power quality, while meeting reliability and comfort requirements of the consumer (Aghaei & Alizadeh, 2013; Kostková et al., 2013; Siano, 2014). However, the impact of DR in such systems is limited by the amount and type of loads that can be deferred or curtailed. While offering a potential for continuous switching of thermostatically

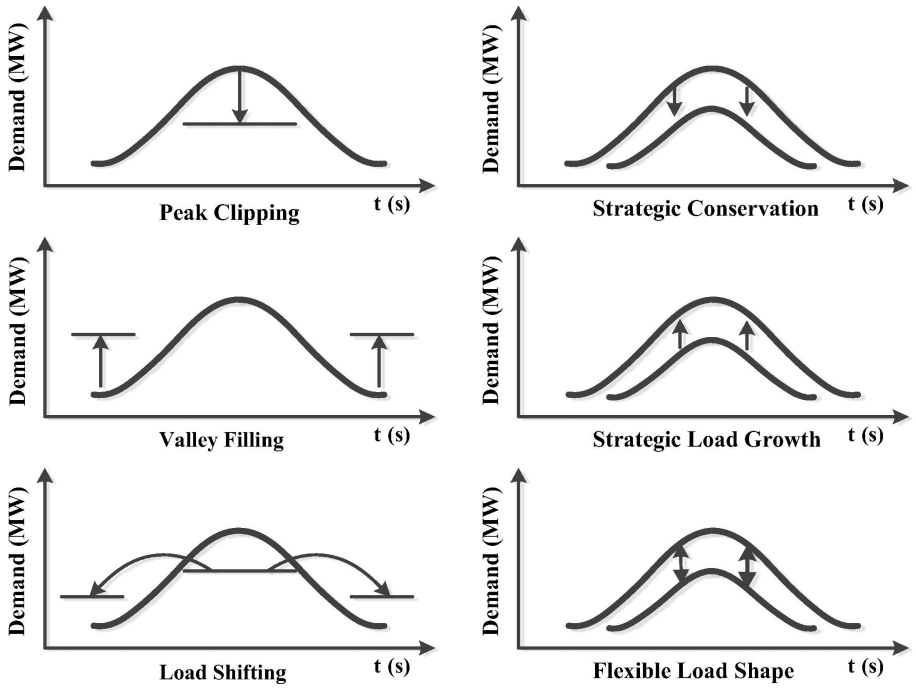

Figure 1.2: Demand Side Management Strategies (Alham et al., 2017)

controllable loads (TCLs) such as electric water heaters and refrigerators, and interruptible shifting of dish washers, washing machines and clothes dryers, *Residential* loads are relatively small (Paterakis et al., 2017). Moreover, the design of efficient DR programs is complicated due to the heterogeneous and varying consumption patterns of residential customers, relatively high investment costs and limited participation of the customer base (Aghaei & Alizadeh, 2013; González et al., 2018; Vardakas et al., 2014). *Commercial* (and other non-residential) consumers offer larger flexible loads. Especially large heating, ventilation and air condition (HVAC) systems in commercial buildings provide easier access to single controllable loads than a large number small residential buildings. Automation equipment may already be largely present, and large spaces have a higher thermal inertia, allowing for longer load interruptions (Paterakis et al., 2017). In addition, many commercial building have identical energy consumption patterns which are determined by weather conditions, design styles and operational behavior (Vardakas et al., 2014). *Industrial* consumers have large flexible loads which makes the implementation of DR programs easier. Even though economic and technical constraints may be render load shifting infeasible, specific large TCLs may be available (Paterakis et al., 2017). Especially electro-thermal heating units equipped with *thermal energy storage systems (TES)* are a promising source of flexibility, which are available at a much lower cost than battery energy storage systems

(BESS). Due to these limitations, it is estimated that only one third of current electricity demand is deferrable at the moment. By 2030 this may be increased to *at most* 55% for residential demand (Parra et al., 2017), leaving a substantial space for flexibility provisions by distributed BESS. Nonetheless, in addition to stationary distributed ESS, Electric Vehicles (EVs) may participate in DSM programs as well. EVs may engage in controlled unidirectional charging or participate in vehicle-to-grid (V2G) programs by controlled bidirectional charging. These measures combine characteristics of energy storage, deferrable loads and curtailable loads and allow a fleet of EVs could provide peak shaving and valley filling, as well as balancing services, which improves the economic efficiency of the energy system (Diekerhof et al., 2018; Paterakis et al., 2017).

At the end-user level, the value of flexible demand and energy storage typically exceeds the economic gains from increasing self-consumption of distributed VRE sources like rooftop solar PV systems - only large C&I consumers can individually reap all value from flexible loads and energy storage(de Heer & van der Laan, 2017). Due to their limited capacity and controlability, flexible loads of smaller end-users must be combined in a single system resource to access the relevant market mechanisms. This service is provided by *aggregators*[2], market intermediaries which provide balancing services to the grid by managing a portfolio of distributed flexible loads (Lampropoulos et al., 2018). Aggregators may also establish *virtual power plants* by combining *uncontrollable* distributed energy resources (e.g. rooftop solar panels or wind turbines) with *controllable* resources (e.g. batteries or generators) (Lampropoulos et al., 2017; Niesten & Alkemade, 2016; Rajabi et al., 2017). In addition to a number of regulatory, market-, and infrastructure-related barriers (see e.g Carreiro et al. (2017), Lampropoulos et al. (2018)), effective aggregation and optimal market participation involves a number of practical and strategic challenges, such as (1) the accurate forecasting of the baseloads of consumers with distributed VRE systems; (2) estimation of available flexible loads; (3) modeling the rebound of demand after DR activation; (4) identifying the most appropriate DR program (e.g. scheduling based on day-ahead prices, or providing real-time balancing services); (5) accounting for the diversity of end-user behavior (Lu et al., 2020); (6) effective customer targeting and clustering in order to exploit similar consumption patterns (Rajabi et al., 2017).

[2]Also referred to as *aggregator companies*, *demand response aggregators*, *aggregation service providers*.

1.2 Problem Description

Research Context

As discussed above, the increasing share of VRES in the electricity generation mix will have a variety of economic repercussions. These "integration costs", which may be decomposed in profile, balancing and grid-related costs, complement direct investment costs at the system level. *Profile costs* are related to the *variability* of VRES, and arise from the temporal profile mismatch between electricity generation and consumption. *Balancing costs* relate to the *uncertainty* of VRE generation, and comprise the additional expenditure to counteract the deviation of actual VRE output from predicted operation. *Grid-related* costs arise from investment in additional grid capacity and transmission losses. Of these components, profile costs and balancing costs have an immediate impact on electricity consumers, producers and suppliers alike: profile costs reduce the market value of VRES vis-à-vis conventional dispatchable energy resources, and thus reduce the feasibility of business cases. Balancing costs are reflected by higher prices in the intraday electricity market and in the balancing market, since forecast error metrics are positively correlated across producers, and thus increase the costs of electricity consumption during specific hours. Meanwhile, this development also offers commercial opportunities for new business models which deploy flexible energy resources to engage in arbitrage (Hirth et al., 2015).

Balancing cost are especially relevant for this research project's host organization, an energy service company (ESCO) which offers - amongst other services - a peer-to-peer energy exchange platform to its clients. This service enables direct (financial) transactions between VRE producers, prosumers[3] and consumers. The ESCO currently executes these transactions within its client portfolio through *ENTRNCE*, an (external) energy market trading platform which provides access to the wholesale electricity market, where residual demand from consumers (and prosumers) can be fulfilled or excess supply by producers (and prosumers) can be sold. Since both peer-to-peer and complementary market transactions have to take place before 11:00 on the day preceding physical delivery, forecasts may differ substantially from actual supply-and-demand (see figure 1.3). The cost of counteracting these portfolio imbalances, i.e. the *imbalance price*, is passed on to the ESCO by the energy trading company which bears balance responsibility for ENTRNCE towards

[3]Prosumers are electricity consumers who produce (a share of) their own demand (Lampropoulos et al., 2013).

the grid operator (see figure 1.5 for an visual representation of this interaction, and section 2.1.1 for the relevant definitions). As the energy transition progresses and the share of intermittent, unpredicatable renewable energy increases, the electricity bills for clients participating in the platform will increase. To address this, the ESCO is currently exploring the potential of a BESS to reduce imbalances within its portfolio. Put differently, it is exploring the value proposition and technical potential of becoming an aggregator.

Knowledge Gap

The past two decades have seen a surge in research on optimal (short-term) DSM strategies, deploying (battery) energy storage and demand response to address the profile- and balancing- and grid related costs that impede the cost-effective integration of high shares of VRES (Balijepalli et al., 2011). Despite the wide variety of research approaches, a (non-exhaustive) review (section 2.2.2) of the literature suggests that most contributions assume a high degree of knowledge about the future states of either the energy market, the physical energy system or both. This is appropriate if DSM programs narrowly focus on profile costs and try to gauge optimal system configurations, define economically optimal schedules based on predetermined RTP (e.g. based on the day-ahead price settlement), or determine the optimal operation of ESSs (e.g. Maheshwari et al. (2020)).

However, balancing costs related to the unpredictability of VRE integration are an important reasons for the necessity of DSM, and higher and more volatile prices occur closer to physical delivery than day-ahead transactions. Research addressing short-term market mechanisms and the unpredictability of VRE supply, typically relies on the perfect foresight assumption, and only estimates the economic impact of forecast errors by performing ex-post sensitivity analyses (e.g. Ding et al. (2014) and J. Wang et al. (2019)). More advanced approaches incorporate stochastic parameters in optimization frameworks to account for the impact of imbalance price and VRE supply uncertainty (e.g. Alipour et al., 2017; Rashidizadeh-Kermani et al., 2019; Tohidi et al., 2018). Alternatively, time-dependent noise terms can be added to the actual VRE supply or imbalance market data to emulate decreasing forecast uncertainty in a model predictive control framework (Okur et al. (2019) and Zhou et al. (2017)). Also Lampropoulos et al. (2015), who employ a hierarchical predictive control scheme which operates on multiple time scales, apply their model to historical data.

Notwithstanding the depth and breadth of the literature base proposing novel DSM

programs, optimization approaches incorporating *actual* market and VRE-supply forecasts are a novelty (see e.g. Terlouw et al. (2019)). Most available research on the potential of (short-term) DSM in the context of VRE integration estimates theoretical economic and technological feasibility of various DSM schemes and appliances, based on historical data. The issue of unpredictability of VRE supply and the stochastic nature of the electricity market are *synthetically* imposed on the historical data. Meanwhile, current business challenges require practically feasible DSM approaches, which use *actual* weather and market data. This thesis seeks to address this gap.

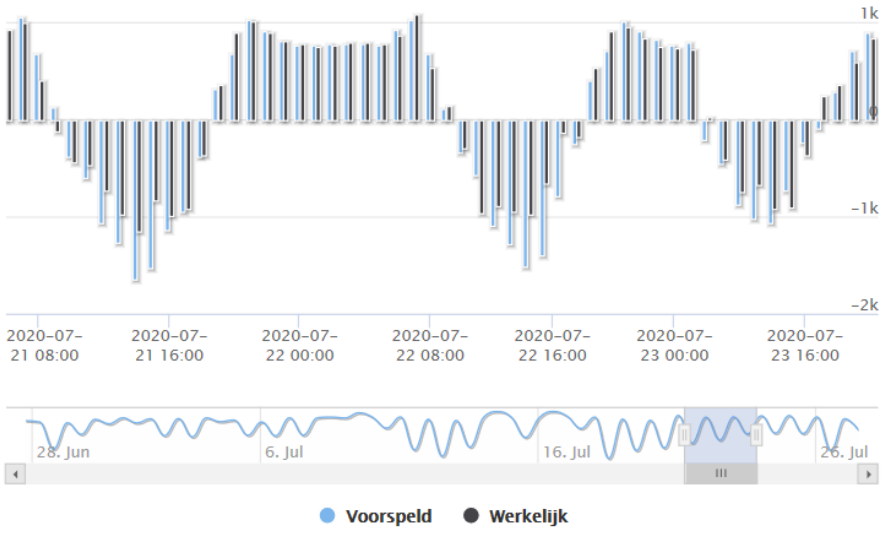

Figure 1.3: Example of Portfolio Mismatches (kWh)

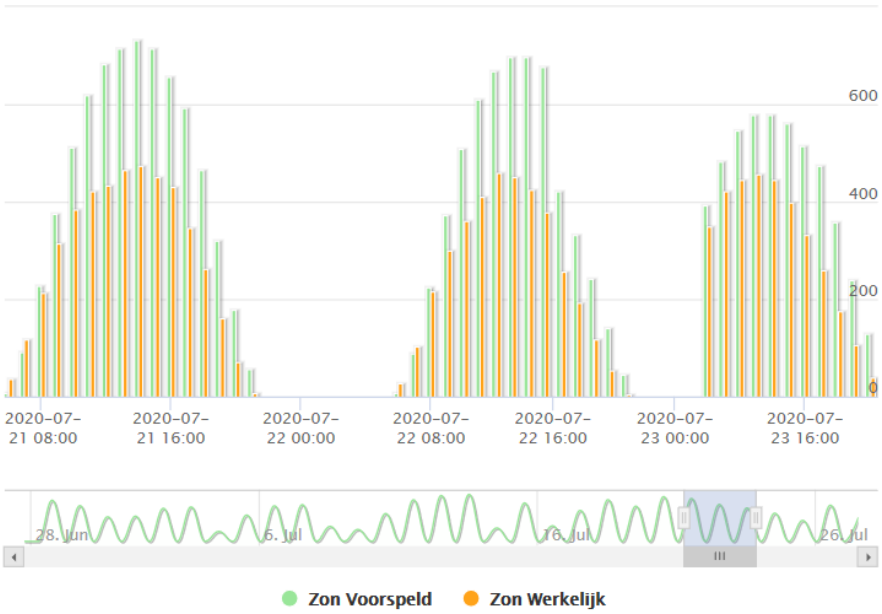

Figure 1.4: Forecasted (green) and actual (orange) solar irradiation (w/cm^2)

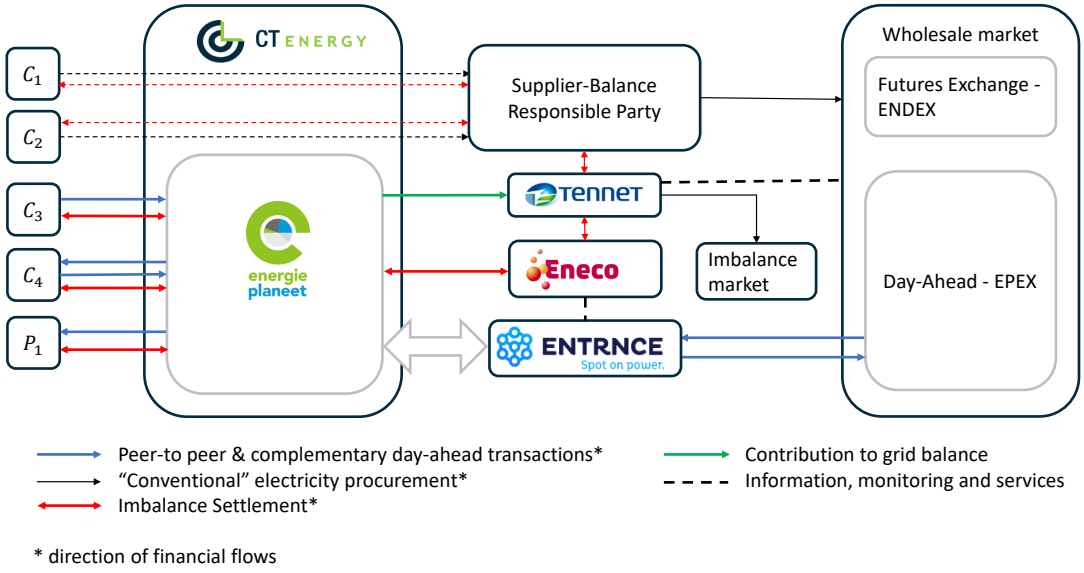

Figure 1.5: CT Energy's Position in the Electricity Market

1.3 Research Scope & Questions

The knowledge gap identified in the previous section is addressed by analyzing the potential of DSM for an aggregator portfolio consisting of several solar PV producers and commercial/industrial consumers and prosumers. Specifically, a case study will be conducted by developing a simulation model in which a number of distributed BESSs are used to reduce internal[4] portfolio imbalances, by shifting loads away from moments of (expected) portfolio shortage towards moments of (expected) portfolio surplus. In addition, BESSs may be used to generate additional revenue by providing balancing services to the grid. To fully capture the unpredictability of both VRE generation and imbalance prices, the proposed ESS should be based on frequently updated and increasingly *near-term* weather forecasts, and the *real-time* imbalance price signal from the transition system operator. This means that the potential of demand side energy storage and DSM will be estimated in an environment of *actual* error in real world forecasting data, as opposed to relying on model-generated uncertainty, or error margins imposed ex-post based on historical forecasting accuracy.

[4]Internal imbalance refers to the difference between the day-ahead expectation and the actual net portfolio result.

Main Question

What is the potential of demand side management using distributed battery energy storage systems to reduce the imbalance costs accrued by the client portfolio of a Dutch electricity supplier-aggregator, based on near real-time weather and market data?

Sub-Questions

1. How can updated weather forecasts be adequately incorporated throughout the model horizon?
2. What characteristics of the battery energy storage systems influence their economic performance?
3. How can imbalance prices be taken into account by the energy management system?
4. What is the optimal battery capacity, considering investment costs and economic gains of demand side energy storage?
5. How can variations in VRE supply, market conditions, forecasting accuracy be accounted for?

Research Framework

Figure 1.6 gives a general overview of the how the (sub) research questions are organized. *Sub-questions 1, 2, 3* relate to model structure and the relevant parameters of the three subsystems explicitly considered by this thesis: (1) the imbalance market, (2) the BESSs, and (3) solar PV production. *Sub-question 4* addresses to the optimal system configuration which is determined using an auxiliary optimization model. *Sub-question 5* addresses the necessity to obtain the final estimation results by applying the model to a *representative* subset of the available input data. In this manner, the intra-annual variation of energy supply and imbalance prices can be adequately captured even if the simulation cannot be applied to the full data-set due to limited computational capacity.

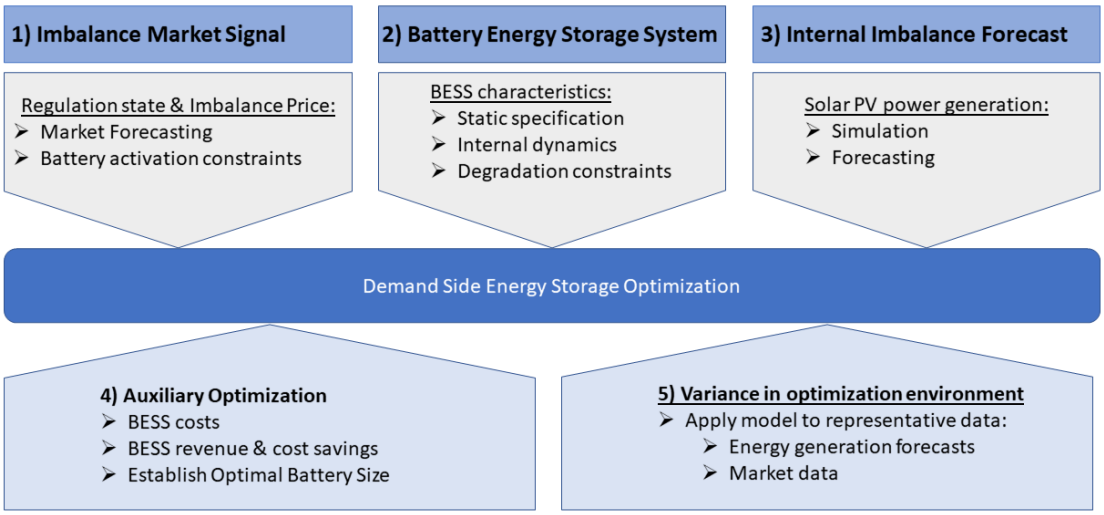

Figure 1.6: Research Framework

1.4 Outline

This thesis is organized as follows: chapter 2 reviews the grey and academic literature on relevant aspects of demand side management, namely (1) the market context; (2) different categories of DSM programs and optimization models; (3) the role of (battery) energy storage system storage in DSM and the key characteristics of battery technology. This review will inform the research strategy (section 3.1), the optimization approach (section 3.2 and 3.5) and the (mathematical) descriptions of the sub-systems (section 3.3, 3.4). The results obtained from the model are presented in chapter 4. Chapter 5 and 6 respectively discuss the results and conclude this report by formulating an answer to the research questions. Figure 1.7 provides a schematic guide to this thesis' structure.

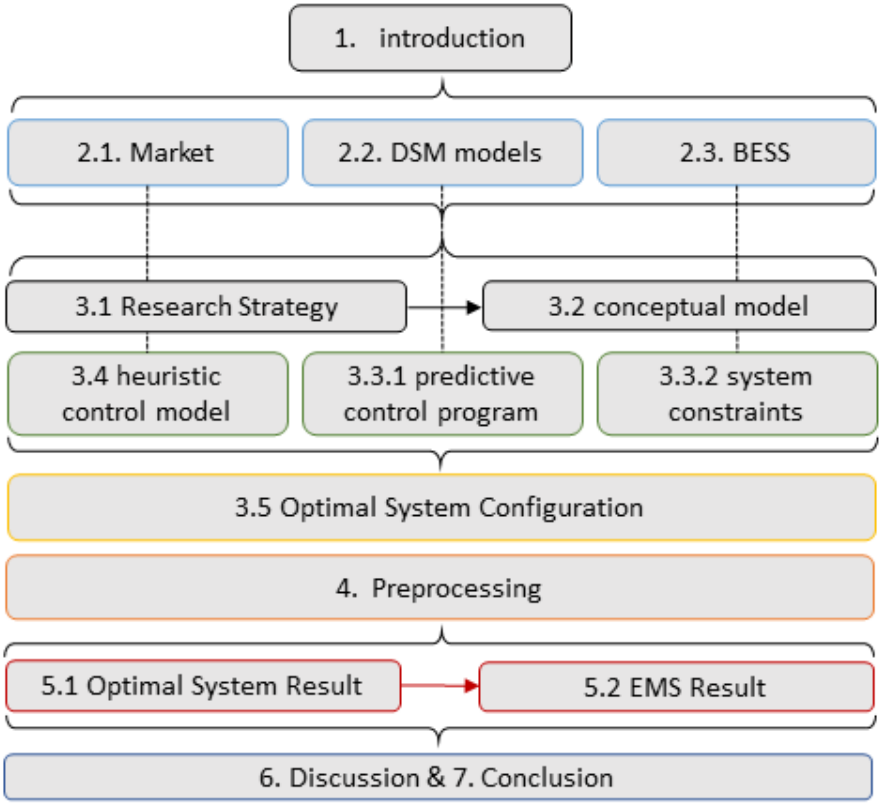

Figure 1.7: Thesis Outline

Chapter 2

Literature Review

2.1 Flexibility in the Dutch Electricity Market

2.1.1 The wholesale electricity market

The European power system is an interconnected network managed by *Transmission System Operators* (TSO) responsible for typically national[1] control areas. *Distribution System Operators* (DSO) connect individual end-users to the transmission network through medium and low voltage networks. Each connection (or main metering) point to the grid has one associated *supplier* and one *Balance Responsible Party*[2] (BRP). Suppliers source electricity from producers, and supply and invoice electricity to end-users. (ENTSO-E, 2020; Lampropoulos et al., 2017). The day before physical delivery, BRPs submit the expected aggregate demand/supply schedules of their grid connections (E-Programs) to the TSO, and are financially responsible for discrepancies between expected and actual net energy injected in or withdrawn from the system during each *Imbalance Settlement Period* (ISP) of 15 minutes. Not all BRPs manage the connections of end-users: *trading* BRPs only engage in energy trading and only manage their own connection (Tanrisever et al., 2015).

Wholesale electricity trading in the Netherlands takes place on three exchanges, which are connected to several other European countries. The European Energy Derivatives Exchange (ENDEX) is the futures market for standardized electricity products, and is active up to 2 days ahead of physical settlement (see figure Figure 2.1). The lion's share of all electricity trading consists of bilateral transactions on this market. Short term trading

[1] Germany has four control areas

[2] Also referred to as Programme Responsible Party (*Programma Verantwoordelijke*, in Dutch)

takes place on the European Power EXchange[3] (EPEX), a spot market consisting of the Day-Ahead Market (DAM) and the Intra-day market (IDM). On the DAM, anonymous bidding results in a supply-demand curve, which determines a uniform clearing price for each hour at market closure (12:00 on the day prior to physical delivery). On the IDM, which closes 5 minutes before physical delivery electricity, the smallest trading unit is 15 minutes, referred to as Program Time Unit (PTU)) (Lampropoulos et al., 2018; Tanrisever et al., 2015). The third exchange, which deals with the discrepancies, or *imbalances*, between traded and actual volumes, is discussed in the subsequent section.

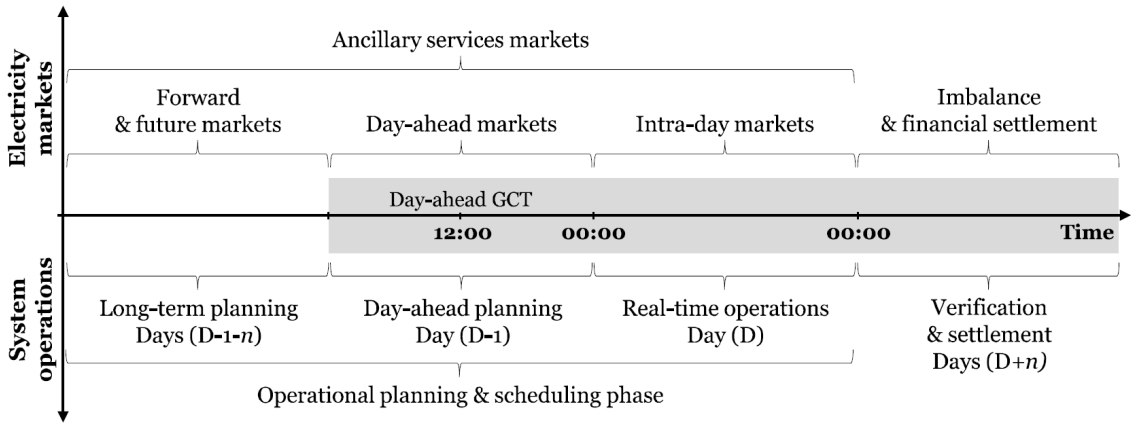

Figure 2.1: Electricity market operation in the time domain. The time scale of interest to this thesis is demarcated in grey (Lampropoulos, 2014)

2.1.2 Imbalance Price Settlement

Since demand and supply cannot be perfectly forecasted, the TSO has to anticipate imbalances to maintain power quality[4]. Hence, the TSO procures operating reserves on the *Ancillary Services Market (ASM)*[5], where it is the single-buyer. During each PTU, these can be activated in response to negative imbalances (i.e. BRPs have a shortage compared to their DAM and IDM commitments) or deactivated in response to positive imbalances (i.e. BRPs have a surplus), respectively. This is referred to as upward regulation (the increase of injection or decrease of withdrawal of electrical energy) and downward regulation (the decrease of injection or increase of withdrawal). The required capacity is provided by Balancing Service Providers (BSPs), offering the different types of reserves, which are

[3]Colloquially still referred to as Amsterdam Power Exchange (APX), its former name

[4]The appropriate voltage level alternating at the appropriate sinewave frequency, which may only deviate by 50 mHz from the nominal value of 50 Hz (European Commission, 2017).

[5]In addition to these balancing services, AS comprise black start capability, the provision of reactive power and the compensation for network losses, but these are of low relevance to (emerging) aggregators and not treated in this thesis.

outlined below and differ primarily in terms of activation time (see figure 2.2). To be complete, it should be mentioned that the TSO may - within the same timeframe - also engage in *imbalance netting* with other TSOs, through International Grid Control Cooperation (IGCC) (Lampropoulos et al., 2018).

1. **Frequency Containment Reserves (FCR)** are contracted ex ante to be fully activated within 30 seconds after a sudden frequency deviation, and are hence "the first line of defense against frequency deviations in the grid" (de Heer & van der Laan, 2017). These formerly called "primary reserves" are subject to strict requirements with respect to metering and data exchange, and are awarded a compensation for standing by with a certain capacity (>1 MW), which is established via a weekly auction (Lampropoulos et al., 2018).

2. **Automatic Frequency Restoration Reserves (aFRR)** (also referred to as *regulating capacity* and previously called "secondary reserves") must be fully activated within 15 minutes in order to restore the nominal value after initial frequency containment. For each ISP, a minimum quantity of bids for upward and downward regulation must placed in the auction, one month ahead of time[6] (Poplavskaya & De Vries, 2019). These bids are complement via a daily auction of "free bids", which can be changed until 30 minutes before the ISP.

3. **Manual Frequency Restoration Reserves (mFRR)** are only activated in case of longer lasting or larger incidents that exhaust aFRR, and were formerly referred to as tertiary reserves. Through a manual procedure, the TSO activates either directly activated reserves (mFRRda (also referred to as *reserve capacity*)), which must reach full activation within the ISP it was called upon, or scheduled activated reserves (mFRRsa (also referred to as *incident reserves*) which are called upon in advance. While mFRRda-bids are selected via a monthly auction and BSPs receive an additional compensation for the electricity supplied based on the DAM prices, the purchasing of mFRRsa is similar to aFRR (Lampropoulos et al., 2018).

4. **Replacement Reserve** used to be referred to as slow tertiary reserves, which were to be activated in case of power plant malfunctioning. However, the IDM has replaced the function of RR, which are no longer used in the Netherlands (Lampropoulos et al., 2018).

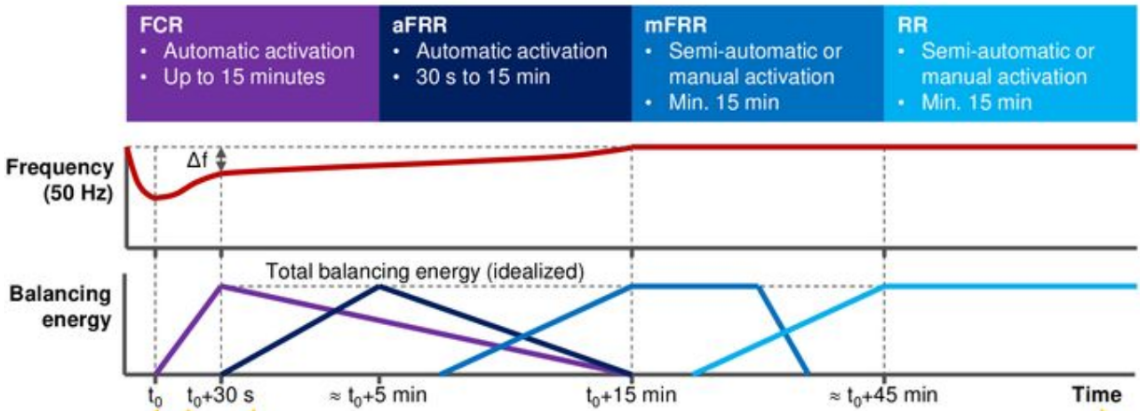

Figure 2.2: Graphical representation of balancing services based on activation time and mechanism. Note that RR does no longer exists in the Netherlands (Aine, 2018)

Bids for both upward and/or downward regulation by all reserve types are ranked based on ascending price. This *merit order* dictates which bids are called upon first, and establishes a uniform balancing energy price based on marginal pricing. Hence, all actived aFRR, mFRRsa and mFRRda offers receive the lowest activated bid price for downward regulation (which is expressed in terms of negative energy) and highest activated bid price for upward regulation (TenneT, 2020). The imbalance price to which BRPs with a shortage or surplus are subject is the result of this pricing scheme and the overall system balance, which is described by the *regulation state*. When no upward or downward regulation takes place (regulation state = 0), small shortages and surpluses are settled based on the average of upward and downward bids (the *mid price*). During regulations states 1 (upward), -1 (downward), and 2 (both upward and downward) the marginal bid prices apply. The direction of its internal imbalance vis à vis the market state, and the sign of the marginal price, determines whether the BRP will be subject to positive or negative costs. For instance, during downward regulation, the settlement price may be negative, which means a positive surplus is penalized. A example of the upward, downward and settled imbalance prices is provided by figure 2.3. While imbalance price settlement takes place *ex-post*, one day after physical delivery, a market forecast is broadcast every minute by the TSO for the current ISP (Okur et al., 2019; Tanrisever et al., 2015).

2.1.3 Aggregators in the Electricity Market

Aggregation services may be implemented in different ways, ranging from integrated approaches were the aggregator-role is assumed by an supplier-BRP, to isolated entities en-

[6]This has recently changed to the day before delivery (en Markt, 2019).

Figure 2.3: example of upward and downward settlement prices

tering into contracts with end-users, suppliers and BRPs to respectively procure flexibility, energy supply and gain access to the wholesale market (de Heer & van der Laan, 2017).

Aggregated flexibility may be offered in all sub-markets. On the DAM, the 1 hour-settlement period is relatively long for the exchange of flexibility and the early market closure results in sub-optimal forecasting of RES (Lampropoulos et al., 2018). Moreover, simulation results show that the contribution to system balancing is more profitable strategy. This is mainly driven by the more frequent and larger price spreads in the imbalance market (IM). On the other hand, IM-risks are higher due to its stochastic nature (Lampropoulos et al., 2017). The IDM is typically too illiquid in the Netherlands: there is a considerable risk that no counter-party bids can be found (Chaves-Ávila et al., 2013). Currently, the technological and capacity requirements for offering the market-based balancing services depicted in figure 2.2 are substantial barriers to entry (Lampropoulos et al., 2018).

However, the preceding section eluded to the fact that BRPs with imbalance positions opposite to the system state may be subject to a negative imbalance price, and may be

rewarded for contributing "voluntarily" to system balance in real time. Since the Dutch TSO provides a market update in near real-time, BRPs may consciously provide "informal" balancing services without actively participating in the ASM, by deviating from their day-ahead schedule in the economically advantageous direction. So-called *passive contribution* may be a more feasible strategy for aggregators seeking market entry (Lampropoulos et al., 2015). Moreover, potential revenues from passive contribution have been increasing steadily over the past years (Lampropoulos et al., 2017).

2.2 Demand Side Management Programs

2.2.1 Categorization

Short term DSM programs are commonly classified based on the underlying motivation mechanism, but may be distinguished based on control mechanisms or decision variables as well (Vardakas et al., 2014). These approaches largely overlap with the more specific, and historical classification by Lampropoulos et al. (2013).

Motivation mechanisms can be either price-based, or market-based (Jordehi, 2019). A range of *price-based*[7] programs exist. Flat Pricing schemes apply constant electricity prices, Time-of-Use Pricing (ToUP) uses a fixed stepped rate structure, and Critical Peak Pricing (CPP) applies an additional pre-set mark-up in case of system stress. Peak Load Pricing and Real Time Pricing (RTP) deploy variable prices based on the actual electricity cost, which are respectively set the day before and in real time (Vardakas et al., 2014). Figure 2.4 gives a sense of the time scale at which these pricing mechanism apply, and demonstrates that today's electricity market effectively combines several pricing mechanisms. *Market-based*[8] DR programs may involve: *(1)* Direct Load Control (DLC), which allow an external entity (traditionally the utility) to remotely adjust end-user appliances; *(2)* Curtailable Load Programs and Emergency Programs, where medium and large consumers are contracted to turn off specific loads when requested by the utility; *(3)* Capacity Market Programs, Demand Bidding and Ancillary Service Market Programs, where end users actively offer balancing services on the electricity market. (Paterakis et al., 2017; Siano, 2014; Vardakas et al., 2014).

[7] Also referred to a *time-based* DR.
[8] Also referred to as *incentive-* or *event-based* DR.

Control mechanisms are either centralized, decentralized, or distributed. In *centralized* control schemes, one single entity monitors and coordinates (schedules) loads, e.g. via remote-controlled relays or internet connections. *Decentralized* schemes disseminate information about the grid state (e.g. through *grid frequency* or RTP) directly to end-user whose demand is adjusted by a local control mechanism(Vardakas et al., 2014). *Distributed* schemes contain a central optimizer which facilitates global coordination of local assets with private objective functions (Diekerhof et al., 2018; Lampropoulos et al., 2013).

Decisions variables may either address the *activation time* of schedulable loads in order to reduce power consumption during instances of peak demand. Alternatively, *Energy-management* reduces specific loads in order to reduce power consumption during peak hours, by controlling appliances with flexible, but non-schedulable loads. Both program-types may also be combined (Vardakas et al., 2014).

Finally, Balijepalli et al. (2011) and Siano (2014) suggest a classification based on *dispatchable* or *physical* DR versus *non-dispatchable* or *market-based* DR. The former refers to ancillary services (e.g. Demand Bidding) and responds to real-time balancing requirements, while the latter refers to all price-based schemes.

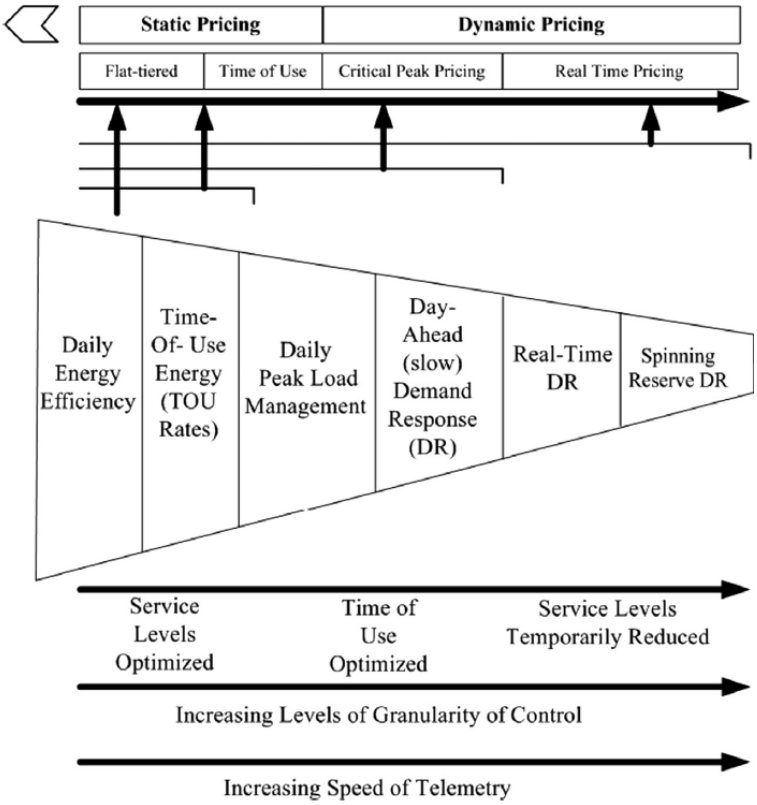

Figure 2.4: Demand Response Approaches (Siano, 2014)

2.2.2 Optimization Methods

The purpose of sections 1.1.1, 1.1.2 was to introduce the concept of flexibility as a scarce resource in the power system. Accordingly, mathematical optimization is the quintessential analytical tool for DSM. As opposed to the classical optimal dispatch problem of (large) electrical power plants, DR programs essentially comprise optimal coordination problems, enabling the scheduling of energy demand, supply and storage based on predefined targets. Numerous optimization techniques have been used to minimize electricity costs, emissions, grid-consumption or volatility, or maximize self-consumption, profits or social welfare (Jordehi, 2019; Vardakas et al., 2014).

A fully fledged DSM system should establish a trade-off between the objectives at the customer and system level, for instance by comprising a two- (or multiple-) level hierarchy to enable the horizontal integration and interaction between individual consumers and producers (e.g. Z. Xu et al. (2016), Salah et al. (2018), (Henríquez et al., 2017)). In addition, a DSM system should: *(1)* be scalable, *(2)* enable each user to determine - within limits - its own objective function, *(3)* take into account relevant sources of uncertainty, *(4)* the algorithm needs to converge to optimal or near-optimal results in a suitable time to stay within the operation time window of the actions of the flexibility provider and the flexibility user, *(5)* the optimization algorithm needs to ensure customer privacy and treat sensitive data carefully. (Diekerhof et al., 2018) Naturally, a DR program may be limited to one, or a subset of these principles, depending on the context of the actual application.

The remainder of this section presents a (non-exhaustive) overview of the most relevant optimization techniques.

Mathematical Optimization

Linear Programming (LP) finds the values of a set (*the design vector*) of *choice variables* that minimize or maximize a *linear* function (or multiple linear functions, in the case of multi-objective optimization), subject to a set of linear *constraints*. The *objective function* determines the desired characteristic of the system that is optimized (e.g. total energy consumption (Vardakas et al., 2014). Typically, LP is applied to *dynamic optimization problems*, in which the objective function is solved over a certain *time horizon*, consisting of consecutive *time steps*. In this case, the parameters in the objective function need not be fixed, but may change over time, despite being exogenously determined. By

contrast, the system's dynamics are captured by *state variables*, whose change is endogenously determined by dynamic equations (Rogosich, 2000).

A common target for DR programs is electricity cost minimization, which is achieved by formulating the a load scheduling procedure and applying an appropriate pricing scheme (Vardakas et al., 2014). For example, Ding et al. (2014) and J. Wang et al. (2019) optimize DR in industrial facilities with PV systems and TCLs, and respectively stationary an ESS and EVs with V2G-functionality. A State Task Network (STN) captures the industrial process by representing the steps of the process as task nodes, and the materials involved as state nodes. The former are schedulable tasks, functioning at different *operation statuses* with a specific electricity demand, number of workers, heat dissipation from equipment, material consumption rate and production rate. Within these status-specific constraints, a production requirement must met at the lowest possible total electricity costs. In both systems, energy management is based on day-ahead TOU-pricing for both selling and buying, assumes PV generation schedules are known in advance, and minimizes total electricity costs using *Mixed Integer Linear Programming*. In MILP, some variables in the design vector are integers - specifically binary integers ({1,0}) representing the ON/OFF-status of appliances (Jordehi, 2019).

Convex programming is the general form of LP, and allows for some non-linearity. Due to the convexity of the objective function(s) and/or constraint(s) some non-linearity is permitted. Since local optima are also global optima, the computation remains efficient (Boyd & Vandenberghe, 2004). Rivera et al. (2016) employ CP to minimize the non-linear costs in an V2G-aggregation scheme. The cost function includes battery degradation as a quadratic function[9]. Sundstrom and Binding (2011) capture the power loss when charging an EV battery with QP, although it is shown that the linear approximation is sufficient. Park et al. (2017) use convexity to characterize user inconvenience form re-scheduling of a set of appliances. The objective function is combined with a quadratic objective function characterizing energy costs of the household with a PV system and an ESS. Non-convex, non-linear programming (NLP) is compared to MILP and LP by Ommen et al. (2014), who optimize a district heating system comprising heat pumps, Combined Heat and Power (CHP) plants and boilers. Sensitivity analysis shows that while NLP is the most accurate, the computational time is orders of magnitude larger than MILP. For this reason (Maheshwari et al., 2020) decompose the non-linear degradation behaviour of a stationary

[9]Quadratic programming (QP) is a subclass of convex programming.

BESS into ten linear segments, which are then included in a linear program.

Stochastic Optimization (SO) methods represent uncertain parameters by random variables instead of deterministic data (Barbato & Capone, 2014). This relaxes the assumption of perfect forecasting implied by the methods discussed above, and thus enables more accurate estimation of optimal scheduling based on RTP and uncertain VRE supply. For instance, Tohidi and Gibescu (2018) use a stochastic MILP to simulate the revenue of a BESS which performs arbitrage between the DAM and IM. The constraints of the optimization problem are probability-weighted summations of a range of possible forecasts, which is iteratively extended until the difference in revenue between two consecutive forecasts are fall below a certain value. Alternatively, uncertainty may be addressed by *Robust Optimization*, which is applied when the probability distribution of uncertain parameters is not accurately known, but instead represented by an *uncertainty set* (Barbato & Capone, 2014).

(Meta)heuristic Optimization overcomes the computational limitations of conventional (exact) optimization, by using artificial intelligence methods to solve nonlinear programs. These nature-inspired algorithms use a combination of randomization and *local search*[10] to find approximate, near-optimal solutions in a more reasonable time-frame. For instance, *Genetic Algorithms (GA)* mimic natural selection of possible solutions ("genes") by reproduction and recombination ("cross-over"), as as well as mutation (Antonopoulos et al., 2020; Dengiz et al., 2019). In (González et al., 2018) and (Morales González et al., 2016) Genetic Algorithms optimize DR frameworks comprising respectively four clusters of medical freezers and a refrigerated warehouse. The differential equations characterizing TCLs, and the binary integers capturing switching result in *Mixed-Integer Non-Linear Programs*, which cannot be solved in a reasonable time-frame by conventional computational method. *Particle Swarm Optimization* is a widely used AI-method for VVP and V2G systems, where are a large number of variables and non-linear functions must be considered. PSO is an iterative process in which a large number of potential solutions ("particles") are moving towards the position of the most optimal particle in the population "swarm" in the preceding iterative step (Antonopoulos et al., 2020).

In addition to these high-level, problem-independent techniques, optimization methods may also be based on explicit, problem-specific rules (heuristics). For instance Dengiz et al. (2019) design use a heuristic control scheme to set the modulation degree ([0,1] for heat

[10]Local Search algorithms find optimal solution by comparing one possible solution to the next (Pirlot, 1996)

pumps, which by inserting the current price p_t to an empirical distribution function $F_t(p)$ based on a range of past price values.

Model Predictive Control

Model predictive control algorithms use a system model to predict future states of the system and determine the best possible control trajectory. This operating schedule contains the values of adjustable independent variables that minimize a certain cost function in the presence of disturbances (independent variables that the system cannot influence). The optimization problem is solved over a given *prediction horizon*. However, in contrast to the methods described above, only the *control horizon* (i.e. the first step(s) of the control sequence) is actually implemented (see figure 2.5) (Afram & Janabi-Sharifi, 2014; Fischer & Madani, 2017).

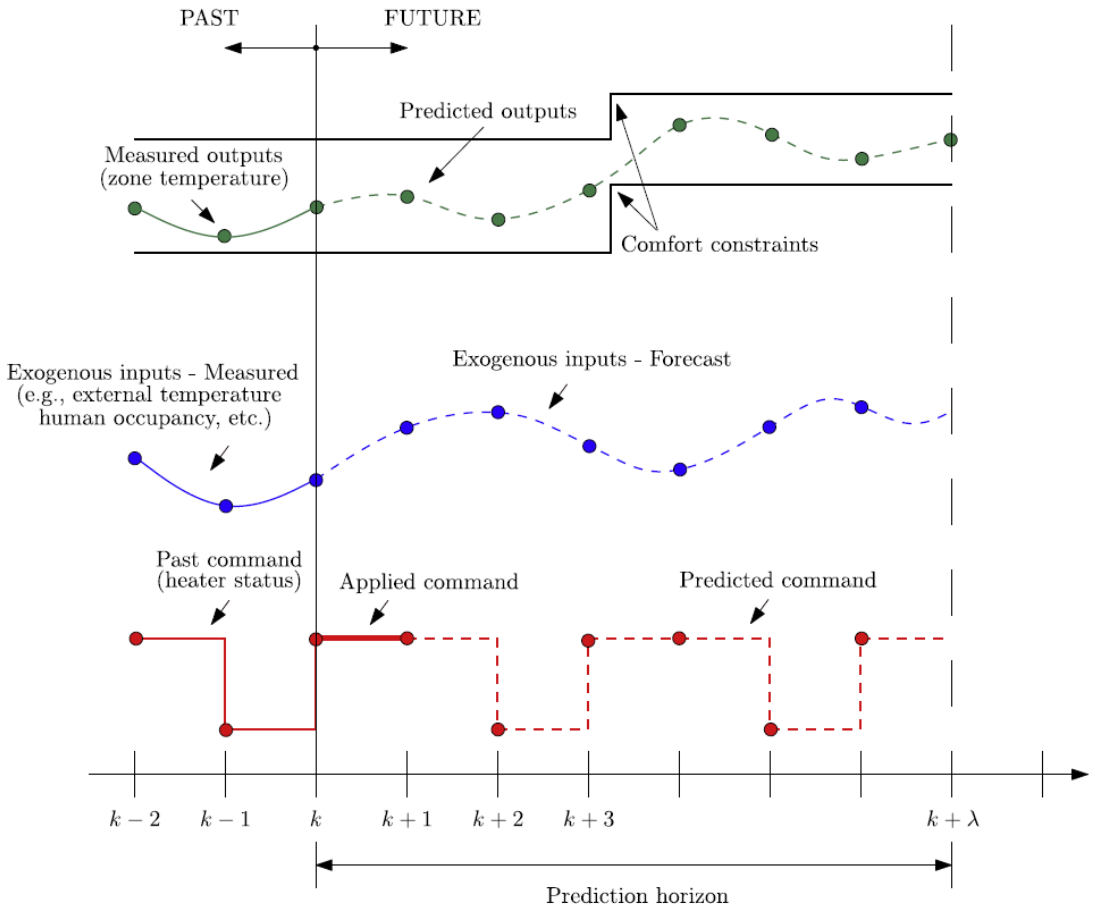

Figure 2.5: evolution of the system variables in an MPC approach for HVAC load control (Bianchini et al., 2016)

Subsequently, the prediction horizon is shifted forward and the optimization is per-

formed again for a prediction horizon starting at the next time instant, based on new measurements and updated forecasts. This so-called *receding horizon* approach introduces feedback to the model since the new state is influenced by past control actions and related disturbances (Avci et al., 2013; Oldewurtel et al., 2012; Privara et al., 2011). MPC can thus be understood as a closed-loop control system.

In recent years, MPC has gained traction as building climate control method aimed at increasing energy efficiency while ensuring end-user comfort. Although MPC is a deterministic method, it is able to incorporate time-varying disturbances and system parameters (e.g. weather conditions, room occupancy) (Afram & Janabi-Sharifi, 2014; Oldewurtel et al., 2010). Since "offline" optimization based on RTP and VRE-generation over a long horizon (e.g. day-ahead) is heavily influenced by uncertainty, MPC is an increasingly popular method for DR programs (Bianchini et al., 2016) and optimal battery charging (Tian et al., 2020). Okur et al. (2019) consider an aggregator which controls heat pumps in residential and commercial buildings with rooftop solar PV. MPC is used to minimize internal imbalances - i.e. "the differences between the DAM bid and the actual energy exchange with the power grid in real-time" - for each PTU. Solar generation is assumed to be the only source of deviation from the DAM bids, i.e. the planned net energy exchange with the grid. Other sources of internal portfolio imbalances, such as errors in the demand forecasts of consumers, are neglected. Increasingly accurate solar irradiance forecasts are simulated from actual measured data, and assumed to be updated every hour. The MPC program runs every 15 minutes, and may shift flexible demand by at most 2 hours. Lampropoulos et al. (2015) construct a hierarchical optimization model which first constructs a arbitrage schedule for a BESS on the DAM. On the operation day, MPC refines the schedule using passive contribution, which is achieved by intra-hour optimization over a receding horizon of 12 hours, based on new, more accurate forecasts. Finally, a real-time control framework minimizes imbalances in the local low voltage grid within each ISP. The authors compare the revenue from the hierarchical model, with only day-ahead scheduling or only intra-hour passive contribution in the imbalance settlement system, and find that the latter is most profitable, whereas the profitability of day-ahead scheduling is sensitive to the efficiency of the battery and the volatility of the DAM. While the battery model uses one nonlinear constraints, it should be noted that the optimization programs employed in MPC are typically linear, despite the non-linear behaviour of loads encountered in MPC-based DR-programs. Linearization or convexification is usually required, since MPC prioritizes computational

performance over model accuracy (Fischer & Madani, 2017). Finally, stochastic MPC allows the remaining short-time forecasting uncertainty to by systematically incorporated by including *chance constraints* in the optimization model, which only must be met in a probabilistic sense (Mesbah, 2016).

2.3 Battery Energy Storage Systems

2.3.1 Energy Storage Technologies and Demand Side Management

As was mentioned before, notwithstanding the relevance of DR, the incorporation of energy storage in the demand side of is imperative for the continued integration of VRES in the power system. Amongst the wide range of applications of ESSs are time-shifting energy over longer periods, avoiding curtailment and network congestion during peak production hours, maintaining power quality and reliability, and providing capacity backup for unexpected contingencies. ESS may play a role on the supply side by offering ancillary services to the grid by responding to imbalances in aggregate demand/supply profiles, or act as flexible loads on the demand side, modifying the profile as seen by the grid operator (Evans et al., 2012; Koohi-Fayegh & Rosen, 2020; Luo et al., 2015; Parra et al., 2017; Zakeri & Syri, 2015).

In all cases, energy storage involves converting energy from a non-storable to a storable form which can be kept for a certain time period in a certain medium. Typically, five classes of energy storage technologies are distinguished: mechanical, electrical, electrochemical, chemical and thermal. An extensive overview of these technologies, which is beyond the scope of this thesis, can be found in Aneke and Wang, 2016; Evans et al., 2012; Guney and Tepe, 2017; Luo et al., 2015. Such publications typically offer a comparison of these technologies based on a variety of metrics: (1) energy density and/or specific energy (amount of energy (kWh) stored per unit volume and/or unit weight (respectively), (2) power density and/or specific power (time rate of energy transfer (W) per kilogram, (3) overall storage capacity (MWh), (4) round-trip efficiency (ratio of total energy input to total energy output), (5) response time, (6) self-discharge (energy dissipation during longer-term storage), (7) life-time and amount of cycles, and (8) techno-economic maturity.

These characteristics inform the suitability of specific technologies for different purposes. For instance, power quality management, which relies on very fast response times

to smooth frequency disturbances on a nano- to milisecond scale, can be adequately fulfilled by flywheels, capacitors and superconducting magnetic energy storage systems. While having a long cycle life, they have among the highest capital costs (€/kWh) due to their short run times once activated. In contrast, Sensible Heat Storage (SHS), the most simple thermal energy storage technology which stores energy by heating or cooling solids or liquids (especially water), has low capital cost and may provide energy over a longer period, but has relatively low charging and discharging rates (Evans et al., 2012). Figure 2.6 provides a schematic overview of different storage technologies relevant in the context of VRE integration.

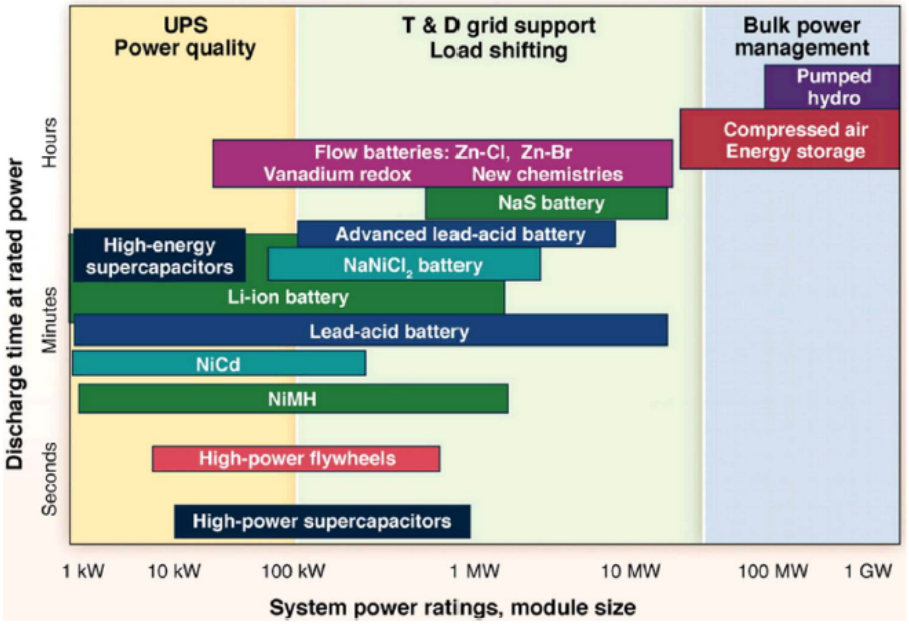

Figure 2.6: Comparison of different ESSs based on system sizing and power output, mapped based on their applicability for the provision of uninterrupted power supply (UPS), transmission and distribution grid support, large scale storage (Guney & Tepe, 2017)

In the context of demand side energy storage and energy management, electrochemical energy storage, and specifically battery energy storage systems (BESS) are most commonly applied. The other type of electrochemical energy storage, redox flow batteries, offer great potential for large scale energy storage, though costs continue to be challenge (Koohi-Fayegh & Rosen, 2020). Even though thermal energy storage is cheaper, for energy management purposes on the demand side, BESS are advantageous, as they are able to simultaneously maintain power quality, shift loads, and offer medium-term standby reserve capacity (Evans et al., 2012). Moreover, batteries have a relatively high efficiency, exhibit low self-discharge, are easily scalable and location independent (Han et al., 2015; Hesse et

al., 2017). Battery types are typically distinguished based on the materials of the *electrodes* and *electrolyte*, the essential components of electrochemical cells (see section 2.3.1. At a higher conceptual level, battery can consist of primary, non-rechargable cells and secondary cells, which can be recharged, and are considered here. Of the various types, lead-acid, sodium-sulfer and lithium-ion batteries are currently of most relevance to the integration of VRES. While sometimes included in related research, nickel-cadmium/-manganese batteries are unlikely to be used for DSM applications, due to high costs, environmental concerns and charging-behaviour dependent degradation (the so-called *memory-effect* (Luo et al., 2015)).

The *Lead-acid* battery is the most widely applied and mature technology on the market, and has been a common choice in isolated power systems to ensure uninterrupted power supply (UPS). While low costs and relatively high cycle efficiencies are beneficial, the cycle life of these Pb-acid batteries is rather low and the anode/cathode/electrolyte give rise to environmental concerns during the production and disposal phase (Evans et al., 2012; Zakeri & Syri, 2015).

Sodium-sulfur (NaS) batteries use a high-temperature reaction between sodium and sulpher which are separated by a solid, beta alumni electrolyte. The technology offers high energy density, relatively high energy efficiency and higher rated power capacity than other batteries, and consists of non-toxic materials. However its high operating costs and operating temperature currently still stand in the way of commercial deployment as utility-scale BESS. (Luo et al., 2015; Zakeri & Syri, 2015).

Lithium-ion batteries play an increasingly import role in electrical energy storage, due to their high energy density, long lifetime ($\tilde{1}$0.000 cycles), relatively high cycle efficiency of up to 97%, and low self-discharge rate (Zakeri & Syri, 2015). Due to their relatively small size and weight, Li-ion batteries have become a prominent energy storage technology for essentially every application, ranging from mobile phones and portable electric tools to electric vehicles. Li-ion batteries are mostly cobalt- or phosphate-based, the latter of which has been developed more recently, but offers higher efficiency while maintaining energy and power density nearly as high as cobalt. Moreover, the availability of cobalt is limited, resulting in higher material costs (Evans et al., 2012).

2.3.2 Battery Technology

Similar to the previous section, the physical and economic characteristics and parameters of BESSs will only be discussed to the extend that these are relevant to the models outlined in section 3.2. Consequently, the thesis focuses on Li-ion (Phosphate) batteries hereafter, based on their applicability to the research context (demand side energy storage, load shifting and grid support). The following paragraph first summarizes the general working principles and parameters of batteries. Secondly, battery degradation, a major contributor to the operating costs of a BESS and a relevant factor for the modelling of battery behaviour, will be discussed.

Working principle

Battery cells consist of positive and negative electrodes. In Li-ion cells, lithium ions are released from the negative electrode, referred to as the anode, during discharging. These ions migrate through the electrolyte, which conducts only ions, and are diffused into to the delithiated positive electrode (the cathode). Meanwhile, electrons are conducted externally from the negative to the positive electrode, which are electrically insulated. This oxidation/reduction process generates a current, and is reversed during charging, when insertion takes place at the negative electrode and oxidation at the positive electrode, which is now referred to as anode. (Chen et al., 2020). The cell's potential power and energy, as well as its safety and lifetime, are determined by the cell's geometry and format. For instance, for a given material composition, a cell can offer either higher energy capacity (mAh), or higher power capacity (V), depending on the thickness of the electrode (Maheshwari, 2018).

The ratio of power output and energy capacity of the battery is called the *c-rate*. While power output determines the rate of (dis)charge, the energy capacity refers to the amount of energy that can be stored. For instance, at 1 C, a 2 Ah battery can provide 2 A current continuously for one hour. When a number of cells are connected in a module, the resulting power and energy arises from the parallel/series configuration. To ensure all cells are charged evenly, and safe operation is guaranteed, all modules are equipped with battery management systems.

The capacity delivered by a module is expressed in kWh, while power output is expressed in kW. *Rated* power and energy output refer to the maximum capacities of the

BESS. The relationship between both quantities is relevant for the specific use case in power systems: for peak shaving and UPS at the demand side, the system should be able to provide energy for a sustained period of time, while ancillary service provision requires shorter energy bursts at high power ratings (McLaren et al., 2016). Here, a distinction can be made between *continuous load current*, which may be sustained for a long time, and *pulse load current*, which may be higher, but can only be sustained for brief period. These maximum currents can be expressed using C-rate and E-rate, since they are capacity dependent. The amount of energy present in the battery as a percentage of its total capacity is referred to as *State of Charge* (SOC). The inverse of this is sometimes referred to as *Depth of Discharge* (DoD), however this thesis refers to DoD as the total difference between the maximum and the minimum SOC (Maheshwari, 2018). The *roundtrip* efficiency of completing a charge/discharge cycle depends on operating conditions of the battery, such as the temperature, the state of charge, the C-rate. For a lithium-ion cell, the efficiency falls within the range of 92%-96% (Renewable, IRENA, et al., 2017).

Battery Degradation

BESSs for DSM applications typically require a relatively large rated power output, and consequently, a large amount of cells. The means the initial investment costs of the system are high, and the preservation of the BESS's life time is of critical importance: once battery capacity degrades below 80% of initial capacity, batteries are typically considered to have reached End-of-Life (EoL) (Muenzel et al., 2015; Omar et al., 2014). Hence, a key factor in the economic optimization of BESSs are the operating costs arising from degradation (B. Xu et al., 2016).

Degradation occurs continuously in both the electrolyte, and the positive and negative electrodes, and comprises changes in the composition of the electrolyte, and the reduction of active lithium in the electrodes. The underlying mechanisms can be decomposed in calendar degradation and cycle degradation (Maheshwari, 2018). Calendar degradation occurs naturally over time, while being influenced by the conditions of the surrounding environment such as temperature, and by usage patterns, such as the average SoC. The rate at which cycle degradation takes place is the result of the (dis) charging behaviour, expressed in terms of DoD and C-rate. The battery life can also be expressed in term of full cycles that can be performed. This *cycle life* depends primarily on DoD, temperature, and C-rate. The results obtained by Omar et al. (2014) who examine the impact of different

cycle depths are visualized in figure 2.7).

Due to their impact on total costs, cycle and calendar aging should be included in system optimization problems (Cardoso et al., 2018). Battery degradation models can be categorized into theoretical and empirical approaches. The former uses explicit equations to capture both physical and chemical characteristics, while the latter fit curves to empirical data to find general equations from discrete cycling measurement points. While electrochemical models are accurate and insightful, empirical models reduce complexity of model tuning. However, adequate empirical models must take into account the relevant charging parameters, such as state-of-charge, (dis)charging currents, depths of discharge and temperature (Muenzel et al., 2015). In fact, empirical models are tailored to specific BES installations, requiring extensive data collection. Alternatively, *semi-empirical* models combine theoretical relations with empirical observations to obtain more generalizable models (B. Xu et al., 2016).

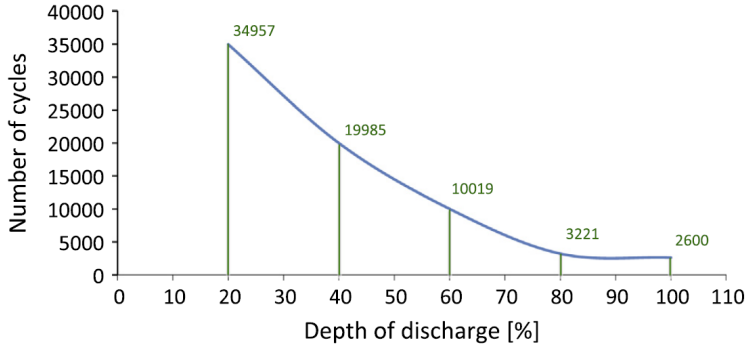

Figure 2.7: Cycle life of a lithium-iron phosphate battery versus cycle depth (Omar et al., 2014).

Chapter 3

Methods

3.1 Research Strategy

3.1.1 Optimal BESS Control

The DSM program proposed in this case study envisages a *centralized energy management system* exerting *direct load control* over distributed demand side battery energy storage systems. Electricity is supplied by 4 utility-scale solar PV systems and 8 prosumers with rooftop solar systems. In addition to the prosumers, the aggregator services the critical electricity demand of 9 consumers. Figure 3.1 provides a schematic representation of the system, whose control scheme aligns *actual* electricity demand from and supply to the grid as much as possible with the supply-demand schedule submitted to the *day-ahead* market, by managing energy flows to and from the battery systems, taking into account *updated* solar energy generation forecasts. Moreover, the system takes note of the imbalance market in order to provide balancing services to the grid. Hence, the EMS must respond to two sources of *dynamic* data: (1) frequently updated solar energy generation forecasts, and (2) *real-time* imbalance market signals. For simplicity, the demand schedules are assumed to be static.

> *Assumption 1:* Perfect foresight is assumed with respect to the day-ahead demand forecasts of all critical loads. Hence, there is no imbalance between actual consumption and the day-ahead schedules of the clients in the portfolio.

Based on to the reviewed literature (e.g. Okur et al. (2019)), MPC is a suitable method to achieve the objective of a DSM program with these general characteristics. The program's objective can be expressed in terms of energy, achieved by reducing imbalances between day-ahead and updated demand/supply-schedules as much as possible, while max-

imizing passive contribution using remaining battery capacity. Alternatively, the objective can be expressed in terms of imbalance costs, achieved by minimizing internal imbalances and/or by generating revenue through passive contribution based on the price signal from the imbalance market. While the problem definition presented in section 1.2 clearly favours the latter formulation, the settlement process of imbalance costs comprises an important caveat for the suitability of MPC. After all, the prediction horizon required for MPC-induced load-shifting exceeds the forecasting horizon of imbalance prices. Research on imbalance price forecasting model beyond a single PTU is few and far between, and it is beyond the scope of both this thesis and the available data to develop an entirely novel price forecasting model. While it is certainly possible to feed (moving)-average imbalance prices in the model and thus account for diurnal or seasonal variations, such a heuristic approach would obfuscate the economic trade-off between *actual* imbalance costs and battery degradation costs.

Instead, this thesis proposes a DSM program with two targets: first, *absolute imbalance* reduction in terms of energy is targeted over the remainder of the optimization period. Secondly, the program may engage in passive contribution *within* the time steps of the model, in response to *imbalance price* forecasts. This hierarchical, two-step framework is loosely inspired by Lampropoulos et al. (2015). The rationale for the first step depends on assumption (2), which is non binding, but does imply that welfare maximization is not actively obstructed by imbalance minimization, and is based on the literature covered in section 1.2.

> *Assumption 2:* The direction of internal imbalances are correlated with the direction of market imbalances and are by and large positive, so internal imbalance will generally not result in negative imbalance costs, i.e. reducing imbalances is generally reduces costs.

Accordingly, the proposed control program consists of two steps:

1. *Before* each PTU starts, an MILP-based MPC program will be used to define an optimal control schedule which minimizes internal portfolio imbalances and battery degradation over the entire prediction horizon, without reference to the imbalance price signal.

2. *During* each PTU, the optimal control schedule defined in step (1) may be amended in *real time* by a heuristic model, using the imbalance market forecasts received

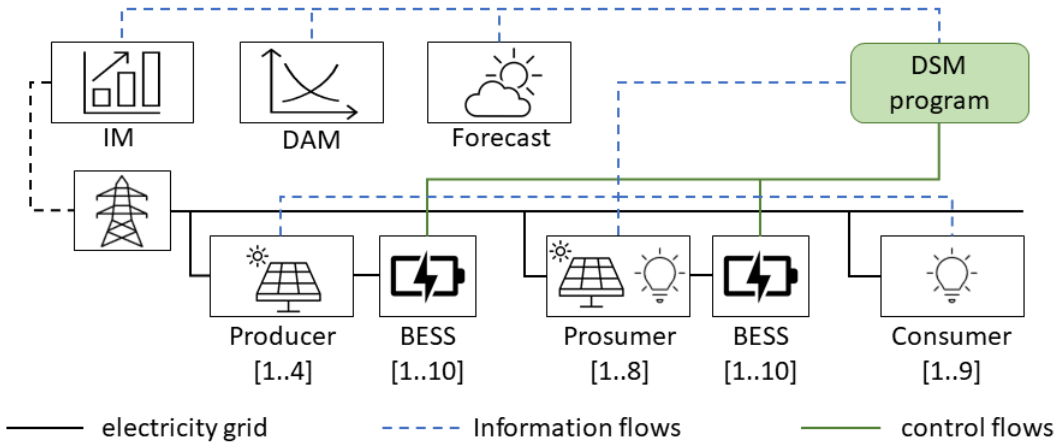

Figure 3.1: Schematic of the case study

during the first minutes of the PTU.

Although in reality the heuristic control program is executed *within* a PTU, i.e. *after* step 1 has been implemented, the proposed mathematical optimization model will treat the impact of this adjustment as taking place during the *entire* PTU. Hence, the resolution of the model can be kept uniform at 15 minute intervals across the two optimization programs. Instead of the time-unit, other variables will be adjusted to account for the shorter duration of the control action. Consequently, intra-PTU augmentation or reversal of control actions set by the MPC program results in a uniform adjustment of the control schedule. This means that the impact of the time duration of the heuristic control action on, for instance, battery degradation, is neglected.

> *Assumption 3:* Once the effect of their shorter duration on net energy input or output is accounted for, the impact of intra-PTU heuristic control actions on the energy system does not differ from the impact of inter-PTU actions by the MPC-program

3.1.2 Optimal BESS sizing

As already alluded to above, there is a definite discrepancy between the thrust of the main research question, which concerns the economic potential of proposed BESS-based DSM scheme, and the EMS proposed in the previous sections, which only targets imbalance costs secondarily. Most importantly, the program is unable to minimize the aggregate of the total capital and operational costs of the BESSs and the total imbalance costs over the entire optimization horizon. To address this issue, a second, auxiliary optimization

program is set up to define the economically optimal static parameters of the system, i.e. the aggregate size of the BESSs and the relative importance of degradation vis á vis imbalance reduction. Based on these optimal parameters, the DSM program's potential in the context of forecasting uncertainty can be examined.

To this end, the program as described above will be restated to optimize the system at once, over a fixed horizon of 96 PTUs, while emulating the components and scope of the MPC program as much as possible. Since the perfect foresight assumption applies, the second step mentioned in section 3.1.1 is no longer required, and the possibility for passive contribution can be included in one single, multi-objective optimization program, which is presented in section 3.5. Due to the single optimization horizon, this program is able to evaluate the potential of the MPC strategy for a range of battery sizes within a more feasible time-frame than the actual MPC program.

3.1.3 Chapter outline

The remainder of this chapter is organized as follows: Section 3.2 describes the specific outline of the model in a conceptual manner, sections 3.3 and 3.4 present the mathematical formulations of each component of the first and second step of the control program, respectively. Section 3.5 presents the adjusted optimization program to determine the optimal configuration. The combined model predictive control program and the heuristic model are represented in *pseudocode* form in algorithm1. This description also includes a number of data pre-processing steps, which are introduced in chapter 4.

3.2 Conceptual Model

Essentially, the DR-model's implementation comprises three generic elements: (1) an optimization program executed over the entire prediction horizon; (2) a heuristic control strategy enabling passive contribution; (3) the overall control sequence, which first executes the optimal control actions during the current PTU, and subsequently updates the prediction horizon for the subsequent model run during the next PTU, changing the state of the battery systems, which introduces feedback to the model. This third element envelops the first two elements and can be sufficiently captured by a rudimentary schematic representation of the control model in flow chart 3.2. In contrast, the optimization program and the heuristic control strategy merit a more detailed discussion.

3.2.1 Predictive Imbalance Minimization

The MPC's prediction horizon consists of two input vectors, which relate to *sub-question 1*: (1) the aggregated critical/non-flexible demand and supply schedules of all clients in the portfolio as submitted on the day-ahead market, and (2) the updated solar energy generation forecasts, which are also aggregated. The latter vector is the predicted element of the MPC program, and is obtained by combining a frequently updated external weather forecast with a moving-average auto-regressive (ARMA) model by making use of a Kalman filter. It should be noted that this step, which is discussed in section 4.3, implies that the future states of the system are, strictly speaking, only in part "model predicted". In contracts, the choice variables of the BESSs (*sub-question 2*) are, except for their starting values, determined entirely endogenously by equations capturing the battery's physical characteristics.

To consider the full solar energy generation forecast and optimally exploit the capacity of the BESS, a prediction horizon of 24 hours (96 PTUs) will be used. This will also allow restrictions to be placed on specific final values (see section 3.3). Since the day-ahead supply/demand schedules are only determined at 11:00 each day, the feasible end-point of the optimization horizon is 23:45 of each day before this moment, but may be extended to 23:45 of the next day after 11:00. For simplicity, to reduce computational times and to maintain closer control over the battery (see section 3.3.2, the computations will keep the final PTU fixed at 23:45. Hence, the optimization occurs over a *shrinking horizon*, as opposed the *receding horizon* as applied in standard MPC programs.

3.2.2 Passive Contribution Strategy

Even after the operating schedules of the controllable distributed energy sources have been adjusted to minimize imbalances, the system may still contain a certain amount of flexibility: the BESS may be (dis)charged further to contribute to grid stability. However, given the scarcity of this resource, passive contribution should only take place when peak imbalance prices occur. This strategy is implemented using a heuristic prediction model, and addresses *sub-question 3*. The model consists of three steps:

1. A price threshold is set based on historical data to ensure only imbalance price peaks of a certain magnitude trigger the activation of the distributed energy resources in the portfolio.

2. Two binary regression models are used to predict (1) the regulation state and (2) whether the settled price will be exceed the price threshold during the current PTU.

3. These predictions will determine whether passive contribution may take place. While the response to the TSO's regulation and price forecast is binary, the magnitude of actual passive contribution is maximized within the general system constraints, and the MPC schedule set by the first part of the DSM program.

The prediction models require 6 minutes of forecast data, which is broadcast by the TSO with a 3-minute delay. If the heuristic model's run-time is sufficiently short, the passive contribution can take place during the last five minutes of each PTU. This means that the first step of the DR program must take place within these 5 minutes, as each subsequent MPC-run requires the passive contribution data as input and must be completed before the start of the next PTU.

3.3 Minimizing Internal Imbalances

3.3.1 Model Predictive Control Program

The proposed MILP is a multi-objective optimization problem, which minimizes the sum of the absolute portfolio imbalances Δ_t^{post} between the day-ahead production/consumption schedule and updated schedule based on the most recent forecast, while also minimizing battery degradation D. The schedule is optimized for the remaining run-time of the model, between current PTU (k) and final PTU ($T = 96$). The multi-objective approach is achieved by including fictitious variable ζ in the objective function (3.1a), which can be varied exogenously between 0 and 1 to determine the optimal weighting factor of the objectives. Both objectives are expressed as percentages (i.e. % imbalance remaining after the optimal schedule is implemented, and % of battery capacity degradation). This section outlines the constraints related to Δ_t^{post}. Δ_t^{pre} are a vector of static parameter set before the optimization is performed, and depend on the updated *expected* demand/supply schedule of the portfolio $\hat{E}_t^{ACT,pre}$, estimated before flexible distributed energy sources are activated (3.1c). Crucially, the demand/supply schedule actually realized (E_t^{ACT}) remains unknown during the model run.

Constraints (3.1d) and the left-hand side of (3.1e) serve a twofold purpose. Mathematically, the formulation ensures Δ_t^{post} is the absolute value of the imbalances at t as both

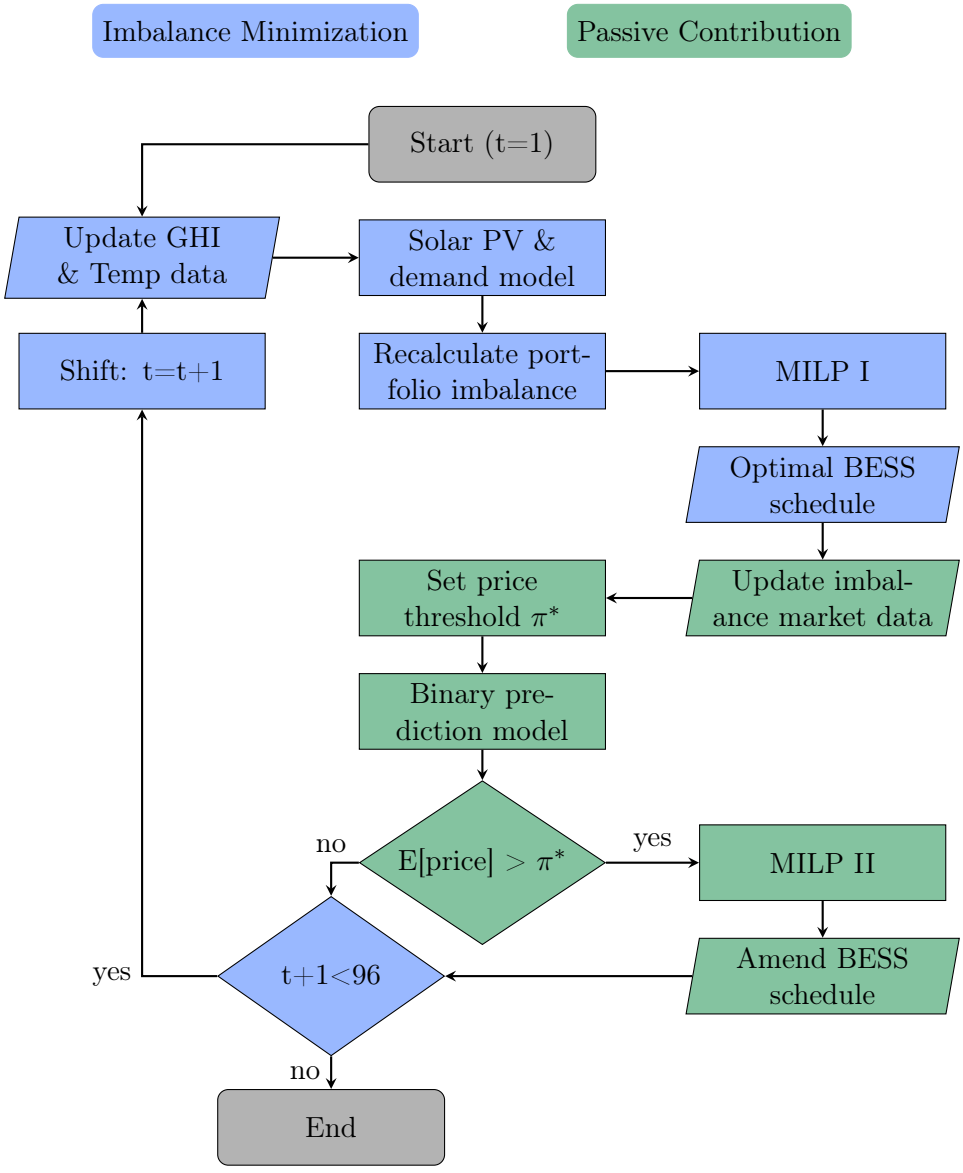

Figure 3.2: Rudimentary flowchart of the MPC and heurstic program

Δ_t^+ (portfolio surplus, $E_k^{DA} - \hat{E}_k^{ACT} > 0$) and Δ_t^- (portfolio shortage, $E_k^{DA} - \hat{E}_k^{ACT} < 0$) are expressed as positive values. Practically, it allows for the straightforward adjustment of the predictive control model to optimize the system configuration. These variables can be adjusted through $\hat{E}_k^{ACT}$ in (3.1e), which aggregates the distributed energy resources described in (sub)section 3.3.2 as expressed by equation (3.1f).

Throughout this thesis, k denotes the current PTU, i.e. the first PTU in the optimal schedule and t refers to each PTU between k and the final PTU T. Figure 3.3 visualizes how the MPC-program solves (3.1a) and implements the model outcome for the upcoming PTU, after which the (*shrinking*) optimization horizon is shifted forward by one PTU. The subsequent section addresses degradation objective D. Algorithm 1 describes the complete program, including the passive contribution model in *pseudo-code*. Note that in the algorithm, the expected/forecasted actual demand/supply schedule $\hat{E}_t^{ACT}$ is denoted as $E_t^{ACT,fcst}$

$$\text{minimize} \quad \zeta \cdot \Delta\% \cdot 100 + (1-\zeta) \cdot D \tag{3.1a}$$

$$\text{subject to} \quad \Delta\% = \frac{\sum_{t=k}^{T=96} \Delta_t^{post}}{\sum_{t=k}^{T=96} |\Delta_t^{pre}|} \tag{3.1b}$$

$$\Delta_t^{pre} = E_t^{DA} - \hat{E}_t^{ACT,pre} \quad \forall \quad t \in \{k, ..., T\} \tag{3.1c}$$

$$\Delta_t^{post} = \Delta_t^+ + \Delta_t^- \quad \forall \quad t \in \{k, ..., T\} \tag{3.1d}$$

$$\Delta_t^+ - \Delta_t^- = E_t^{DA} - \hat{E}_t^{ACT} \quad \forall \quad t \in \{k, ..., T\} \tag{3.1e}$$

$$\hat{E}_t^{ACT} = \underbrace{\sum_{i=1}^{I=n_c} E_{t,i}^{ACT,NF} - \sum_{i=1}^{I=n_p} \hat{E}_{t,i}^{ACT,PV}}_{\text{not controllable}} + \underbrace{\sum_{i=1}^{I=n_b} E_{t,i}^{BESS}}_{\text{controllable}} \quad \forall \quad t \in \{k, ..., T\} \tag{3.1f}$$

$$E_t^{DA} = \underbrace{\sum_{i=1}^{I=15} E_{t,i}^{DA,NF} - \sum_{i=1}^{I=6} E_{t,i}^{DA,PV}}_{\text{by definition}} \quad \forall \quad t \in \{k, ..., T\} \tag{3.1g}$$

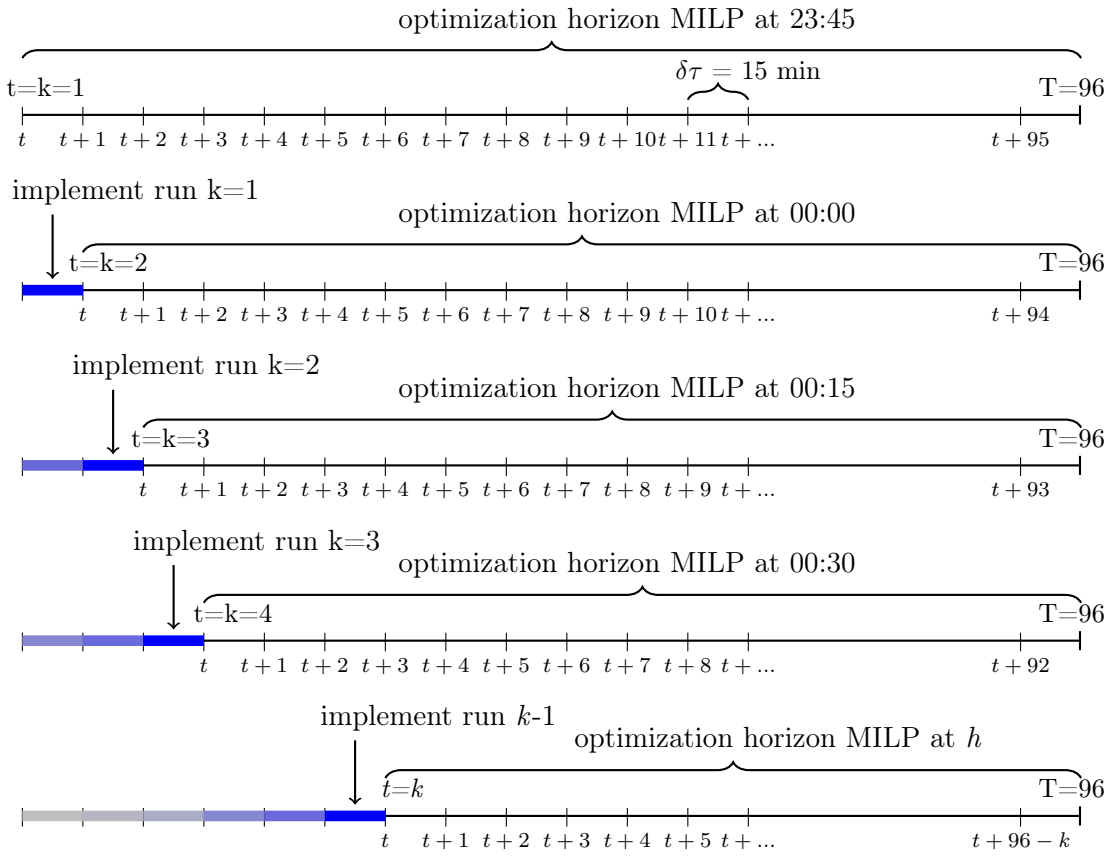

Figure 3.3: Optimization horizons of the MILP-based predictive control model at PTUs k=[1,4] and at one undefined PTU k. Aach MILP is solved during the previous PTU, after which the control action is implemented (indicated in bright blue), after which the MPC shifts forward on the time axis.

3.3.2 Battery Energy Storage System Model

The reduction of imbalances by charging or discharging the BESSs is governed by the charging and discharging dynamics of the modules, and by the additional objectives reducing the total degradation of the batteries over the optimization horizon. These quantitative characteristics, which where qualitatively introduced in section 2.3.2, are introduced here.

The specific BESS analyzed in this thesis comprises n $LiFePO_4$ modules which contain 45 cells of 17 Ah with a nominal voltage of 3.2 V, in a *15s3p* configuration, delivering a rated capacity of 2,4 kWh. All relevant characteristics of the battery module are listed in table 3.1. The BESS's total capacity (or rather, rated battery energy (kWh)) stems from the combination of an optimal number of modules in the battery pack. It should be noted that the model remains agnostic with respect to the series/parallel configuration of the BESS, and only uses the maximum (dis)charge current and rated voltage to establish maximum (dis)charging capacity (i.e.$P_{max,dis(charge)}(W) = I_{max,(dis)charge} * U_{nom} * n_{modules}$):

Assumption 4: The configuration of the modules does not alter the BESS characteristics in terms of power (kW), energy (kWh) and degradation rate.

The cycle life of the battery, which is assumed to be static, is taken from (Omar et al., 2014), and only depends on the maximum DoD of 60% (C-rate is limited and it is assumed high temperatures do not occur) The next section outlines the physical limitations of the BESS,comprising the battery's rated capacity and energy, maximum (dis)charge current, round-trip efficiency of the entire BESS, and static restrictions to prevent high rates of degradation. The second objective of the MILP, the amount of degradation caused by battery activation, will be introduced subsequently. In algorithm 1, the complete vector of (static) battery parameters is referred to as $\mathbf{Z}^{BESS}$.

Charging and Discharging

Whilst the optimization program targets *energy* (costs), battery input and output are modeled in terms of *power* (kW). Therefore equation (3.2a) includes time duration $\delta\tau = 0.25h$ during which power transfer takes place. Note that the model treats the combined BESSs as one system, with an aggregate output. During each PTU t of duration $\delta\tau$, the aggregated BESSs must either demand energy by charging, or supply energy by discharging, or remain inactivate, but simultaneous charging and discharging may not occur. This limitation is ensured by introducing binary variable β_t in constraints (3.2b), (3.2c), (3.2d) and (3.2e). These equations also imply non-negativity and constrain the battery maximum (dis)charge rate (kW) (Antoniadou-Plytaria et al., 2020; Maheshwari et al., 2020; J. Wang et al., 2019). The latter is primarily determined by the grid[1]: the decentralized BESS hypothesized here is distributed amongst a predetermined number of end-users (see section 3.5), so the grid capacity is the aggregate of all connections with a BESS. However, up to a certain BESS size, (3.2d) and (3.2e) will be binding. After all, the amount of modules determines the (dis)charge power of the total BESS, due to the upper limits of (dis)charge current and voltage).

The battery system's charging and discharging dynamics are governed by SoC-equation (3.3a). By including Q_{BESS} in the equation, the total energy storage capacity of the BESS is included in the model. The energy ultimately stored and recovered is reduced by efficiencies η_{ch} and η_{dis}, which comprise both conversion and internal battery losses

[1]The assumed 3-phase connection has a maximum current of 160 A and maximum voltage of 230 V, resulting in a maximum (disc)charge power of approximately 100 kW per connection (Liander, 2014)

(Antoniadou-Plytaria et al., 2020). In order to limit calendar degradation, the state of charge is kept within health constraints (3.3b). SoC at $t = 0$ (i.e. at 23:45 of the preceding day) and $t = 96$ (i.e. the final PTU) is set at 50% (3.3c) (Schneider et al., 2020). However, when the shrinking optimization horizon is still relatively long and the potential for passive contribution is still uncertain, a uniform constraint for $t = 96$ is needlessly binding: the MPC program may (dis)charge the battery early on in the day to meet the constraint, thus *increasing* imbalance. This activation may turn out to be unnecessary or even counterproductive during subsequent model runs as new weather forecasts come in, or opportunities for passive contribution arise. Hence, constraint (3.3d) tightens linearly as the horizon shrinks.

$$\sum_{i=1}^{I=n_b} E_{t,i}^{BESS} = (P_t^{ch} - P_t^{dis}) \cdot \delta\tau \quad \forall \quad t \in \{k, ..., T\} \tag{3.2a}$$

$$0 \leq P_t^{ch} \leq \beta_t \cdot P_t^{grid,max} \quad \forall \quad t \in \{k, ..., T\} \tag{3.2b}$$

$$0 \leq P_t^{dis} \leq (1 - \beta_t) \cdot P_t^{grid,max} \quad \forall \quad t \in \{k, ..., T\} \tag{3.2c}$$

$$0 \leq P_t^{ch} \leq \beta_t \cdot P_t^{ch,max} \quad \forall \quad t \in \{k, ..., T\} \tag{3.2d}$$

$$0 \leq P_t^{dis} \leq (1 - \beta_t) \cdot P_t^{dis,max} \quad \forall \quad t \in \{k, ..., T\} \tag{3.2e}$$

$$SoC_t = SoC_{t-1} - \frac{1}{\eta_{dis} \cdot Q_{BESS}} \cdot P_t^{dis} \cdot \delta\tau + \frac{\eta_{ch}}{Q_{BESS}} \cdot P_t^{ch} \cdot \delta\tau \quad \forall \quad t \in \{k, ..., T\} \tag{3.3a}$$

$$SoC^{min} \leq SoC_k \leq SoC^{max} \quad \forall \quad t \in \{k, ..., T\} \tag{3.3b}$$

$$SoC_0 = 50\% \tag{3.3c}$$

$$50\% \cdot \frac{k}{96} \leq SoC_{96} \leq 50\% \cdot (2 - \frac{k}{96}) \tag{3.3d}$$

While the model predictive control program does reduce calendar degradation through constraint (3.3b) and cycle degradation through objective D, the techno-economic reper-

cussions (i.e. power fade) of these mechanisms on the battery capacity Q_{BESS}, is not considered by the optimization programs in the MPC-framework. However, the optimal sizing program in section 3.5, does explicitly include degradation costs. Finally, self-discharging of the BESS is neglected.

Assumption 5: The maximum energy capacity (kWh) (dis) charge rate (kW), and (dis)charging efficiency (%) remain constant over the life-cycle of the battery, and are not influenced by environmental or operating conditions (Antoniadou-Plytaria et al., 2020; Maheshwari et al., 2020).

Assumption 6: Since self-discharge rate of Li-ion batteries is very small, this variable is neglected in the SoC-formula.

Table 3.1: battery module parameters

minimum rated energy capacity	2.4 kWh
rated voltage	48 V
nominal capacity	50 Ah
max. charge current	50 A
max. discharge current	75 A
max. charge C-rate	1C
max. discharge C-rate	1.5C
min. State of Charge	20%
max. State of Charge	80%
battery costs	500€/kWh
cycle life[2] at 60%DoD	10000
(dis)charging efficiency	94%
grid capacity	100 kWh (·10 connections)

Battery Degradation

Whilst constraints (3.2e) and (3.3a) limit calendar degradation, the life-cycle costs of the BESS is also affected by cycle aging, which depends on (dis)charging rates and current throughput (Schneider et al., 2020). Hence, the second part of the objective function minimizes total battery degradation D over the control horizon. The degradation formula

applied here is based on Schimpe et al. (2018), who present a range of semi-empirical models to capture several cycle aging effects that occur under different temperature conditions. The model is parameterized on experimental data obtained from a life-time test study conduced on a commercial $LiFePO_4$ cell with a nominal capacity of 3 Ah and a nominal voltage of 3.2V, designed for stationary applications (Schimpe et al., 2018). While the model error for cell capacity loss is below 1% of initial cell capacity, it should be noted that application of this model to the current problem presupposes that the parameters can be reliably generalized to a $LiFePO_4$ cell of 17 Ah. Moreover, the(dis)charging power of the entire BESS should arise from a uniform current through the battery. These assumptions (7 and 8) implicitly follow Cardoso et al. (2018) and D. Wang et al. (2016), who utilize a semi-empirical model parameterized on a 1.5 Ah $LiNiCoO_2$ cell by J. Wang et al., 2014, to optimize BESSs with energy ratings of multiple kilowatt-hours.

Assumption 7: The battery energy management system ensures uniform (dis)charging behaviour across all modules and cells, regardless of the BESS module and cell configuration.

Assumption 8: The parameters in equation (3.4) do not depend on battery cell capacity.

Since the application of the model proposed here assumes the reference temperature (298.15 K) is maintained throughout, a number of capacity loss mechanisms pertaining to the temperature dependence of both calendar and cycle degradation are not considered. Similarly, SOC_{max} is below the region in which the cycle aging mechanism for high SOC-levels applies . Consequently, the capacity loss model reduces to (3.4), where $k_{cycle,lowT,Ref}$ refers to the cycle degradation stress factor ($4.009 \cdot 10^{-4} \cdot Ah^{-0.5}$) which applies at the low reference temperatures. This equations depends on the current rate in two ways. The charge throughput in the charge direction Q_{Ch} (which is half of the total charge throughput) , captures the assumed mechanism for lithium loss, while the current rate also enters via an exponential correlation term with the charge current I_{Ch}, nominal cell capacity C_{nom}, and maximum charging current $I_{Ch,ref}$. Finally, $\beta_{lowT} = 2.64h$. To facilitate implementation, (3.5b) restates the model in term of C-rate (3.5a). The total degradation accumulated over the optimization horizon is simply (3.5c)

$$Q_{Loss,Cyc,LowT} = k_{cycle,lowT,Ref} \cdot exp[\beta_{lowT} \cdot \frac{I_{Ch} - I_{Ch,ref}}{C_{nom}}] \cdot \sqrt{Q_{Ch}} \tag{3.4}$$

$$\text{C-rate}_t = \frac{P_t^{ch} + P_t^{dis}}{Q_{BESS}} \tag{3.5a}$$

$$Q_{loss,t} = 4.009 \cdot 10^{-4} \cdot exp[2.64 \cdot \frac{\text{C-rate}_t \cdot C_{nom} - I_{Ch,ref}}{C_{nom}}] \cdot \sqrt{\frac{\text{C-rate}_t \cdot C_{nom} \cdot \delta\tau}{2}} \tag{3.5b}$$

$$D = \sum_{t=k}^{T=96} Q_{loss,t} \quad \forall\, t \in \{k, ..., T\} \tag{3.5c}$$

In the implementation of the model, (3.5b) is captured by a piecewise linear function to circumvent the formula's non-linearity in C-rate$_t$. To ensure computational efficiency, a rather coarse linearization in 5 domains is used (see figure 3.4)

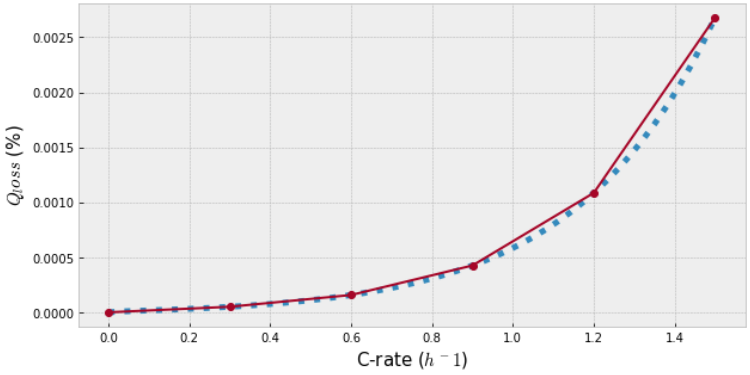

Figure 3.4: Piecewise linearization of capacity loss model 3.5b

3.4 Heuristic Control Program

The control method enabling passive contribution proposed in this thesis is referred to as 'heuristic', because the control actions are based on a number of pre-determined 'rules', as opposed to exact empirical or theoretical models. The rule underlying the heuristic model proposed in this thesis is expressed as a percentile in the frequency distribution of historical imbalance prices, and approach loosely borrowed from Dengiz et al. (2019). The value is related to this percentile is the price threshold referred to in section 3.2.2. The percentile itself, which relates to the "scarcity" of the flexibility available in the system, is introduced in section 3.4.1. The subsequent steps of the program, i.e. (1) the combination

of statistical models to predict regulation states and imbalance prices, and (2) the optimization program to determine the maximum feasible amount of passive contribution, are outlined in subsections 3.4.2 and 3.4.3.

3.4.1 Price Threshold Setting

To ensure a certain calendar life, the number of charging cycles that may be performed during on model run is constrained. This number, N_0 is obtained from the system optimization model introduced in section3.5. The difference between this number and the amount of cycles already performed determines the "scarcity" of the available battery capacity at a particular point in time. After each run of the MPC-model, the amount of full equivalent cycles (FEC) performed over the entire optimization horizon (both to minimize imbalances and engage in passive contribution) is calculated. The cycle counting method adopted by this thesis may be referred to as *half-cycle counting*. This is a more rudimentary approach than *rainflow cycle counting*, the most common alternative, which is a separate algorithm. However, Antoniadou-Plytaria et al. (2020) find that results obtained using both approaches largely correspond. The FECs performed to minimize imbalance determines the potential amount of BESS *activations* "left" for passive contribution in terms of n PTUs (3.7). As mentioned earlier, the maximum depth of discharge (DOD_{max}) is defined as the difference between SOC_{max} and SOC_{min}.

$$\text{FEC}_t = \frac{1}{2}\sum_{t=0}^{T=96} \frac{P_t^{BESS,ch} + P_t^{BESS,dis} + \frac{1}{3}\cdot P_t^{pc,D} + \frac{1}{3}\cdot P_t^{pc,U}}{Q_{BESS}} \cdot \delta\tau \quad (3.6)$$

$$\text{activations}_t = (N_0 - FEC_t) * \frac{Q_{BESS} * DOD_{max}}{P_{(dis)charge,max}\cdot\frac{1}{3}\cdot\delta\tau} \quad (3.7)$$

$$\text{percentile}^{up} = max\{(1 - \frac{\text{activations}_k}{T-k}) * 100\%, 50\%\} \forall \quad \text{activations}_k > 0 \quad (3.8a)$$

$$\text{percentile}^{down} = min\{(\frac{\text{activations}_k}{T-k}) * 100\%, 50\%\} \quad \forall \quad \text{activations}_k > 0 \quad (3.8b)$$

The number of activations still available at PTU=k must be exploited optimally during the remaining horizon. The heuristic proposed by this model is the ratio of n remaining

activation to n remaining PTUs $(T-k)$, which is converted into percentile. For instance, if the BESS may be activated twice during a remaining horizon of 20 PTUs (i.e. between 18:45 and 00:00), the passive contribution should only take place if the upward imbalance price (which is paid by the TSO) is above the 90^{th} percentile of historical upward imbalance prices (3.8a). Alternatively, downward imbalance prices should be below the 10^{th} percentile, as these prices are paid by the aggregator (3.8b). To account for seasonal variation, a (rolling) window of 30 days around the operation date during the previous 5 years is used. This approach ensures that, if the day progresses without any activation taking place, the activation threshold will decline. The 50^{th} percentile is used as the lower and upper bound for the upward and downward regulation price respectively.

3.4.2 Intra-PTU Imbalance Price Forecasting

Hypothetically, the objective funciton of the heuristic control model is (3.9), where λ_t^U and λ_t^D are binary variables distinguishing downward and upward regulation from all other possible states, respectively. On account of the imbalance settlement system of the TSO, the optimal upward regulation price, π_t^U is positive from the perspective of the aggregator, and the optimal downward imbalance price π_t^D is negative. Corresponding to the sign convention of Δ_t in constraint (3.1d) in section 3.3.1, both upward and downward contribution, $E_t^{pc,up}$ and $E_t^{pc,down}$ are modeled as positive values, allowing for more straightforward formulation in combination with the imbalance price. It should be noted however, that this crucially contrasts with the sign convention of the underlying subsystems, where energy production is expressed as a negative value (3.1f).

$$\begin{aligned} \text{maximize} \quad & \sum_{t=0}^{T=96} E_t^{pc,up}\lambda_t^U\pi_t^U + E_t^{pc,down}\lambda_t^D\pi_t^D \qquad (3.9) \\ \text{where} \quad & \lambda_t^U + \lambda_t^D = \quad 1 \\ & \lambda_t^U, \lambda_t^D \quad \in \quad \{0,1\} \end{aligned}$$

Since both λ_t and π_t, are unknown ahead of time, (3.9) cannot be actually implemented. Instead, the heuristic control program employs two pairs of binary regression models to formulate predictions about both components of the market state. The first pair is used

to forecast if either regulation state 1 or -1 will occur, the second to forecast if either the upward or downward imbalance price threshold will be surpassed. For simplicity, this approach ignores the possibility of regulation state 2, which is treated as 0. The probability of a regulation state occurring is estimated conditional on a vector $\mathbf{X}$ of market forecast data. This data consists of a relevant subset of all market data published by TenneT during the first 6 minutes of each PTU, i.e. upward and downward adjustment capacity activated, upward and downward reserve capacity activated and the highest and lowest bid price for upward and downward regulation, respectively (see table 4.4. In addition, the differences of all variables and several time-related dummy variables will be included. The sequential selection of relevant variables from data accumulated during the first 6 minutes of each PTU is outlined section 4.3.

The prediction of a certain regulation state occurring is obtained from logistical regression models (3.10a) and (3.11a), which estimate the probability of one particular state occurring. Upward and downward regulation are thus expressed as predicted binary variables $\hat{\lambda}_t^D$ and $\hat{\lambda}_t^U$. The binary settlement price variables $\pi_t^{D \leq D_{Th},pr}$ and $\pi_t^{U \geq U_{Th},pr}$ take on 1 if the settlement price respectively falls below or above the upwards or downwards regulation price percentile determined by (3.8a) and (3.8b). Since these variables are determined by the conditional probability $Pr(\pi_t \leq / \geq \pi_t^{Th} | \lambda = 1)$, the forecast data on which models (3.12a) and (3.13a) are estimated a subset of the total historical sample where $\lambda_t^D = 1$ and $\lambda_t^U = 1$, respectively.

$$Pr(\lambda_t^D = 1|X_t) = \frac{1}{1 + e^{-(\beta_0 + \beta X_t)}} \tag{3.10a}$$

$$\hat{\lambda}_t^D = \begin{cases} 0, & \text{if} \quad Pr(\lambda_t^D = 0) \leq 0.5 \\ 1, & \text{if} \quad Pr(\lambda_t^D = 1) > 0.5 \end{cases} \tag{3.10b}$$

$$Pr(\lambda_t^U = 1|X_t) = \frac{1}{1 + e^{-(\beta_0 + \beta X_t)}} \tag{3.11a}$$

$$\hat{\lambda}_k^U = \begin{cases} 0, & \text{if} \quad Pr(\lambda_t^U = 0) \leq 0.5 \\ 1, & \text{if} \quad Pr(\lambda_t^U = 1) > 0.5 \end{cases} \tag{3.11b}$$

$$Pr(\pi_t^D \leq \pi_t^{D_{Th}} | X_t^D) = frac11 + e^{-}(\beta_0 + \beta X) \tag{3.12a}$$

$$\hat{\pi}_t^{D \leq D_{Th}} = \begin{cases} 0, & \text{if} \quad Pr(\pi_t^D < \pi_t^{D_{Th}}) \leq 0.5 \\ 1, & \text{if} \quad Pr(\pi_t^D < \pi_t^{D_{Th}}) > 0.5 \end{cases} \tag{3.12b}$$

$$Pr(\pi_t^U \geq \pi_t^{U_{Th}} | X_t^U) = \frac{1}{1 + e^{-}(\beta_0 + \beta X)} \tag{3.13a}$$

$$\hat{\pi}_t^{U \geq U_{Th}} = \begin{cases} 0, & \text{if} \quad Pr(\pi_t^U > \pi_t^{U_{Th}}) \leq 0.5 \\ 1, & \text{if} \quad Pr(\pi_t^U > \pi_t^{U_{Th}}) > 0.5 \end{cases} \tag{3.13b}$$

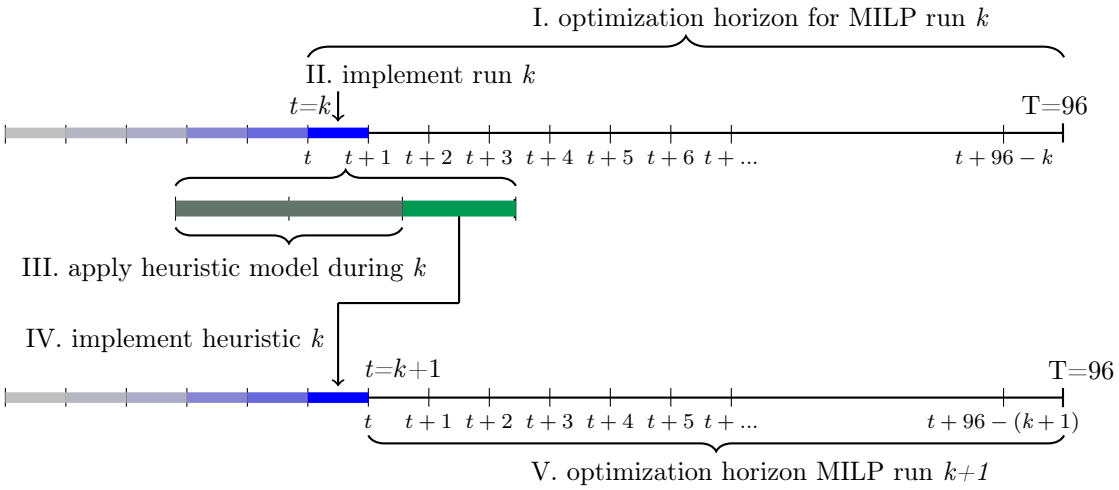

Figure 3.5: The timeline of the heuristic program as integrated in the MPC timeline. Data is obtained and the model is applied during the first 10 minutes (the dark gray area), after which the blue PTU is updated with the control action set for the final 5 minutes, which are indicated in green.

3.4.3 Passive Contribution Model

The products of the regulation state prediction and the settlement price prediction enter as parameters $\hat{\lambda}_t^U \hat{\pi}_t^{U \geq U_{Th}}$ and $\hat{\lambda}_t^D \hat{\pi}_t^{D \leq D_{Th}}$ in an MILP which largely mirrors the constraints of imbalance minimization problem. However, the objective equation (3.14a) is singular, and does not include battery degradation since high levels of degradation are already prevented by (3.7). Crucially, passive contribution (kWh) should be maximized when high regulation prices occur, but within the limits of the previously reduced imbalance. This is achieved

by constraints (3.14b) -(3.14f), where $\overline{P}_t$ is output of the imbalance minimization problem. While the (dis)charging schedule may not be changed *during* the current PTU k, the schedule may change for upcoming PTUs, but only if no imbalance (Δ_t^{pre}) is forecast. Figure 3.5 visualizes how the passive contribution model is embedded in the optimization horizon of the MPC-program.

$$\text{maximize} \quad E_t^{pc} = (P_t^{pc,D}\lambda_t^{D,pr}\pi_t^{D\leq D_{Th},pr} + P_t^{pc,U}\lambda_t^{U,pr}\pi_t^{U\geq U_{Th},pr})\frac{\delta\tau}{3} \,\forall\, t = k \quad (3.14a)$$

$$\text{subject to} \quad P_t^{pc,D} = P_t^{pc,U} = 0 \qquad \forall \quad t \in \{k+1,.,T\} \quad (3.14b)$$

$$P_t^{ch} = \overline{P_t^{ch}} \qquad \forall \quad t = k \quad (3.14c)$$

$$P_t^{dis} = \overline{P_t^{dis}} \qquad \forall \quad t = k \quad (3.14d)$$

$$P_t^{ch} = \overline{P_t^{ch}} \quad \forall \quad t \in \{k+1,.,T\} \quad \wedge \quad \Delta_t^{pre} \neq 0 \quad (3.14e)$$

$$P_t^{dis} = \overline{P_t^{dis}} \quad \forall \quad t \in \{k+1,.,T\} \quad \wedge \quad \Delta_t^{pre} \neq 0 \quad (3.14f)$$

$$0 \leq P_t^{pc,D} \leq \gamma_t \cdot (P_t^{grid,max} - P_t^{ch}) \,\forall \quad t = k \quad (3.14g)$$

$$0 \leq P_t^{pc,U} \leq (1-\gamma_t) \cdot (P_t^{grid,max} - P_t^{dis}) \forall \quad t = k \quad (3.14h)$$

$$0 \leq P_t^{pc,D} \leq \gamma_t \cdot (P_t^{ch,max} - P_t^{ch}) \quad \forall \quad t = k \quad (3.14i)$$

$$0 \leq P_t^{pc,U} \leq (1-\gamma_t) \cdot (P_t^{dis,max} - P_t^{dis}) \,\forall \quad t = k \quad (3.14j)$$

$$0 \leq P_t^{ch} \leq \beta_t \cdot P_t^{grid,max} \qquad \forall \quad t \in \{k,.,T\} \quad (3.14k)$$

$$0 \leq P_t^{dis} \leq (1-\beta_t) \cdot P_t^{grid,max} \qquad \forall \quad t \in \{k,.,T\} \quad (3.14l)$$

$$0 \leq P_t^{ch} \leq \beta_t \cdot P_t^{ch,max} \qquad \forall \quad t \in \{k,.,T\} \quad (3.14m)$$

$$0 \leq P_t^{dis} \leq (1-\beta_t) \cdot P_t^{dis,max} \qquad \forall \quad t \in \{k,.,T\} \quad (3.14n)$$

$$SoC_t = SoC_{t-1} - \frac{1}{\eta_{dis} \cdot Q_{BESS}} \cdot (P_t^{dis} + P_t^{pc,U} \cdot \frac{\delta\tau}{3})$$

$$+\frac{\eta_{ch}}{Q_{BESS}} \cdot (P_t^{ch} + P_t^{pc,D} \cdot \frac{\delta\tau}{3}) \; \forall \quad t \in \{k, ., T-1\} \tag{3.14o}$$

$$SoC^{min} \leq SoC_t \leq SoC^{max} \qquad \forall \quad t \in \{k, ., T\} \tag{3.14p}$$

$$SoC_0 = 50\% \tag{3.14q}$$

$$50\% \cdot \frac{k}{96} \leq SoC_{96} \leq 50\% \cdot (2 - \frac{k}{96}) \tag{3.14r}$$

3.5 Optimal System Size

An estimation of the economically optimal BESS size must consider the cost reduction realized by minimizing imbalance reduction and the revenue generated by engaging in passive contribution, as well as the capital and operating costs of the battery. Hence, the analysis compares the total costs accrued under the business as usual scenario with the costs accrued under demand side management. The BAU costs can be simply determined by equation (3.15), where π_t is the settled imbalance price. π_t is taken as a negative, since a positive portfolio imbalance (i.e. a portfolio surplus) in combination with a positive settlement price results in payment from the TSO to the aggregator (TenneT, 2020). The imbalance costs accrued by the MPC-program, depend on the interaction of (remaining) portfolio surplus Δ_t^+ and shortage Δ_t^- after imbalance minimization, with the regulation state and imbalance market price. When upwards regulation, downwards regulation and mid imbalances price (π_t^U, π_t^D and π_t^M, respectively) are positive, portfolio shortage results in costs. Specifically, (3.16) demonstrates these possible interactions, where (A) comprises costs associated with a portfolio shortage and (B) comprises costs associated with a portfolio surplus.

Algorithm 1: Model Predictive and Heuristic Control Program

Input: $\mathrm{E}^{\mathrm{NF,\ hist}}, \mathrm{E}^{\mathrm{PV,\ hist}}, \mathrm{GHI}^{\mathrm{hist}}, \mathrm{Temp}^{\mathrm{hist}}$
$\mathrm{E}^{\mathrm{DA}}, \mathbf{Z}^{BESS}$
$\pi^{\mathrm{hist}}, \lambda^{\mathrm{hist}}, \mathbf{X}^{\mathrm{TSO,\ hist}}, \pi^{\mathrm{FCST}}, \lambda^{\mathrm{FCST}}, \mathbf{X}^{\mathrm{TSO,\ FCST}}$

for *PTU=1 to T=96* **do**

Input: $\mathrm{GHI}^{\mathrm{fcst}}, \mathrm{Temp}^{\mathrm{fcst}}, \mathrm{GHI}^{\mathrm{act}}_{[1\ldots PTU-1]}$

function (1) `Demand Model(`$E^{NF,\ hist}$`):`
  return $\mathrm{E}^{\mathrm{NF\ fcst}}$

function (2) `Kalman Filter(`$GHI^{hist}_{[\ldots,0]}$, GHI^{fcst}, $GHI^{act}_{[1\ldots PTU-1]}$`):`
  return $\mathrm{GHI}^{\mathrm{KF}}$

function (3) `PV Regression Model(`GHI^{KF} , $Temp^{fcst}$, $E^{PV,\ hist}$, GHI^{hist}, $Temp^{hist}$`):`
  return $\mathrm{E}^{\mathrm{PV,\ fcst}}$

$\mathrm{E}^{\mathrm{ACT,\ fcst}} \leftarrow \mathrm{E}^{\mathrm{NF,\ fcst}} - \mathrm{E}^{\mathrm{PV,\ fcst}}$

$\Delta^{\mathrm{pre,\ fcst}} \leftarrow \mathrm{E}^{\mathrm{DA}} - \mathrm{E}^{\mathrm{ACT,\ fcst}}$

MILP I `Imbalance Minimization(`$\Delta^{pre,\ fcst}$, $\boldsymbol{Z}^{BESS}$, SOC^{*}_{PTU-1}`):`
  return $\mathrm{E}^{\mathrm{BESS}}$, $\mathrm{P}^{\mathrm{BESS}}$, D, SOC_{PTU}, $\Delta^{\mathrm{post,\ fcst}}$

Output: $\mathrm{E}^{\mathrm{BESS}}$ schedule for [PTU,...,T]

function (4) `Full Equivalent Cycle(` P^{BESS}, $\boldsymbol{Z}^{BESS}$`):`
  return FEC

function (5) `Remaining Activations(` *FEC, n cycles,* $\boldsymbol{Z}^{BESS}$`):`
  return n remaining activations

Input: $\mathbf{X}^{TSO,fcst}$

if *n remaining activations* > 0 **then**

function(6) `Set Price Threshold(`$\boldsymbol{X}^{TSO,hist}$, *n activations*`):`
  return $\pi_t^{U_{Th}}$, $\pi_t^{D_{Th}}$

Heuristic `Logistic Regression 1(`$\boldsymbol{X}^{TSO,hist}$, $\boldsymbol{X}^{TSO,fcst}$, λ^{hist}`):`
  return $\hat{\lambda}^{U}$, $\hat{\lambda}^{D}$

Heuristic `Logistic Regression 2(` $\boldsymbol{X}^{TSO,hist}$, $\boldsymbol{X}^{TSO,fcst}$, π^{hist}, $\pi_t^{U_{Th}}$, $\pi_t^{D_{Th}}$`):`
  return $\hat{\pi}_t^{U \geq U_{Th}}$ $\hat{\pi}_t^{D \leq D_{Th}}$

MILP II `Passive Contribution(` $\hat{\lambda}^{U}$, $\hat{\lambda}^{D}$, $\hat{\pi}_t^{U \geq U_{Th}}$, $\hat{\pi}_t^{D \leq D_{Th}}$, $\Delta^{pre,\ fcst}$, $\boldsymbol{Z}^{BESS}$, SOC_{PTU}, $\Delta^{post,\ fcst}$, P^{BESS}, D`):`
  return E^{PC}, P^{PC}, SOC^{*}_{PTU}

Output: adjusted $\mathrm{E}^{\mathrm{BESS}}$ activation for [PTU]

end

$\mathrm{PTU} \leftarrow PTU + 1$

end

$$Cost_{BAU} = \sum_{t=0}^{T=96} (E_t^{DA} - E_t^{ACT}) \cdot -\pi_t \tag{3.15}$$

$$Cost_{\Delta,MPC} = \sum_{t=0}^{T=96} \underbrace{\Delta_t^- \cdot (\lambda_t^U \pi_t^U + \lambda_t^D \pi_t^D + (1 - \lambda_t^D - \lambda_t^U) \cdot \pi_t^M)}_{\text{A: } (E_k^{DA} < E_k^{ACT})}$$

$$- \underbrace{\Delta_t^+ \cdot (\lambda_t^U \pi_t^U + \lambda_t^D \pi_t^D + (1 - \lambda_t^D - \lambda_t^U) \cdot \pi_t^M)}_{\text{B: } (E_k^{DA} > E_k^{ACT})} \tag{3.16}$$

where $\lambda_t^U + \lambda_t^D = 1$

$\lambda_t^U,\ \lambda_t^D \in \{0, 1\}$

The costs of the BESS model costs comprise capital expenditure (CAPEX) and operational costs (OPEX). Since this thesis does not perform a long-term investment analysis, and only applies the model to single-day horizons, it uses a simplified cost calculation approach. CAPEX are uniformly divided by the total lifetime of the BESS, without accounting for interest or discount rate (Blok & Nieuwlaar, 2020). OPEX are estimated based on the assumption that total operating costs during the cycle life of the battery are 33% of the total CAPEX (Renewable, IRENA, et al., 2017). In this optimization problem, a total number of 5000 cycles is used, which 50% of the amount used in the MPC program. This more conservative estimate is adopted to account for the definitional unclearity of DOD, which has a major impact on the cycle life (Maheshwari, 2018), combined with the fact that the battery's is used more intensively when the perfect foresight assumption applies.

Except for the calendar life and FEC_t, all variables in (3.17) enter into the MILP as parameters. To identify the optimal number of modules, the MILP is run for a range of BESS sizes. The calendar life of the BESS depends on the degradation rate of the battery and the end of life capacity (80%) (3.18) [3] Since the degradation rate $Q_{loss,t}$ is calculated for each PTU with equation (3.5b), CAPEX is directly influenced by (dis) charging behavior. In contrast, equation (3.6) of the heuristic model must be restated as (3.19) to determine the full equivalent cycles during a single PTU.

The revenue accrued by upward and downward passive contribution is determined by

[3] Note that 3.18 is obtained from the discrete exponential decay formula.

(3.20). Note that the revenue from downward regulation arises from negative imbalance prices π_t^D. Finally, the total net costs of the DSM system during the entire optimization horizon are calculated by (3.21), in which the *avoided* imbalance costs are included as a negative cost of the battery.

$$\begin{aligned} Cost_{BESS} &= \sum_{t=0}^{T=96} \frac{N_{\text{modules}} \cdot Cost_{\text{module}}(\frac{EUR}{kWh}) \cdot E_{BESS,rated}(kWh)}{\text{calendar life}_t(PTU)} \\ &\quad + \frac{0.33\% \cdot N_{modules} \cdot Cost_{\text{module}}(\frac{EUR}{kWh}) \cdot FEC_t}{\text{cycle life}(PTU)} \end{aligned} \tag{3.17}$$

$$\text{calendar life}_t = \frac{log(0.8)}{1 - 0.01 * Q_{loss,t}(\%)} \tag{3.18}$$

$$FEC_t = \frac{1}{2} \frac{P_t^{BESS,ch} + P_t^{BESS,dis} + \frac{1}{3} \cdot P_t^{pc,D} + \frac{1}{3} \cdot P_t^{pc,U}}{Q_{BESS}} \cdot \delta\tau \tag{3.19}$$

$$Revenue_{PC} = \sum_{t=0}^{T=96} P_t^{pc,U} \cdot \lambda_t^U \pi_t^U \cdot \frac{\delta\tau}{3} - P_t^{pc,D} \cdot \lambda_t^D \pi_t^D \cdot \frac{\delta\tau}{3} \tag{3.20}$$

$$Cost_{net} = Cost_{BESS} - (Cost_{\Delta,BAU} - Cost_{\Delta,MPC}) - Revenue_{PC} \tag{3.21}$$

In order to emulate the DSM-program as much as possible, the resulting costs for a range of different battery sizes are obtained using a *Lexicographic* optimization approach, which optimizes multiple objectives subject to a predefined preference order (Castro-Gutiérrez et al., 2009). The optimal solutions of each objective function are compared with respect to this order.

In the present case, the sequential minimization of internal imbalances and passive contribution can be reflected by optimization program (3.22a)-(3.22g), which has a fixed optimization horizon ($t = [1, 96]$). Also note that constraint (3.22g) now contains the actually realized, as opposed the expected supply/demand schedule of the portfolio E_t^{ACT}. The objective function of the imbalance minimization program, f_1, is prioritized over the objective of the costs minimization/passive contribution program, f_2 by (3.22b). Hence, the optimal solution of the latter must ensure the minimal imbalances f_1^*, achieved by choice variables $\mathbf{X}^*$. Vector g_1 in (3.22d) contains all constraints of the energy system, i.e.

(3.1d) - (3.5c).

$$\text{minimize} \quad f_2(\mathbf{X}) = -(Revenue_{PC} - Cost_{BESS}) \tag{3.22a}$$

$$\text{subject to} \quad f_1(\mathbf{X}) \leq f_1(\mathbf{X^*}) \tag{3.22b}$$

$$g_1(\mathbf{X}) \leq 0 \tag{3.22c}$$

$$\text{where:} \quad f_1(\mathbf{X}) = \zeta \cdot \Delta\% \cdot 100 + (1 - \zeta) \cdot D \tag{3.22d}$$

$$\Delta\% = \frac{\sum_{t=1}^{T=96} \Delta_t^{post}}{\sum_{t=1}^{T=96} |E_t^{DA} - E_t^{ACT}|}) \qquad \forall t \in \{1, ..., T\} \tag{3.22e}$$

$$\Delta_t^{post} = \Delta_t^+ + \Delta_t^- \qquad \forall t \in \{1, ..., T\} \tag{3.22f}$$

$$\Delta_t^+ - \Delta_t^- = E_t^{DA} - E_t^{ACT} \qquad \forall t \in \{1, ..., T\} \tag{3.22g}$$

Chapter 4

Data Preparation and Exploratory Analysis

4.1 Production-Consumption Portfolio

The production-consumption portfolio considered here consists of 21 clients, which have been classified based on their production/consumption ratio[1]. A typical profile of each client type can be seen in figure 4.1. The rudimentary data of the entire portfolio is shown in table 4.1. Since the perfect forecasting assumption is applied to demand data, no specific analysis are performed on the energy demand data. The solar energy supply data, imbalance market data and the selection of representative sample periods, are addressed hereafter.

4.2 Solar Energy Supply Simulation

The forecasted solar PV generation schedule is estimated based on frequently updated weather forecasts, comprising *Global Horizontal Irradiance* (GHI) and temperature (T). GHI (W/m^2) is the amount of shortwave solar radiation received by one square meter horizontal to the earth's surface. While predicted day-ahead and actual solar PV generation schedules are available for all locations, weather forecast updates are only available for a single location. To achieve consistency between the schedules, the raw day-ahead and actual data is replaced by simulated forecasts and actual generation schedules. These simulations are based on a baseline regression model commonly applied in solar PV forecasting. While this model is less accurate than state of the art estimation techniques, the difference appears to be minimal (Gigoni et al., 2017). Moreover, the analysis of thesis focuses on the reduction of imbalances between day-ahead predictions and actual energy

[1] If the maximum net uptake from the grid is less than one third of total production, the client is labeled as a producer

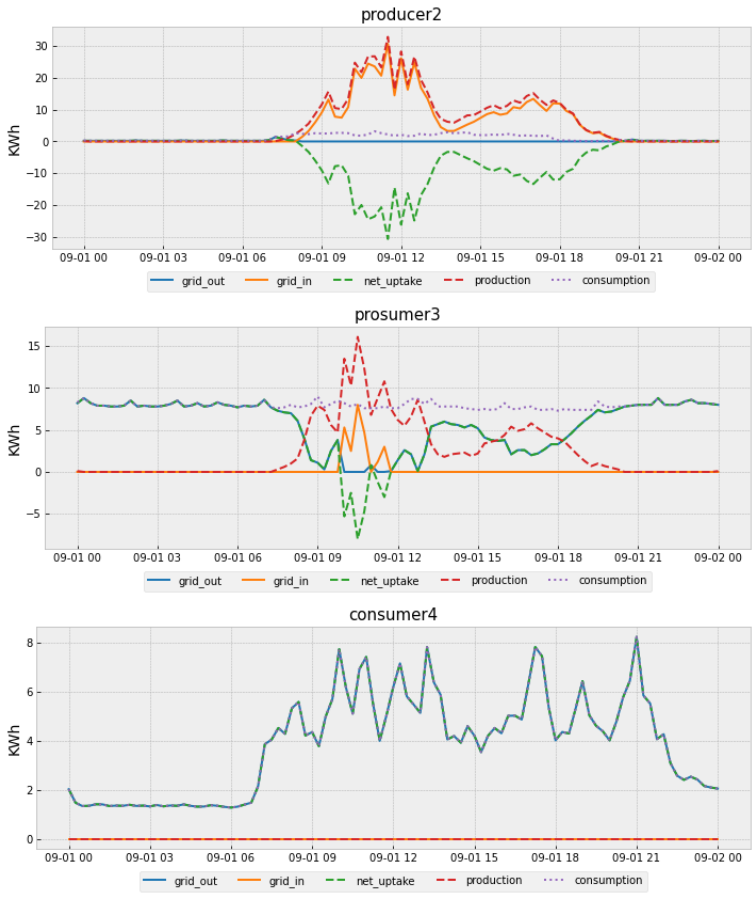

Figure 4.1: Typical supply-demand profiles of each customer type

supply, based on *relative* improvements in forecasts over time, as opposed to the *absolute* accuracy of the generation schedules. Finally, the model is not used for out-of-sample predictions, but instead simulates generation schedules for the same installations based on actual measurements over the same time period. Nonetheless, it should be noted that especially the volatility of solar energy generation cannot be captured by these regression based simulations (see figure 4.2).

The multivariate linear regression model proposed by (Gigoni et al., 2017) relates solar power generated at hour t to GHI, which enters equation (4.1) as its level and its quadratic term, and in interaction with temperature. The model parameters $\beta_1 > 0$, $\beta_2 < 0$, and $\beta_3 < 0$, indicate, that (1) power generation increases with higher GHI, but decreasingly so as (1) solar radiation intensifies and (2) temperature increases. To take into account unknown environmental factors that may vary over time, the regression model is applied to a rolling window of d days in both directions. To prevent the straight application of proposed regression model from producing sub-optimal simulations, and to select the

Table 4.1: Daily average contribution to portfolio supply/demand from each client

	net_uptake (kWh/day)	production (kWh/day)	consumption (kWh/day)	PV_{max} (kWh/day)	kW-peak (kW)
producer1	-495.23	497.35	2.12	1185.52	200.00
producer2*	-202.88	243.34	40.47	1483.10	230.00
producer3*	-143.79	246.79	103.01	1539.80	230.00
producer4	-6188.29	6262.28	73.98	15582.96	2000.00
prosumer1	-346.52	572.19	225.67	1497.15	266.00
prosumer2	774.29	434.17	1208.47	973.10	134.00
prosumer3	171.40	291.22	462.62	693.90	100.00
prosumer4	564.07	1024.24	1588.31	2409.41	360.00
prosumer5	202.68	469.12	671.81	1170.25	150.00
prosumer6*	618.60	426.79	1045.40	1087.62	170.00
prosumer7*	756.17	240.20	996.38	1213.46	180.00
prosumer8	-107.09	249.09	142.00	657.40	93.00
consumer1	496.69	0.00	496.69		
consumer2	549.30	0.00	549.30		
consumer3	624.69	0.00	624.69		
consumer4	392.72	0.00	392.72		
consumer5	7393.89	0.00	7393.89		
consumer6	202.05	0.00	202.05		
consumer7	5438.67	0.00	5438.67		
consumer8	3872.85	0.00	3872.85		
consumer9	2381.86	0.00	2381.86		
mean	807.44	521.75	1329.19	2457.81	342.75

optimal rolling window, all different configurations of the level, square and interaction of the explanatory variables were tested. Results of this analysis for all solar PV producers and prosumers, which were performed using the *Statsmodels* libary in Python, are presented in appendix tables A.1 and A.2. In most cases the model proposed in the literature performs best, while the optimal window size varies.

$$E^{PV} = \beta_1 \cdot GHI + \beta_2 \cdot GHI^2 + \beta_3 \cdot GHI_t \cdot T_t + \upsilon_t \tag{4.1}$$

$$\begin{aligned} E_{t,d}^{PV,*} &= \sum_{i=1}^{I} \hat{\beta}_1^{i,[d-4,d+4]} \cdot GHI,*_t + \hat{\beta}_2^{i,[d-4,d+4]} \cdot GHI,*_t^2 \\ &\quad + \hat{\beta}_3^{i,[d-4,d+4]} \cdot GHI,*_t \cdot T,*_t \forall \quad i \in \quad \{i...I\} \end{aligned} \tag{4.2}$$

The total solar PV production during each time step is estimated with the general function formula (4.2), where the $\hat{.}$ signifies fitted parameters, i refers to the individual

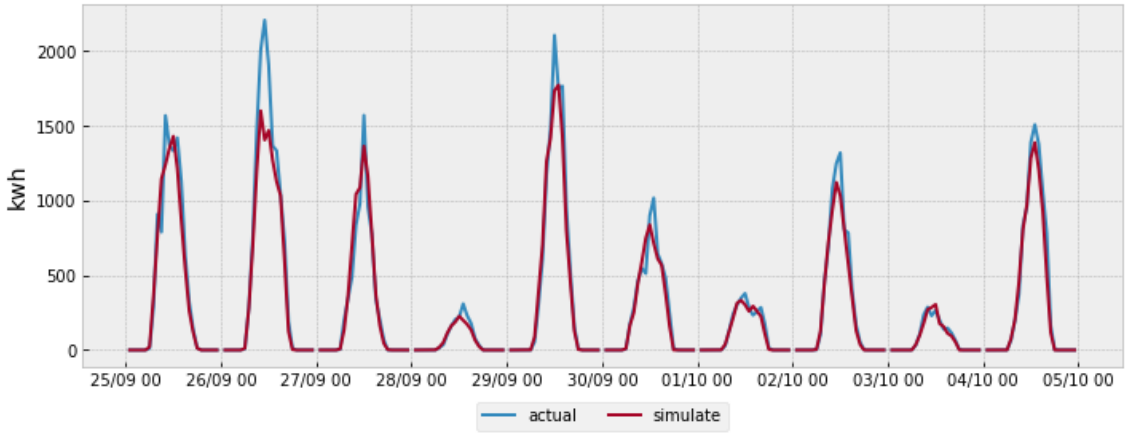

Figure 4.2: Sample of a simulated vs original solar PV energy generation profile

solar system to which the parameters are fitted, t refers to the hour to which the forecast is applied, and d to the day in the training data. * May either refer to actual measurements (ACT), day-ahead forecasts (DA) or the most recent updates available at PTU=k.

4.3 Solar Irradiance Forecasting

Actual GHI and Temperature data with an hourly resolution are obtained from the Dutch public broadcaster KNMI (2019-2020). Hourly day-ahead and updated GHI and Temperature forecasts were obtained from two sources. Primarily[2], data from the commercial forecaster *Buienradar* (BR), which is available for the period September 2020 - Januari 2021 is used. To provide more context to these results, forecasts by the KNMI are used for the period 2019 - 2020. Since these dates do not overlap, exact comparisons are not possible, however, the wider range of especially the KNMI-data allows for a better representation of the model outcome under different circumstances.

New forecast updates by *Buienradar* are obtained every 15 minutes, while updates by the *KNMI* forecasts are updated at a 6 hours frequency. However, actual changes in the GHI forecasts are less frequent. The histograms in figure 4.3 visualize th probability distribution of updates per forecasted hour in the dataset (the hours before sunrise and after sundown are excluded).

Crucially, weather forecasts should increasingly approach the actual values if the model predictive control program is to reduce imbalances. Counter-intuitively, this is not necessarily the case (see table 4.2). Section 4.3.1 introduces a recursive post-estimation technique

[2]The models presented in sections 4.2, 4.3.1, and 4.4 are trained on the data until September 2020, which means the time period of the KNMI forecasts is part of the training data

Table 4.2: forecast error BR

date	RMSE DA	RMSE 1h	RMSE 4h	RMSE 8h	cluster
2020-12-09	45.9786	45.4342	45.259	45.1693	0
2020-10-03	47.9875	56.3015	57.4785	49.5992	0
2020-12-04	33.0914	33.9172	34.1461	31.1304	0
2020-12-23	12.418	11.8831	11.2235	11.3867	0
2020-11-27	42.9402	45.2881	46.8129	43.5699	0
2020-09-18	35.9889	31.9574	31.7835	36.63	1
2020-09-30	67.405	69.2736	67.8651	70.2153	1
2020-09-21	30.6668	29.2456	28.8001	32.2222	1
2020-09-12	120.782	114.578	116.202	117.425	1
2020-09-07	32.9689	28.5984	28.2025	31.6646	1
2020-12-06	34.785	42.3636	44.467	42.9323	2
2020-10-20	28.6072	25.9979	25.4502	26.965	2
2020-10-06	44.6053	37.2971	37.4747	36.8752	2
2020-11-10	38.9379	38.7094	38.2676	37.8046	2
2020-11-22	12.7031	12.476	14.1419	13.1208	2
mean	41.991	41.5548	41.8383	41.7807	

to tune these forecasts based on actual data. This method is applied to hourly data, which is subsequently upsampled and linearly interpolated to match the resolution of the MPC program. Hence, h as opposed to t is adopted as the time-subscript in this subsection.

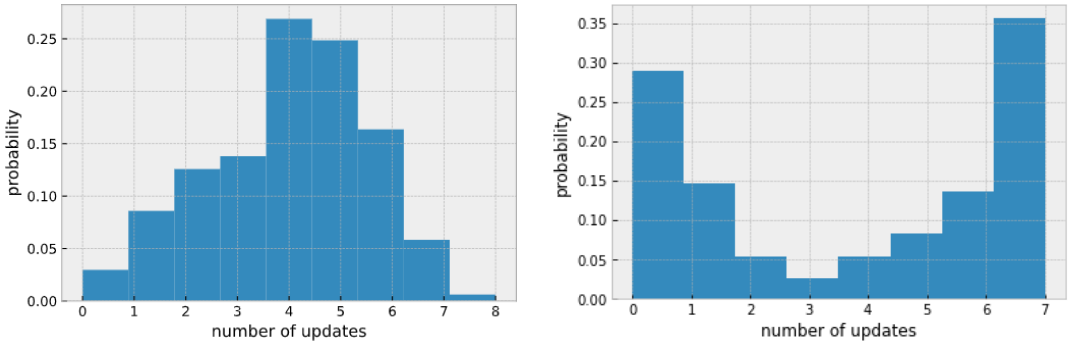

Figure 4.3: Distribution of number of forecast revisions for each hour. Left: Buienradar; Right: KNMI

4.3.1 Recursive Forecast Improvements

The recursive post-estimation method proposed in this thesis employs a *Kalman Filter* (KF). This algorithm estimates the *states* of a stochastic dynamic system at h by combining model-generated *predictions* $\hat{x}_{h|h-1}$ with actual *measurements* Z_{h-1}. The process disturbance and measurement noise are used to determine the contribution of each estimation component to a new revised (i.e. filtered) estimation. This approach effectively

enables the estimation of unknown disturbances in measurement data by using existing knowledge of the system. As this noise is recorded during the previous states of the system, the KF is a recursive algorithm, which comprises a form of feedback control. The KF has been successfully used in many engineering applications, traditionally to more accurately estimate the trajectory of aircraft and satellites Simon (2001). Moreover, the KF has been used in a variety of energy systems applications, such as Hokoi et al. (1990), Kim and Park (2017), Louka et al. (2008), and Pelland et al. (2013).

In the absence of a theoretical model, this thesis uses an (rolling) Auto-regressive Moving Average (ARMA) model as the state equation of in the Kalman filter, similar to Hokoi et al. (1990). In the proposed set-up, the externally obtained GHI-forecasts [3] are treated as as measurement data Z_h. The subsequent paragraph introduces the ARMA model, section 4.3.1 outlines the implementation of the Kalman Filter.

Auto-regressive Moving Average Model

The *ACF and PACF plots* 4.4 of GHI for 2020-2021 provides insights in the most appropriate prediction model. The Autocorrelation Function (ACF) plot indicates that GHI_h is positively correlated with 5 of its lags, and also shows a clear seasonal pattern[4]. Moreover, the Partial Autocorrelation Function (PACF) plot indicates that the part of GHI_h that is not predicted by its lags (i.e. the prediction error), is also correlated with *its* lags. This means an Autoregressive Moving Average Model is most appropriate. To find the optimal combination of between auto-regressive and moving average orders (respectively p and q), a grid search is performed using the *Statsmodels* libary in Python. The results of this analysis are presented in the left section of appendix table B.1. While the Dickey-Fuller test provides a strong evidence against the presence of a unit root (i.e. the data is stationary), the diurnal trend of GHI within shorter time horizons may render an ARIMA model more suitable. Hence, the grid search also includes order of integration d.

The right section of appendix table B.1 sorts all ARMA(p,q) combinations by the Aikaike Information Criterion. This common metric estimates the trade-off between goodness of fit and overfitting the model Stock and Watson (2015). The ARMA(4,0,2) model, which exhibits both low prediction errors and has a relatively low AIC-score has functional

[3] For simplicity, and in order to reduce computational complexity, the temperature forecasts is not included in the Kalman filter, based on its smaller role in the regression models (4.2)

[4] While SARIMA models may yield more accurate forecasting results, a more elaborate model would complicate the formulation of the Kalman filter, and the delay the computation time of the model. Hence, SARIMA models are not considered here.

form 4.4. Parameters ϕ_p and γ_q are estimated on the optimal a backward looking window of 16 days.

$$x_h - \phi_1 \cdot x_{h-1} - \phi_2 \cdot x_{h-2} - \phi_3 \cdot x_{h-3} - \phi_4 \cdot x_{h-4} = w_h + \gamma_1 \cdot w_{h-1} + \gamma_2 \cdot w_{h-2}$$
$$\text{where} \quad w \quad \sim \quad N(0, \sigma^2) \tag{4.4}$$

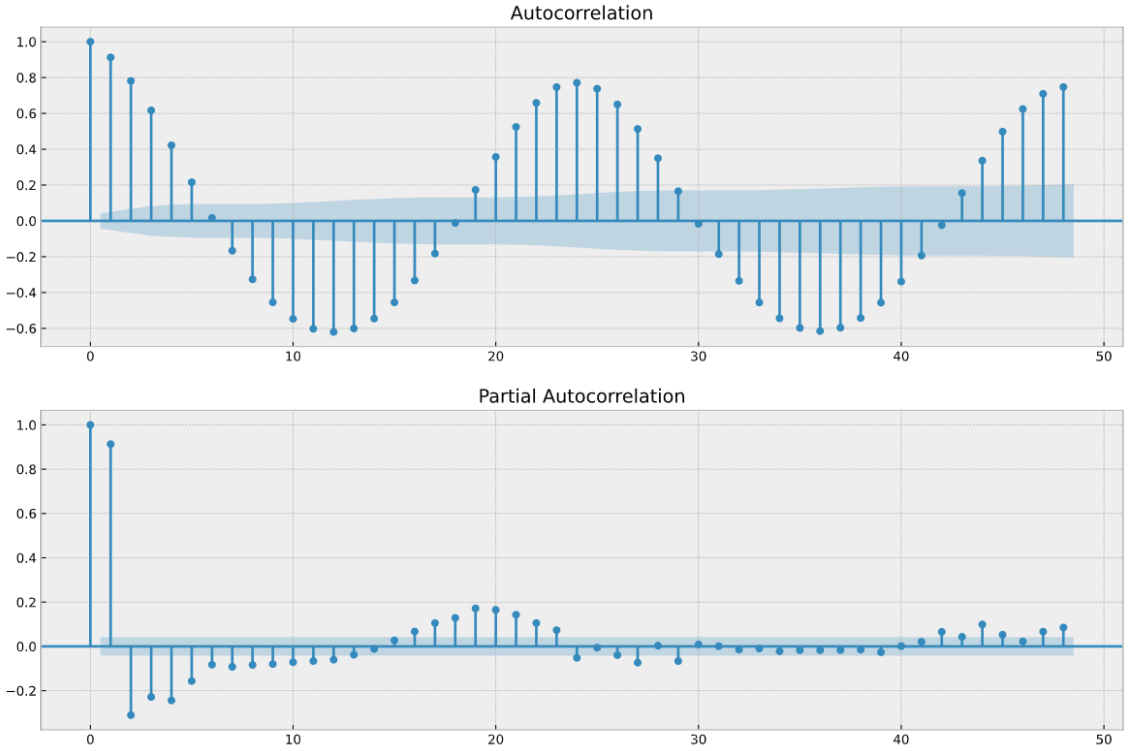

Figure 4.4: ACF and PACF plots of GHI data

Kalman Filter

The Kalman filter is typically modeled as a sequence of two sets of matrix equations, which record the propagation of estimated states and error co-variance. The first set are referred to as *time update* equations, and project forward the system state and modeling error. The second set are referred to as *measurement update* equations which revise these *a priori* estimates by incorporating new measurements and measurement noise (Bishop, Welch, et al., 2001). The calculation procedure thus consists of the prediction and correction steps outlined below. Note that in the proposed application of the KF, a clear distinction is made between *predictions*, which are obtained from the model, and *forecasts* which are treated as measurement data.

1. Prediction The prediction step simply applies the ARMA-model, which is restated in matrix form by equation(4.5), where the state vector $\mathbf{X}_h^-$ is the *a priori* prediction obtained from the ARMA(4,2) model, fitted to a window of 15 days prior to h using the Statsmodels-library in python. System state matrices, and the [1x1] variance matrix of residual w_h are subsequently used in the *a priori* error covariance calculation (4.6) $\mathbf{P}_h^-$, which itself relies on the previous KF iteration. As starting value, $\mathbf{P}_0^-$ is used, which is the variance-covariance matrix of the auto-regressive parameters ϕ.

$$\hat{\mathbf{X}}_h^- = \mathbf{F}_{h-1} \cdot \mathbf{X}_{h-1} + \mathbf{G}_{h-1} \cdot w_h \tag{4.5}$$

$$\text{where} \quad \mathbf{F}_h = \begin{bmatrix} \phi_1 & 1 & 0 & 0 \\ \phi_2 & 0 & 1 & 0 \\ \phi_3 & 0 & 0 & 1 \\ \phi_4 & 0 & 0 & 0 \end{bmatrix}, \mathbf{X}_h = \begin{bmatrix} x_h \\ x_{h-1} \\ x_{h-2} \\ x_{h-3} \end{bmatrix}, \quad \mathbf{G}_h = \begin{bmatrix} 1 \\ \gamma_{h-1} \\ \gamma_{h-2} \\ 0 \end{bmatrix}$$

$$\mathbf{P}_h^- = \mathbf{F}_{h-1} \cdot \mathbf{P}_{h-1}^+ \cdot \mathbf{F}_{h-1}^T + \mathbf{G}_{h-1} \cdot \sigma_{h-1}^2 \cdot \mathbf{G}_{h-1}^T \tag{4.6}$$

$$\text{where} \quad \mathbf{P}_0^- = \begin{bmatrix} \sigma_{\phi_1}^2 & \sigma_{\phi_{1,2}} & \sigma_{\phi_{1,3}} & \sigma_{\phi_{1,4}} \\ \sigma_{\phi_{2,1}} & \sigma_{\phi_2}^2 & \sigma_{\phi_{2,3}} & \sigma_{\phi_{2,4}} \\ \sigma_{\phi_{3,1}} & \sigma_{\phi_{3,2}} & \sigma_{\phi_3}^2 & \sigma_{\phi_{3,4}} \\ \sigma_{\phi_{4,1}} & \sigma_{\phi_{4,2}} & \sigma_{\phi_{4,3}} & \sigma_{\phi_4}^2 \end{bmatrix}$$

2a. Kalman Gain Calculation The Kalman gain, which expresses the weight that should be placed on the contribution of the externally obtained forecasts, as opposed to the model prediction, is estimated based on the variance of the forecasting error $v$up to *h-1*, which is obtained from the "measurement" equation 4.8. Due to matrix $\mathbf{H}$, $v$this is simply the latest forecasting error. Consequently, the KF is able quickly adjust the *revised* predictions if forecast accuracy improves or deteriorates.

$$\begin{aligned} &\mathbf{Z}_h = \mathbf{H} \cdot \mathbf{X}_h + v_h \\ &\text{where} \quad v \sim N(0, \mathbf{R}_{h-1}^-), \qquad \mathbf{H} = \begin{bmatrix} 1 & 0 & 0 & 0 \end{bmatrix} \end{aligned} \tag{4.8}$$

$$\mathbf{K}_h = \mathbf{P}_h^- \cdot \mathbf{H}^T \cdot (\mathbf{H} \cdot \mathbf{P}_h^- \cdot \mathbf{H}^T + \mathbf{R}_{h-1})^{-1} \tag{4.9}$$

2b. Correction In common applications, the KF-algorithm minimizes the noise in *real-time* estimations, e.g. of the position of a satellite (e.g. Wickert and Siddappa (2018). In contrast, the proposed application of the KF reduces the error in solar irradiance *forecast*. Hence, $\hat{\mathbf{X}}^+$ and $\hat{\mathbf{X}}^-$ now refer to the prediction model's projection over the entire forecasting horizon, which is (i.e. $24 - h$). Therefore the Kalman gain obtained from the most recent prediction and forecast is applied to the entire forecasting vector.

$$\hat{\mathbf{X}}^+_{h,..,24-h} = \hat{\mathbf{X}}^-_h + \mathbf{K}_h \cdot (\mathbf{Z}_{h,...,24-h} - \mathbf{H} \cdot \hat{\mathbf{X}}^-_h) \tag{4.10}$$

$$\mathbf{P}_h^+ = \mathbf{P}_h^- - \mathbf{K}_h \cdot \mathbf{H} \cdot \mathbf{P}_h^- \tag{4.11}$$

In figure 4.5, the sequentially generated 1-hour ahead KF-forecasts are presented for 6 representative[5] MPC-runs, together with the actual GHI record and the original GHI forecast. A similar figure (B.1) for the KNMI forecasts is included in appendix B. The corresponding table **??** demonstrates that the application of the KF indeed reduces the forecast error, and is most succesful in doing so when applied to the KNMI forecasts.

Table 4.3: Error metrics of Kalman filtered vs original forecasts

2020	RMSE_kf	RMSE_org	cluster
12-09	37.84	47.60	0
10-03	39.94	43.65	0
12-04	31.16	36.53	0
12-23	12.49	12.58	0
09-18	41.64	43.92	1
09-30	83.93	88.58	1
09-21	33.68	36.12	1
09-12	140.64	140.70	1
12-06	31.07	36.89	2
10-20	32.71	35.49	2
10-06	67.68	65.72	2
11-10	40.8	47.09	2
mean	46.4649	49.4930	

2019	RMSE_kf	RMSE_org	cluster
01-07	10.58	12.29	0
09-03	55.17	48.25	0
03-06	25.482435	43.600219	1
01-04	10.446324	31.709782	1
09-06	59.43	61.58	2
07-04	20.15	20.66	2
07-03	89.88	112.99	3
07-06	78.52	100.49	3
w. mean	47.35	56.96	

[5]The selection of representative days are discussed in section 4.5.1.

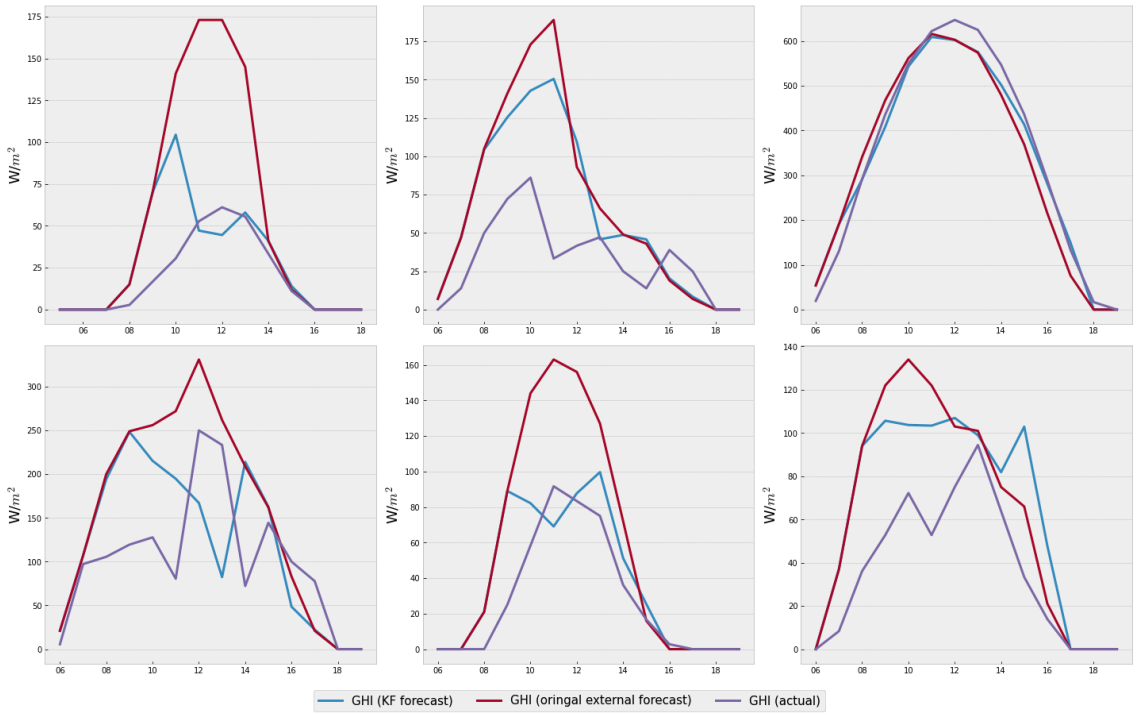

Figure 4.5: 1-hour ahead forecast before and after applying the Kalman filter

4.4 Imbalance Market Forecasting

4.4.1 Data Preparation

The LR models introduced in section 3.4.2 are applied to the first 6 minutes of market data published by TenneT, displayed in table 4.4. The data is augmented by taking the differences and the overall slope of each variable. Moreover, the probability distribution of imbalance prices varies depending on the hour and month in which price settlement takes place, especially at the margins (see figures 4.6 and 4.7). To take into account this variation, both hours (in periods of 6 hours) and months (in periods of 2 months) are added to the data as dummy variables in forecasting models 3.12a and 3.13a. The data set, which covers 2015-2021 is split in a training set (before 01-09-2020) and testing set (after 01-09-2020) to avoid overfitting. Moreover, the *class balance* of regulation state dummies and price threshold dummies is evaluated. While the regulation state data is fairly balanced (see figure 4.8), the price threshold dummy represents only fraction of the data below 30%. An LR model trained on this data is likely to frequently fail to identify the minority class (i.e. the imbalance prices above threshold). For LR models applied to large datasets, the preferred method to address this issue is *undersampling*, reducing

Table 4.4: imbalance market settlement forecast

variable	mean	min	max
$IGCC_{up}$	30.00	0.00	735.00
$IGCC_{dow}$	40.75	0.00	953.00
upward	31.06	0.00	666.00
downward	29.05	0.00	672.00
upward reserve	0.15	0.00	145.00
downward reserve	0.03	0.00	225.00
emergency	0.00	0.00	1.00
highest price upwards	22.50	0.00	936.12
mid price upwards	31.86	-31.07	107.40
lowest price downwards	8.70	-500.00	186.51

the size of the majority class by randomly removing a certain amount of instances in the dataset (Tantithamthavorn et al., 2018). The result of this method can be observed in figure 4.9.

4.4.2 Variable Selection

The 25 independent variables with the most predictive power are selected using the *recursive feature elimination* (RFE) algorithm in the *Scikit-learn* library in Python (Guyon & Elisseeff, 2003; Kuhn, Johnson, et al., 2013). In order to construct both feasible and parsimonious models, LR models with random combinations of these features are tested in a loop, each time dropping those that do not increase the goodness of fit (pseudo R^2). In the case of regulation state forecasting, this coincides with high significance levels of the selected variables (lower than $p = 0.01$). Moreover, a small number of previously eliminated variables turn out to improve the predictive power and are thus included in the model. The selected features are highlighted in appendix tables C.1 and C.2.

The statistical output of the resulting models as implemented in *Statsmodels* can be found in the appendix as well, where output tables C.3 and C.4 correspond to logistic regression equations (3.10a) and (3.11a). C.5 and C.6 correspond to equations (3.12a) and (3.13a). Note that in the threshold prediction models, the p-values of some variables exceed 0.1, despite improving the model's goodness of fit. These variables are nonetheless retained, as the models are judged based on their predictive performance, in terms of true positive and true negative rate. These metrics are visualized by *confusion matrices* 4.10(b) - 4.10(e). The models exhibit low false positive rates, meaning battery activations are very unlikely to result in negative passive contribution revenue. However, the false negative

rates are relatively high. To address this, the binary classification models 3.10a-3.13a can be made more sensitive by lowering the classification criteria 0.5 (Provost, 2000).

4.5 Selecting Representative Days

Due to computational limitations, the DSM-program cannot be applied to the entire dataset. This is a common challenge in energy systems optimization studies, which can be addressed by selecting a "limited number of well-chosen representative historical periods" (Poncelet et al., 2016) (Schütz et al., 2018). After all, in order to obtain reliable (cost) estimates it is essential to correctly capture the variability of VRES (Nahmmacher et al., 2016). This issue can be addressed by simply selecting days which diverging conditions, which capture the model outcome in different scenarios. However, since there is no consistent criterion to make this selection, more advanced selection methods may be preferred (Poncelet et al., 2016). The most common strategy, the application of a clustering algorithm, is applied in this thesis as well. Specifically, Ward's hierarchical clustering method is used to identify days with similar characteristics following a procedure proposed by Nahmmacher et al. (2016) who utilize it to produce input data for the European electricity system model LIMES-EU, which adequately replicates the variability of electricity demand and multi-regional VRE generation.

4.5.1 Hierarchical Clustering

(1) Data Normalization

The dates from which representative days can be selected are constrained by the dates for which forecast updates are available, i.e. 1 September 2020 - 31 December 2020 for the BR forecasts and one week per month for 1 Januari 2020 - 31 December 2019 for the KNMI forecasts.

A subset of the other key variables that define the optimization environment - the (mean) solar irradiance, the errors in the day-ahead solar irradiance forecasts, (mean and maximum) upward and downward settlement price and price volatility - are selected from the available data. In order to correctly compare the "distances" between the days based on each of these variables, the data is normalized.

(2) Clustering Algorithm

The (agglomerative) hierarchical clustering algorithm minimizes the deviation between historic days *dd* with a vector of selected variables (V_d) V_d and their cluster "representative" c with vector (V_c) (4.12).

$$min \sum_{c} \sum_{d \in D_c} ||V_d - V_c^*||^2 \tag{4.12}$$

The procedure starts with clusters of just one member, and iteratively combines these clusters in a way that achieves the smallest increase in the Sum of Squares between the data in the cluster and a vector of the means of these variables, i.e. the cluster centroid c (Ward Jr, 1963). The algorithm implements these iterations by sequentially combining the clusters with the smallest euclidean distance until there is only one cluster left. In this thesis, the algorithm is applied to the data using the python-based *Scikit-learn* library.

(3) Define n Clusters

Based on the resulting *dendrogram* (figure 4.11), seven clusters may be identified in both the BR- and the KNMI-dataset. However, since some initial clusters are very small, this thesis adopts a higher level clustering in three *BR-clusters* and four *KNMI-clusters*[6].

(4) Select Representative Days

Finally, for each cluster, a number of dates closest to the centroid are selected as representative days. This "distance" is the simple mean deviation between all measured values of the respective day and the centroid values. The selected representative days can be found in table 4.5.

For the BR-clusters, it can be observed that the most relevant distinguishing features of the hierarchical clusters are average GHI, with clusters 0, 1 and 2 respectively representing higher, lower and medium average solar energy generation. Secondly, average upward regulation price and price volatility are distinguishing features, with clusters 0, 1 and 2 respectively representing, higher, lower and medium average prices and price volatility. In addition, the maximum upwards imbalance price is noticeably higher for cluster 0. The KNMI-clusters exhibit a similar pattern. In addition, there are noticeable differences between the market environment in 2019 and 2020. Especially maximum and average

[6]This corresponds to the results of additional k-means clustering, which estimates the ideal amount of clusters (see appendix figure D.1)

upwards regulation prices are higher in 2020.

Based on these days, the total model outcome of the entire dataset can be estimated. To this end, the weighted average of the results of each cluster is taken, to account for the size of each cluster relative to the size of the dataset[7].

Table 4.5: Days selected using Ward's Hierarchical Clustering Method

2020	HC	$\overline{ghi}$	RMSE	$\overline{up}$	$\overline{down}$	max *up*	max *down*	σ^2_{up}	σ^2_{up}	x-$\overline{x}$
12-09	0	11.0	44.0	78.0	4.0	450.0	-101.0	10110.0	335.0	0.0
10-03	0	19.0	49.0	57.0	3.0	450.0	-82.0	9021.0	433.0	0.0
12-04	0	20.0	31.0	52.0	11.0	523.0	-124.0	11605.0	609.0	0.0
12-23	0	6.0	11.0	81.0	9.0	397.0	-31.0	12226.0	303.0	0.0
11-27	0	7.0	43.0	41.0	12.0	450.0	-74.0	5433.0	337.0	0.0
09-18	1	198.0	36.0	47.0	7.0	250.0	-100.0	6213.0	338.0	0.0
09-30	1	59.0	69.0	60.0	9.0	347.0	-78.0	6810.0	250.0	0.0
09-21	1	180.0	32.0	40.0	6.0	352.0	-79.0	5437.0	322.0	0.0
09-12	1	92.0	115.0	37.0	2.0	248.0	-143.0	3549.0	1298.0	0.0
09-07	1	187.0	31.0	28.0	9.0	362.0	-19.0	2793.0	137.0	0.0
12-06	2	16.0	42.0	39.0	9.0	260.0	-129.0	3634.0	395.0	0.0
10-20	2	21.0	26.0	32.0	9.0	259.0	-29.0	2604.0	185.0	0.0
10-06	2	49.0	36.0	21.0	8.0	252.0	-72.0	1682.0	402.0	0.0
11-10	2	53.0	37.0	32.0	3.0	257.0	-133.0	4392.0	1090.0	0.0
11-22	2	31.0	13.0	30.0	14.0	217.0	-42.0	817.0	178.0	0.0
w. mean[8]		53.31	39.55	46.52	6.67	334.75	-93.33	6298.90	494.40	0.0

2019	HC	$\overline{ghi}$	RMSE	$\overline{up}$	$\overline{down}$	max *up*	max *down*	σ^2_{up}	σ^2_{up}	x-$\overline{x}$
01-07	0	9.0	15.0	41.0	15.0	267.0	-53.0	2796.0	484.0	0.0
09-03	0	64.0	35.0	42.0	7.0	244.0	-9.0	3564.0	103.0	0.0
11-07	0	21.0	20.0	31.0	12.0	451.0	-41.0	4736.0	233.0	0.0
03-06	1	33.0	44.0	50.0	9.0	348.0	-147.0	5040.0	509.0	0.0
01-04	1	4.0	20.0	60.0	14.0	270.0	-130.0	3845.0	961.0	0.0
11-02	1	58.0	33.0	52.0	0.0	215.0	-138.0	4201.0	596.0	0.0
09-06	2	120.0	88.0	19.0	4.0	227.0	-74.0	1049.0	342.0	0.0
07-04	2	313.0	20.0	25.0	7.0	258.0	-151.0	1627.0	404.0	0.0
09-04	2	63.0	62.0	30.0	5.0	247.0	-71.0	3642.0	276.0	0.0
07-03	3	223.0	124.0	19.0	8.0	268.0	-40.0	1445.0	146.0	0.0
07-06	3	185.0	67.0	36.0	7.0	350.0	-75.0	4253.0	209.0	0.0
08-04	3	244.0	106.0	15.0	10.0	108.0	-1.0	471.0	125.0	0.0
w. mean[9]		130.99	57.94	31.84	7.77	264.38	-75.41	2786.46	334.01	0.0

[7] Nahmmacher et al. (2016) perform one final scaling step to account for the difference between the weighted average of the clusters and the historical data. However, due to time restraints, and since the analysis in this thesis does not involve multi-year extrapolation, this step is skipped.

[8] Cluster 0, 1, and 2 respectively represent 37.2%, 19.8%, and 43.0% of the total sample

[9] Cluster 0, 1, 2, and 3 respectively represent 3....

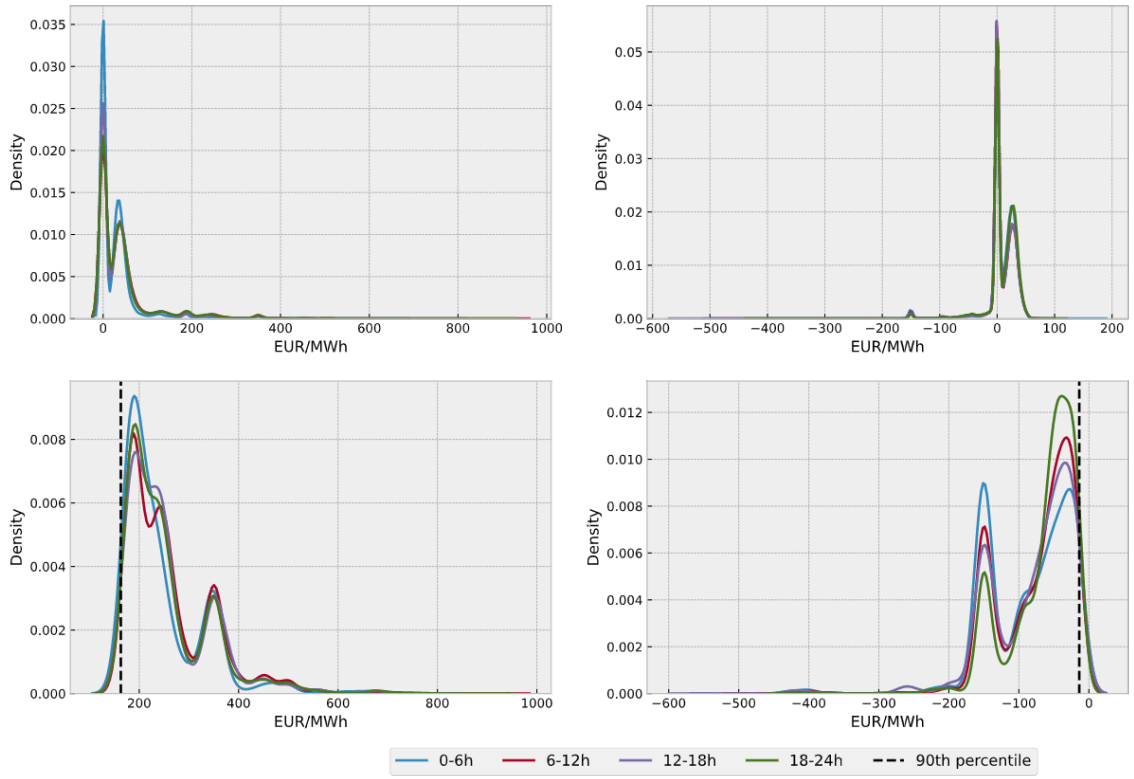

Figure 4.6: Probability distribution of the settlement price for different time intervals (top: full price range; bottom left: above 90th percentile (upward regulation); bottom right: below 10th percentile (downward regulation))

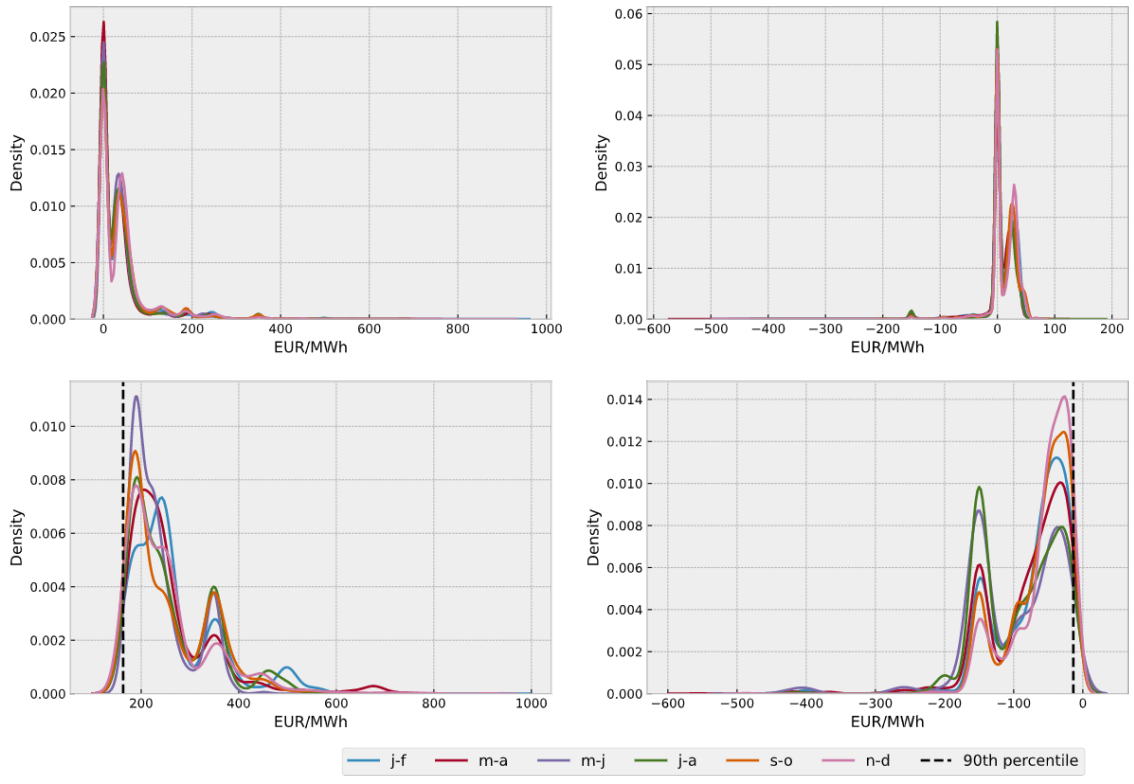

Figure 4.7: Probability distribution of the settlement price for different months, e.g. 'j-f' refers to January and February (top: full price range; bottom left: above 90th percentile (upward regulation); bottom right: below 10th percentile (downward regulation))

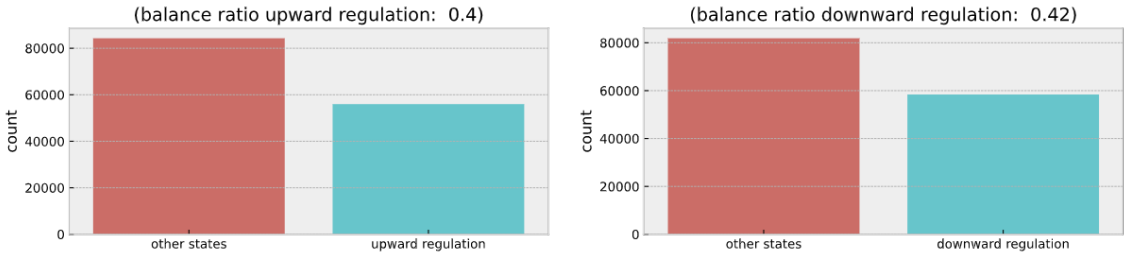

Figure 4.8: Class balance of regulation states (2015-2019)

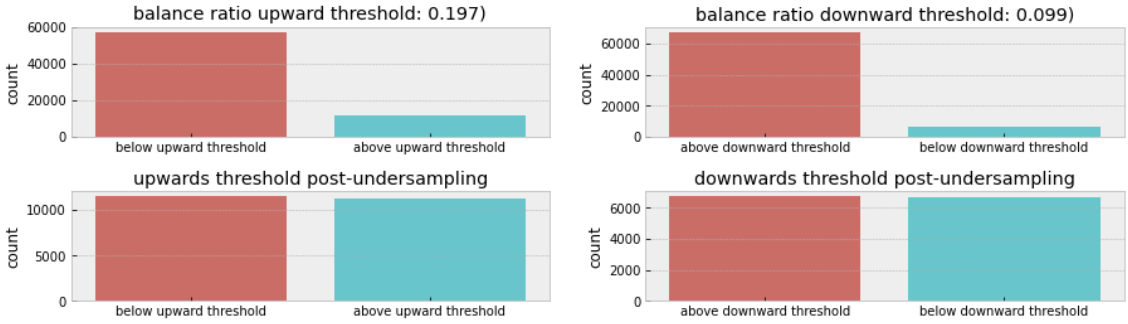

Figure 4.9: Class balance of price thresholds before and after random undersampling (2015-2019)

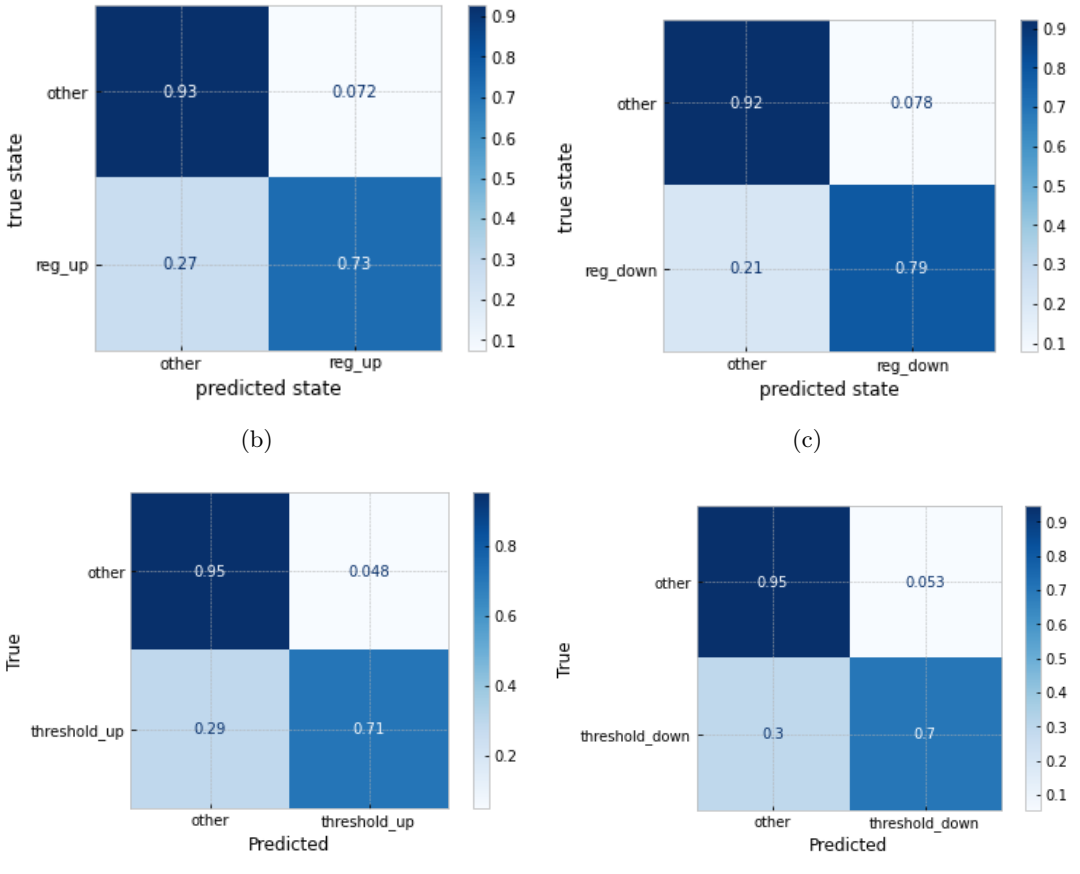

Figure 4.10: (b) upward regulation (87% accurate); (c) downward regulation (86% accurate); (d) upward threshold (91% accurate); and (e) downward threshold, (92% accurate).

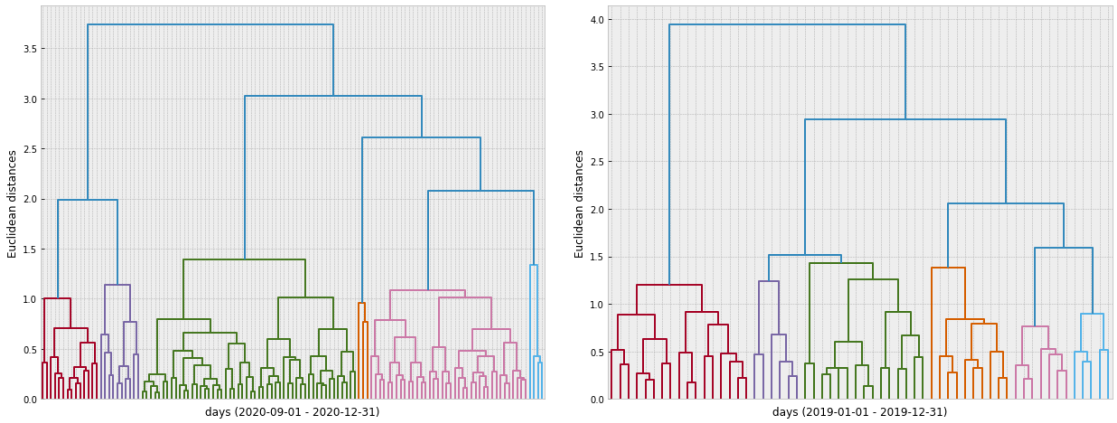

Figure 4.11: Dendrograms of Hierarchical Clustering (Buienradar (left) and KNMI (right))

Chapter 5

Results

This chapter first presents the results of the auxiliary system optimization model outlined in section 3.5. The implications of these results motivate the parameters chosen for the model predictive-heuristic control framework. Subsequently, the outcomes of the actual program are presented in section 5.2, separately in terms of imbalance reduction and imbalance costs reduction achieved by the DSM program, and in terms of the revenue generated by passive contribution.

5.1 Optimal System Conguration

5.1.1 Optimal Battery Energy Storage Size

The BESS modules under consideration are small relative to the average imbalance, and are equally divided over a 10 grid connections with a maximum capacity (100 kWh). The optimal system configuration model is thus applied to a range of aggregated BESS sizes of up to 50 modules per connection. Based on historical data, solar PV energy generation is simulated, both actual supply, and the day-ahead forecast. The difference between both (the internal portfolio imbalance (see figure 5.8 and 5.7)) is minimized by optimally deploying the aggregated BESSs. The optimization program is executing using Gurobi Optimization (2021), an optimization solver available for Python, and applied to the representative days in the BR-clusters. The optimal battery size can be determined in terms of imbalance reduction achieved by the system, battery degradation, total costs, and net costs.

As can be observed in figure 5.1, beyond a certain aggregate BESS size (250 modules),

the additional capacity only reduces imbalances when daily balance is unusually high[1]. A similar pattern exists for the degradation rate (figure 5.2). Figure 5.3 visualizes equation (3.21) and demonstrates that additional capacity beyond 250 modules is mainly used for passive contribution during days with high imbalance prices and high price volatility (i.e. BR cluster 0). Nonetheless, this ability does have a positive impact on the economic feasibility of the BESS. Figure 5.4 demonstrates that the system must consist of approximately 200 modules to break even. Under the perfect foresight assumption, a BESS of approximately 350 modules appears to be optimal. However, it appears that a battery with the assumed characteristics is not able to substantially reduce imbalance costs in general. Naturally, the amount of FECs decreases as with increasing battery size. The smallest configuration performs approximately 2 cycles more cycles per day than the largest configuration. The economically optimal amount of cycles (performed by a 350-module system) is rounded downward to 4.

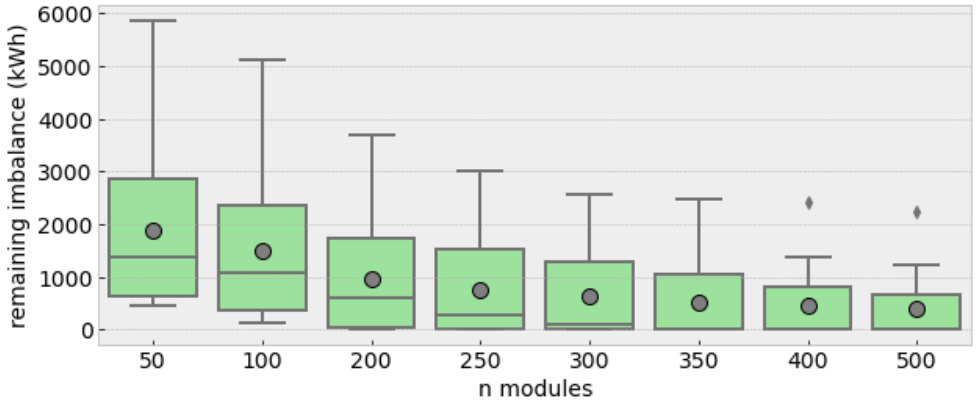

Figure 5.1: Remaining absolute daily imbalance for different BESS sizes

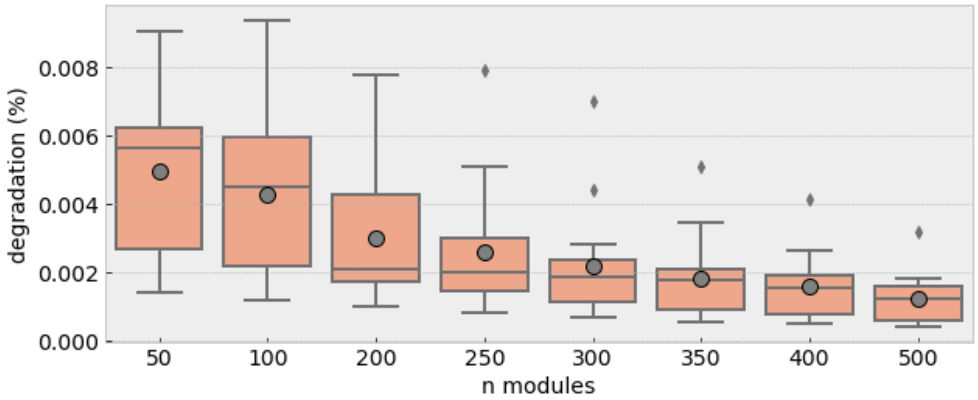

Figure 5.2: Degradation for different BESS sizes

[1]This can be observed from the "boxes" in the box-plot, which contain the interquartile range of the imbalance data and decrease only slightly after a certain capacity

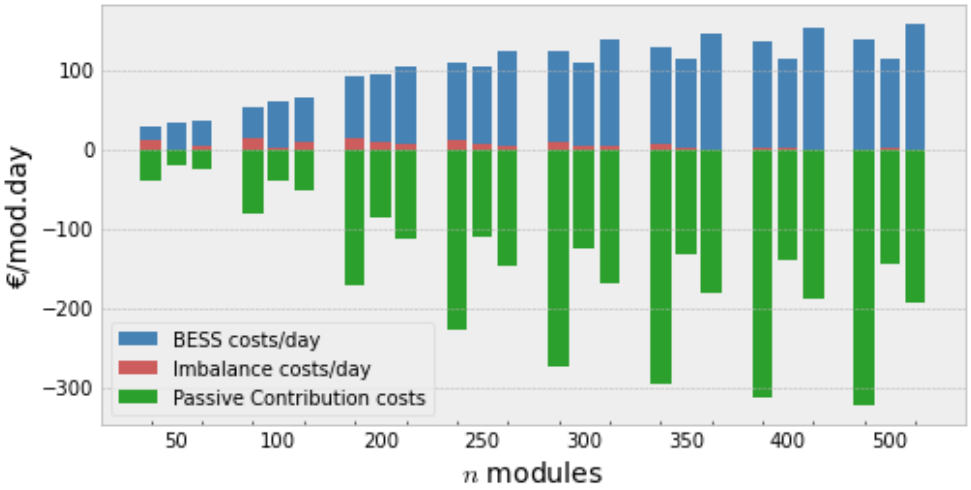

Figure 5.3: Full cost structure for different BESS sizes, respectively grouped from left to right for clusters 0, 1 and 2

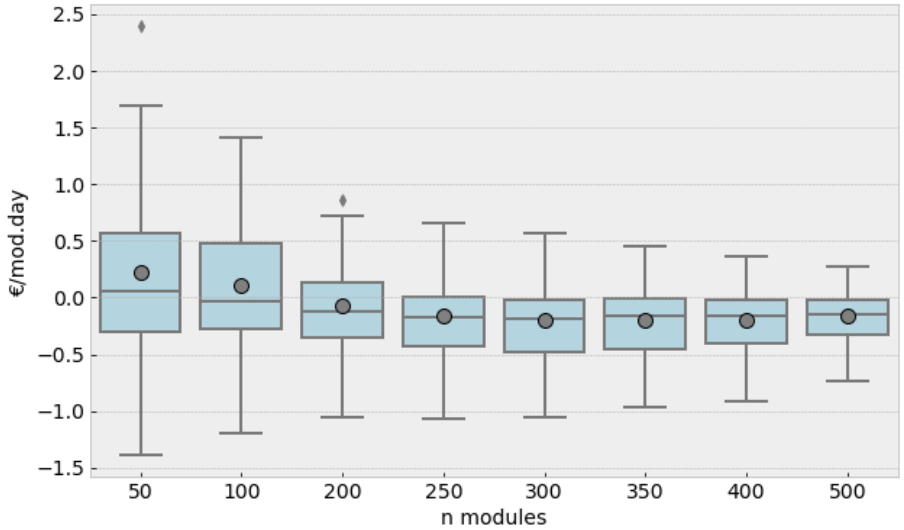

Figure 5.4: Net system costs per module

5.1.2 Optimal Multi-Objective Optimization Weight

The system optimization model also allows for the comparison of the results achieved by different optimization weights ζ in equation (3.22e). The resulting scatter-plot visualizes the *pareto frontier*, which consists of weights produce dominant solutions, for which degradation rates cannot be reduced without increasing the remaining imbalance. Other solutions are dominated, and can be improved without increasing degradation or decreasing imbalance reduction (Certa et al., 2011).

Primarily, figure 5.5, demonstrates that the differences between all solution are most

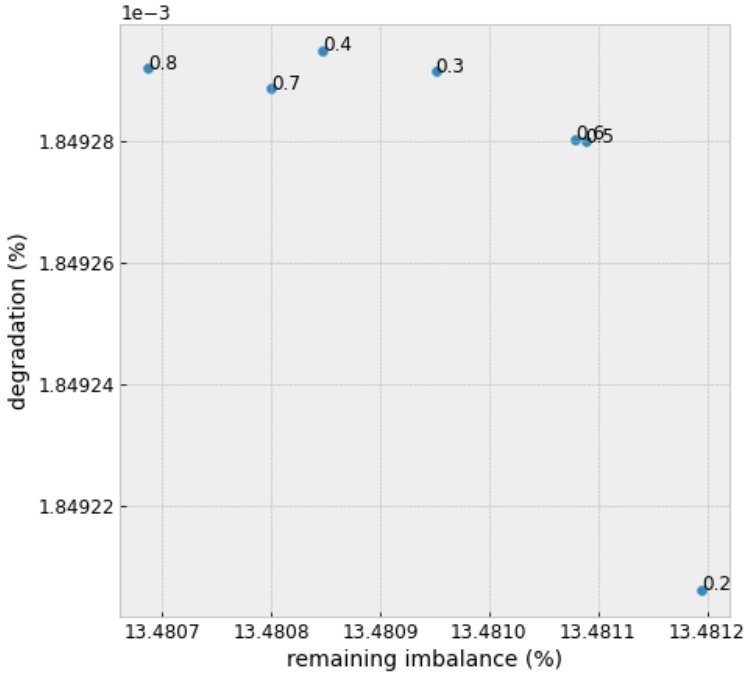

Figure 5.5: Average model outcomes for different weight (ζ)

likely negligible. Nonetheless, $\zeta = 0.5$ yields a dominant, Pareto optimal solution, which also results in a relative balance between both objectives, as opposed to dominant weights on the boundaries. Hence, weight $\zeta = 0.5$ is used in the implementation of (3.1a) .

5.2 Model Predictive & Heuristic Control

5.2.1 Imbalance Minimization

The DSM program introduced in chapter 3 is implemented in Gurobi Optimization (2021) as well. The program produces an optimal BESS activation schedule, which is updated for the remainder of the day by every iteration of the program. The generated BESS schedule reduces the *expected* remaining total imbalance $\sum_{t=k}^{T=96} \Delta^{post}$, but aims to reduce *actual* remaining total imbalance. Figures 5.9, 5.10 and 5.11 provide a single example of the DSM program's iteratively defined schedule for BR-clusters 0, 1 and 2, and figures 5.12, 5.13, 5.14 and 5.15 for KNMI-clusters 0, 1, 2 and 3, respectively. Additional output examples can be found in appendix E. While the top three sub-graphs are based on the optimization output with respect to the *forecasted* data used by the model, the bottom sub-graph visualizes the impact of the control actions on *actual imbalance* ex-post. The top figures distinguish positive imbalance (surplus) and negative imbalance (shortage) as positive and negative

values. The bottom figure shows absolute imbalance, which can either decrease (green) or increase (red) as a result of battery charging. The frequent occurrence of red areas clearly indicates that important discrepancies exists between actual and forecasted data, even after applying the Kalman filter. In addition, imbalances are caused by the end of the day, in order to meet constraint (3.3d).

This issue is summarized in table 5.1, which compares the mathematical and the conceptual (actual) objective of the model for 4 days per BR-cluster and 2 days per KNMI-cluster. For both clusters, the model generally manages to successfully reduce *forecasted imbalance* reduction. On some days this is not the case due to a combination of one-directional imbalance throughout the run-time and the final SoC constraint (3.3d). However these expected results do not reflect the *actual* imbalance. Specifically, the column "imbalance reduction" contains the program's conceptual/intended objective, as opposed to the mathematical objective of the MILP. This is the difference between "actual imbalance" and "actual remaining", the later referring to the imbalance after the DSM program has been implemented. Positive values indicate positive, successful, imbalance reduction, while negative values indicate that the imbalance is actually exacerbated by the program's control actions. Although the results of cluster 1 are somewhat positive, this is a minority cluster in the sample. A similar pattern emerges in the KNMI-cluster.

5.2.2 Imbalance Costs Reduction

The ultimate goal of the MILP-based MPC program is the reduction of imbalance costs, which are calculated using equations (3.20) and (3.21), and presented in table 5.2. By design, the model reduces imbalance costs regardless of the direction, even if imbalance costs are negative. However, as can be expected from table 5.1, the DSM program does not manage to reduce imbalance costs in all but two cases, if the BESS is rescheduled based on the BR forecasts. If the KNMI forecasts are used, the model is more successful in absolute terms, but this is most likely more indicative of the different market conditions in 2020. In addition, since negative imbalance costs are also reduced, the mean imbalance costs are still higher compared to the BAU-case.

5.2.3 Passive Contribution

Finally, the revenue from passive contribution can be found in table 5.3. While revenue from upward passive contribution is decidedly positive, the magnitude of the revenue varies

Table 5.1: Actual and forecasted imbalance reduction

BR 2020	HC	actual imbalance (kWh)	actual remaining (kWh)	forecast imbalance (kWh)	forecast remaining (kWh)	imbalance reduction (kWh)	degradation (%)
10-03	0	10702.93	11151.51	4563.69	4702.51	-448.58	0.000421
12-04	0	2384.62	2517.70	1940.37	1875.17	-133.07	0.000225
12-09	0	3628.44	3897.99	3323.03	3592.58	-269.55	0.000234
12-23	0	683.0	731.58	140.97	163.26	-48.53	0.000175
09-18	1	6972.23	6235.33	4409.43	3895.55	736.91	0.006184
09-21	1	5358.98	4943.12	2844.93	2263.13	415.85	0.001376
09-30	1	7591.08	7715.82	4162.52	4048.59	-124.74	0.000510
09-12	1	19179.45	19102.86	12399.52	11824.89	76.58	0.004448
10-06	2	8684.19	8550.57	4928.90	4359.38	133.62	0.005208
10-20	2	728.05	999.02	486.28	397.77	-270.96	0.000490
12-06	2	2949.49	2994.02	2523.56	2568.10	-44.54	0.000282
11-10	2	8225.59	8377.27	8730.42	8241.24	-151.68	0.000175
w. mean		5767.97	5833.19	3898.66	3725.70	-69.61	0.00138

KNMI 2019	HC	actual imbalance (kWh)	actual remaining (kWh)	forecast imbalance (kWh)	forecast remaining (kWh)	imbalance reduction (kWh)	degradation (%)
01-07	0	574.02	607.61	240.75	264.21	-33.59	0.000344
09-03	0	1273.41	2780.57	1940.28	1235.22	-1507.16	0.003734
01-04	1	910.57	1085.32	523.47	495.01	-174.75	0.000423
03-06	1	1693.33	1512.39	2051.55	1244.80	180.94	0.001173
07-04	2	838.14	1218.63	900.21	314.43	-380.49	0.000910
09-06	2	4785.22	4569.98	5935.61	4888.54	215.24	0.008789
07-03	3	4340.74	4198.89	3009.11	2569.32	141.85	0.000527
07-06	3	3100.88	3493.51	3341.15	2662.93	-392.63	0.000870
w. mean	1.72	2440.05	2658.06	2528.58	1946.68	-218.01	0.002441

significantly, both within and between clusters. This corresponds to the large differences in (negative) passive contribution costs encountered in the results of the static MILP. Moreover, the differences in maximum imbalance prices between 2019 and 2020, also effects the weighted mean of the revenue. Finally, downward passive contribution does not always yield positive revenue, since negative price peaks occur less frequently, and are less pronounced.

5.2.4 Computational Feasibility

A crucial element of the model is the time its takes to compute the optimal control actions. The passive contribution step should take place after the 9th and before the 10th minute of each PTU, i.e. after the market data is received and before the final five minutes in which

Table 5.2: Imbalance costs without (BAU) and after applying the DSM program

BR (2020)	HC	BAU (€)	DSM (€)
10-03	0	1150.53	1176.47
12-23	0	71.64	85.01
12-04	0	128.23	133.14
12-09	0	338.16	354.51
09-18	1	445.54	428.33
09-21	1	315.69	319.44
09-30	1	496.01	489.31
09-12	1	744.92	750.57
10-06	2	230.67	283.98
10-20	2	40.33	43.56
12-06	2	170.33	178.47
11-10	2	177.22	212.29
w. mean		322.73	338.36

KNMI (2019)	HC	BAU (€)	DSM (€)
2019-01-07	0	-34.52	-6.69
2019-09-03	0	-14.62	22.70
2019-03-06	1	-58.25	6.26
2019-01-04	1	86.54	82.50
2019-07-04	2	-8.42	11.73
2019-09-06	2	102.11	115.32
2019-07-03	3	92.23	90.09
2019-07-06	3	85.20	80.64
w. mean		38.98	55.42

Table 5.3: passive contribution revenue

BR (2020)	HC	down (€)	up (€)
10-03	0	0.40	121.08
12-23	0	-4.15	281.13
12-04	0	56.08	586.28
12-09	0	51.20	352.96
09-18	1	-1.49	292.09
09-21	1	6.89	275.86
09-30	1	-9.31	147.98
09-12	1	43.24	90.69
10-06	2	66.35	125.95
10-20	2	0.00	33.35
12-06	2	-5.71	13.00
11-10	2	36.66	89.17
w. mean		22.03	192.81

KNMI (2019)	HC	down (€)	up (€)
01-07	0	18.17	232.55
09-03	0	-1.06	227.28
03-06	1	0.00	412.40
01-04	1	25.91	102.79
07-04	2	0.00	78.95
09-06	2	-1.46	68.38
07-03	3	8.80	0.00
07-06	3	29.47	-0.00
w. mean		9.04	114.70

the passive contribution must take place begin. Li-ion batteries have a short response time with an order of magnitude of microseconds (Evans et al., 2012). Hence, the time window in which the heuristic predictions models and the passive contribution program must be completed can be close to 60 seconds. After the passive contribution step has been implemented, 5 minutes remain for the MPC-program to shift forward and re-optimize the battery schedule based on new data. The simulations were carried out on a Intel Core i5 processor with 8 GB RAM. Figure 5.6) shows a histogram of the runtimes of each part of the DSM program, both of which fit (by and large) in the available time window.

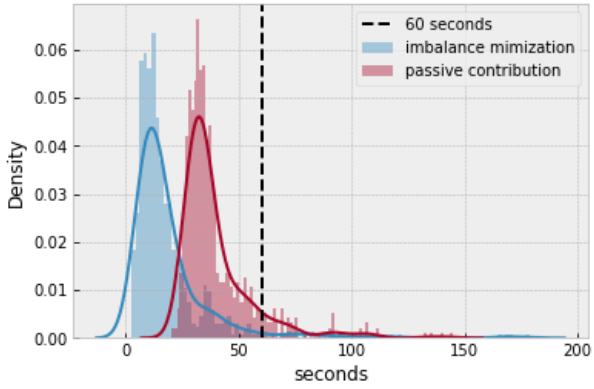

Figure 5.6: Histograms of the time duration of running the imbalance market minimization program and the passive contribution program.

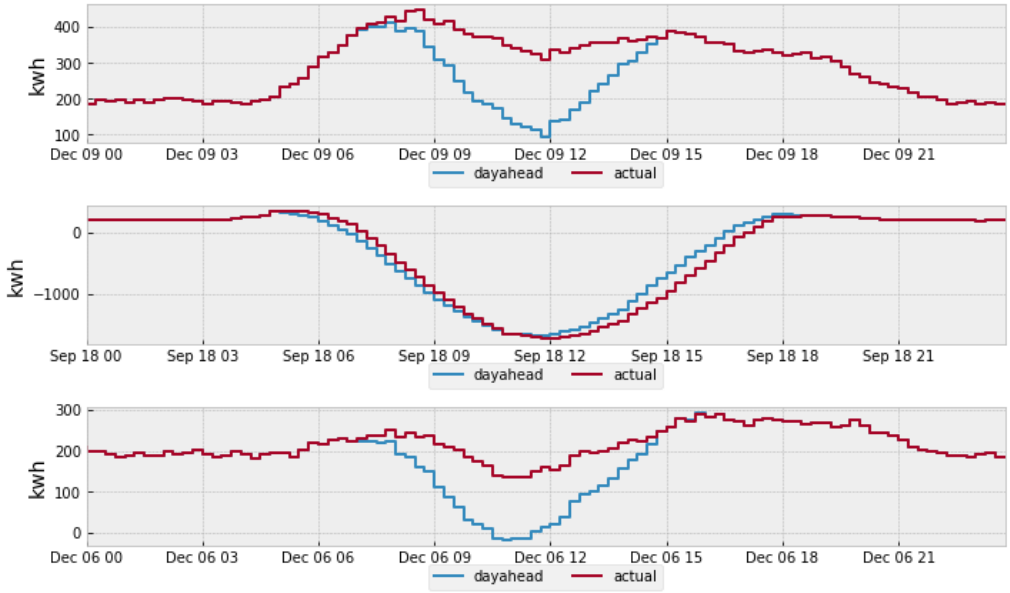

Figure 5.7: Portfolio imbalance BR (2020) - one day for each cluster

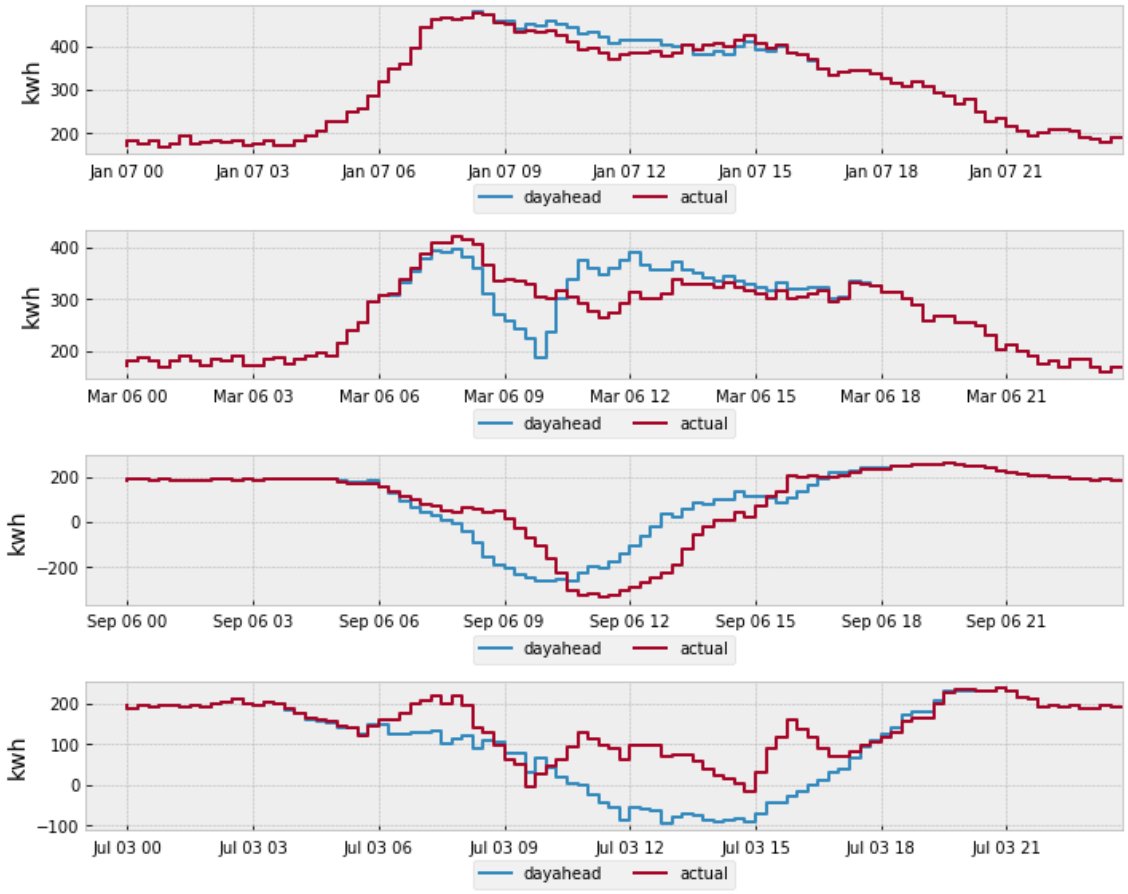

Figure 5.8: Portfolio imbalance KNMI (2019) - one day for each cluster

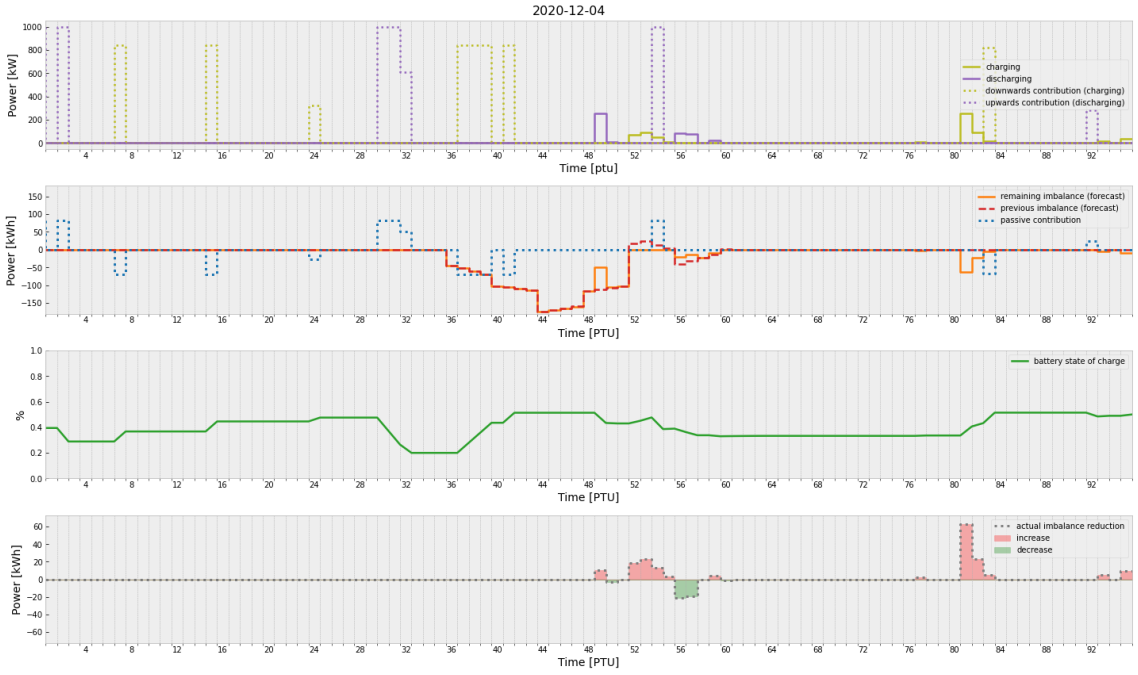

Figure 5.9: Example of model run BR-cluster 0 (4 december 2020)

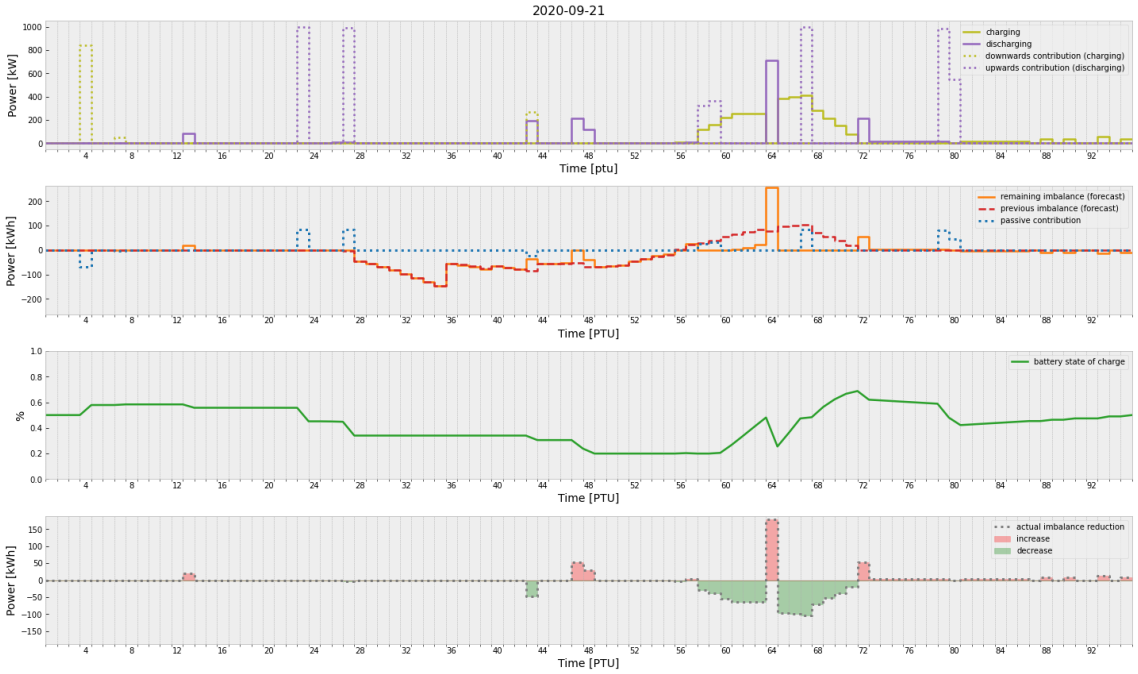

Figure 5.10: Example of model run BR-cluster 1 (21 September 2020)

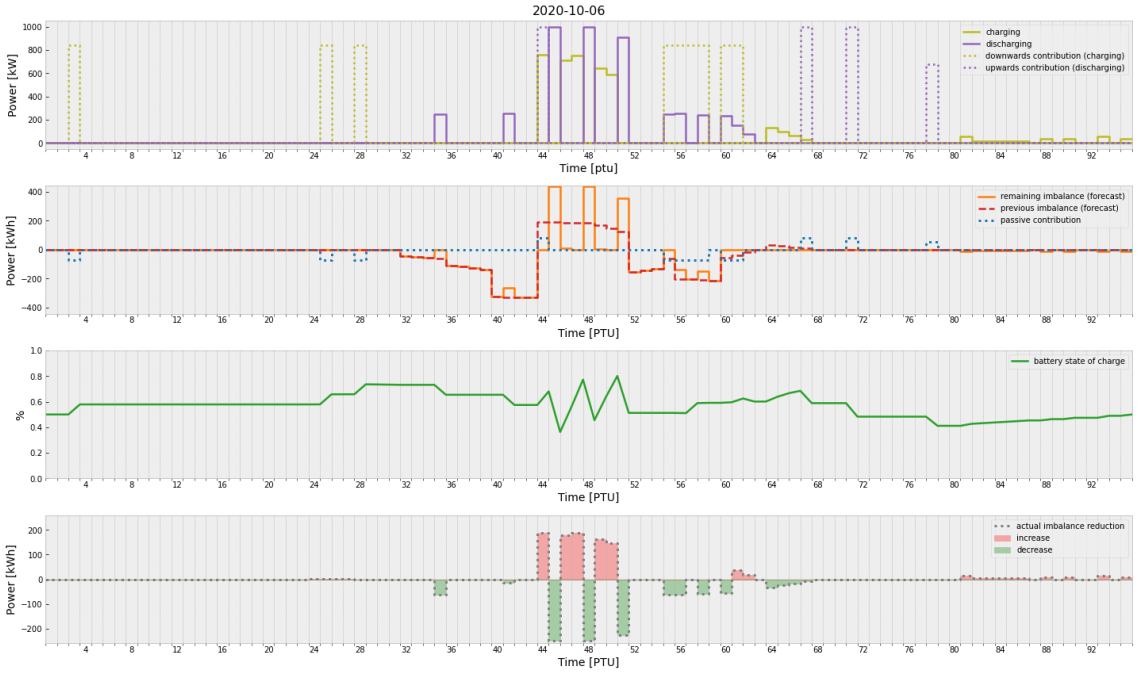

Figure 5.11: example of model run BR-cluster 2 (20 Oktober 2020)

Figure 5.12: Example of model run KNMI-cluster 0 (7 January 2019)

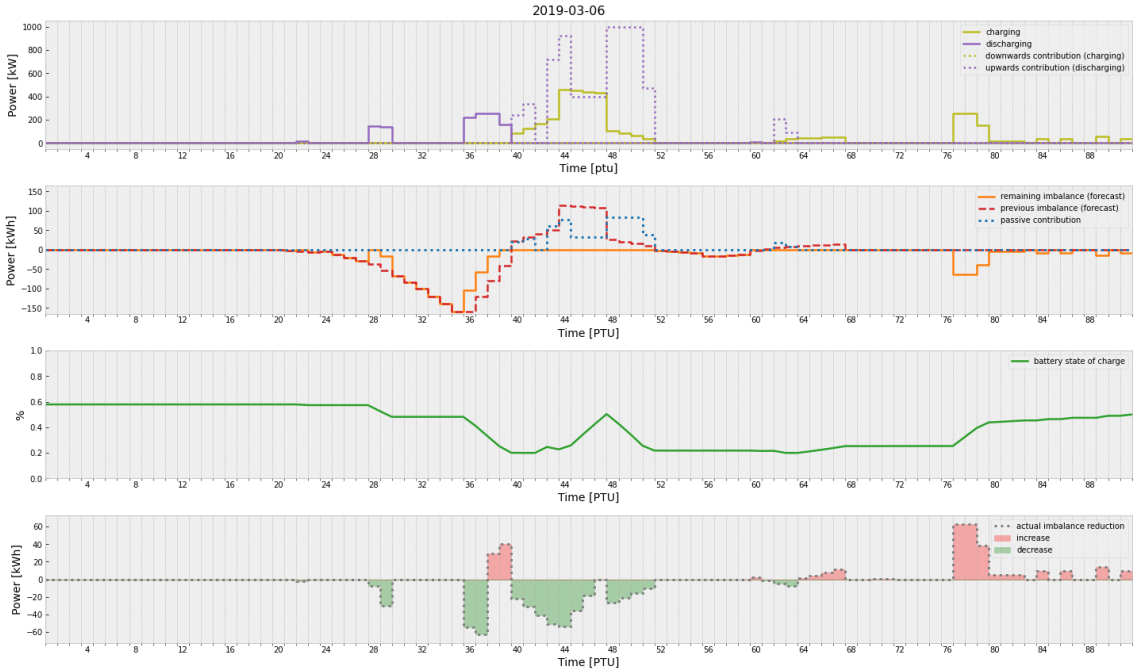

Figure 5.13: Example of model run KNMI-cluster 1 (6 March 2019)

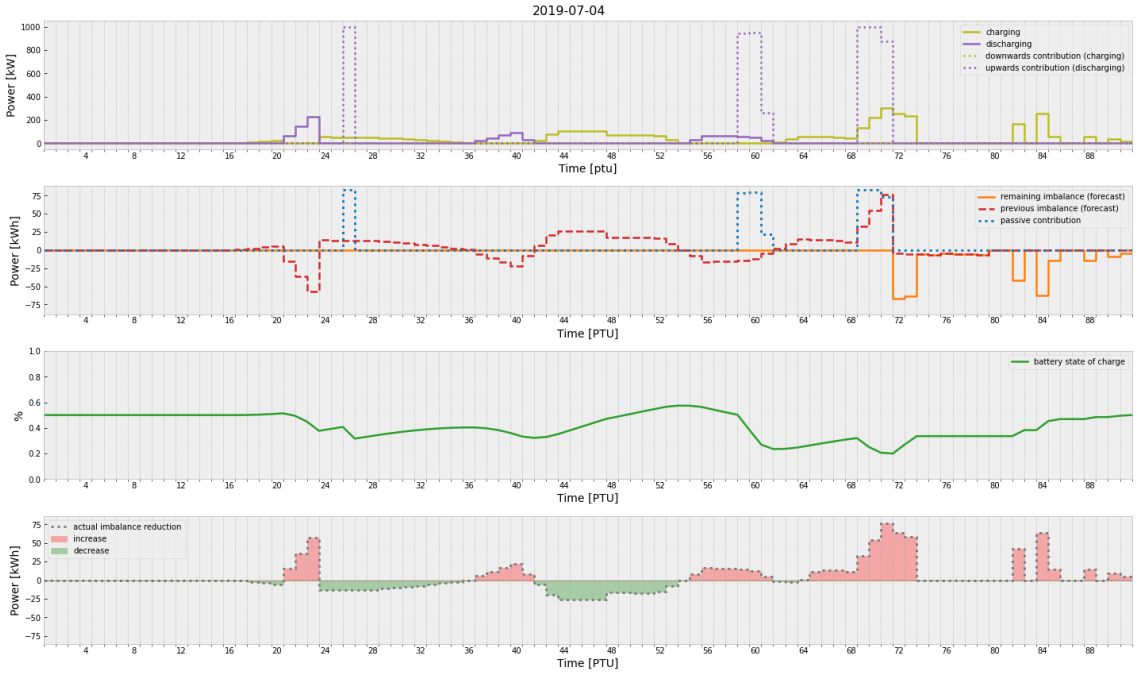

Figure 5.14: Example of model run KNMI-cluster 2 (4 July 2019)

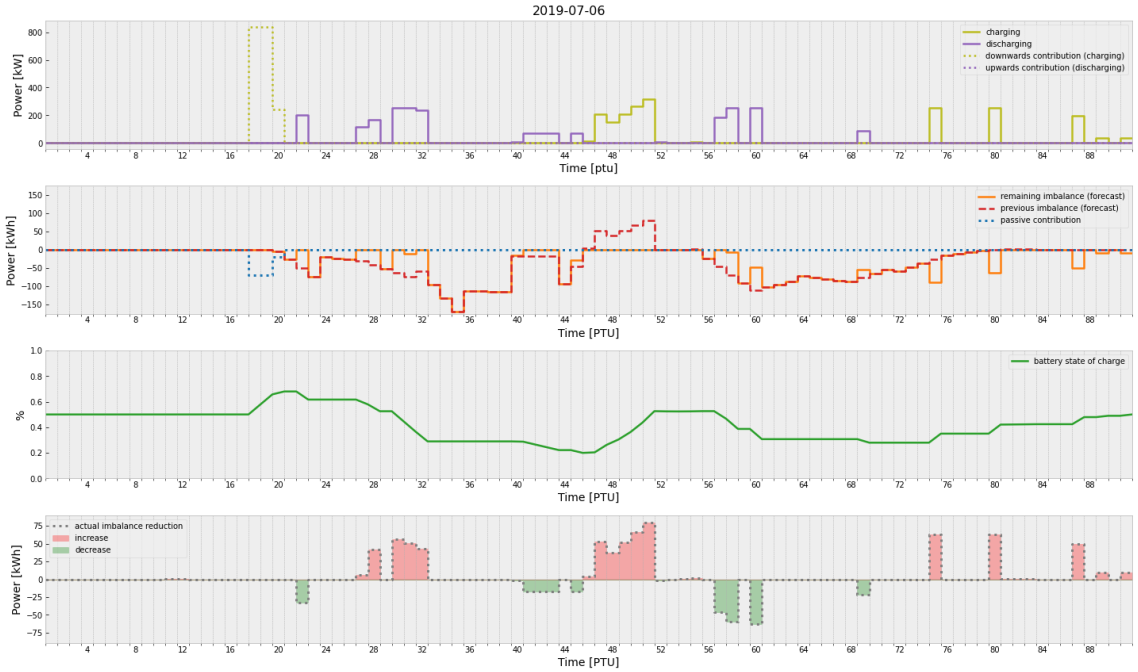

Figure 5.15: Example of model run KNMI-cluster 2 (6 July 2019)

Chapter 6

Discussion

6.1 Reflection & Interpretation

6.1.1 Research Context

Several distinct features of VRES complicate their integration in the power system, and thus impede the phasing out of GHG emitting capacity. In short, VRE supply is obtained from (1) intermittent and (2) unpredictable primary energy resources, by (3) non-synchronous[1] generators which have (4) a relatively small size, is (5) location-dependent and (6) has low short-term costs (Sinsel et al., 2020). The research effort addressing these challenges has surged in recent years, especially regarding the intermittency and unpredictability of solar and wind energy, and their effect on electricity prices. An overwhelming literature base examines technological and economic optimization schemes to counteract the increasing variability of supply by leveraging latent demand flexibility or by optimally deploying (distributed) energy storage systems.

This thesis belongs within this strand of research, with a specific focus on the unpredictability of VRE supply. In fact, aspects (1) and (3)-(5) were explicitly not considered: the EMS proposed focuses exclusively on *mismatches* caused by erroneous solar energy supply forecasts. At the market level, imbalance price peaks also occur due to forecast errors. To reap higher economic and environment gains from the demand side flexibility offered by distributed BESS, a DSM program should probably address simultaneously more challenges posed by VRE supply, for instance by increasing self-consumption. This would require a DSM program with additional optimization objectives, steps or hierarchies. However, the scope of this thesis was purposefully limited to a relatively rudimentary DSM

[1] Conventional electricity generation exhibits a high degree of rotational inertia, which helps stabilize the system frequency

program. Instead, the underlying goal was to examine the potential and challenges of the real world application of more elaborate models proposed in the literature, whose merit is often evaluated theoretically, based on simulated stochasticity and post-estimation techniques such as sensitivity analysis. Instead, the DSM program proposed is based on *actual* solar irradiance and temperature forecasts and employs computationally feasible forecasting and optimization techniques.

6.1.2 Results

To create a realistic economic optimization environment, a non-linear battery degradation model is adopted, and the optimal size of the distributed BESSs is determined based on a fixed horizon MILP. The latter enables a comparison of the model outcome based on perfect foresight, versus forecast data. The economic potential of passive contribution is clear, and allows the BESSs to break even: when the CAPEX and OPEX of the battery are included, the BESS is able to substantially reduce imbalance costs and achieve slightly negative costs if the batteries are optimally sized. This means that the potential economic gain from the system is not substantial. Moreover, the actual implementation of the DSM program shows that these results can hardly be obtained in a forecast-based simulation environment.

The MPC framework of the DSM program clearly demonstrates the benefit of rescheduling the BESSs as new forecasts are received. Throughout the model run, substantial changes in the magnitude and timing of battery activation occurs. However, there is a persistent discrepancy between forecast and actual measurements, which is not reliably reduced over time by new forecasts. These results provide an insight in the remaining challenges of VRE integration: even with additional pre-processing of the forecast data using a Kalman filter, the program does not reliably reduce actual imbalances.

The passive contribution strategy developed in this thesis does approach the economic potential estimated by the perfect foresight-optimization. Especially upward regulations can be a reliable source of revenue, even though the contributions to the grid only last for 5 minutes. This revenue has the same order of magnitude as the capital and operational costs of the BESSs, and can therefore ensure the break-even point its reached, while the remaining capacity is deployed for other objectives.

6.2 Assumptions & Limitations

Data Availability

The goal of this thesis is to provide an insight in the challenges of implementing DSM programs in practice. Hence, the DSM program is based on actual data accumulated by the host organization of this research project. However, since the available forecast data is limited to one location over a 6-month period, the presented results have some caveats. Even though additional forecast data by a different forecasting agency adds to the validity of the analysis, the periods of the data-sets do not overlap, which means a one-on-one comparison is not possible. This discrepancy is exacerbated by the changing imbalance price environment between 2019 and 2020.

More importantly, weather forecasts for the 6-month period in 2020 are only available for one location. Consequently, predicted and actual VRE supply data must be aligned artificially. Hence, the actual supply data of the PV installations is simulated using regression models based on historical data, which are applied to the measurement data at the forecast location. Consequently, the original resolution of 15 minutes of actual energy production data was reduced to one hour and then interpolated, due to the 1 hour-resolution of the measurement and forecast data. While the KNMI forecasts are available for more locations, the period of the KNMI data (2019) does not correspond to the period for which PV generation data of the entire producer-prosumer-portfolio is available at a 15-minute resolution (2020). Also in this case, actual production would have to be simulated. These 1-hour resultion, regression-bases simulation do not account for the full volatility of actual solar PV supply.

Modeling Assumptions

A number of modeling assumptions imply an simplification of the actual portfolio imbalances, which may result in overly optimistic results. These assumptions (1-7) have been demarcated in throughout this report. Of these assumptions, the perfect foresight with respect to the energy demand has the most substantial impact on the results. Secondly, the operating costs of the BESS when engaging in passive contribution may be underestimated, since 5-minute (dis) charging "bursts" are "spread out" over 15 minutes (*assumption 3*). The battery model in general does not consider (1) the configuration of modules in the BESS; (2) capacity fade and decline of efficiency over time; (3) self-discharge; (4). At a

more conceptual level, the model only includes grid constraints at the individual level, and only considers the market mechanism afterwards. This means that the location of the distributed BESSs is essentially irrelevant.

6.3 Suggestions for Further Research

Model Predictive Control Framework

Further research may apply more advanced forecasting methods within the same framework. First of all, more accurate solar PV generation forecasting models are available, and may be successfully replace the regression models (Antonanzas et al., 2016). Likewise, the diurnal trend nature of solar PV generation could be more accurately captured by *seasonal* ARIMA models, improving the Kalman Filter. Due to time constraints this could not be tested, though especially further ahead model predictions may benefit from this approach, enabling more effective scheduling.

The Kalman Filter proves to be an effective method in the context MPC-based DSM programs. However, applying KF to absolute solar irradiance values may not reap its full potential. In a real world application, it would likely be more effective to apply KF to forecast *errors* in *energy generation*, based on measured data with a 15 minute resolution. This would enable the filter, which now only targets forecasting error in solar irradiance, to account for the full range of "hidden" noise in the system.

Given the frequent occurrence of days with a unidirectional imbalance, it would be worthwhile to research the benefits of extending the optimization horizon beyond 24 hours. This would reduce the impact of SoC-constraint (3.3d) on the battery charging, allowing the battery to (dis)charge during more benefial hours.

Finally, due to time constraints caused by the encountered inaccuracy of the original solar irradiance forecasts, additional flexible distributed energy resources could not be included in the model. Given the impact of the battery costs on the overall EMS costs, and absence of potential revenue, it would be worthwhile to run these simulations for a combined distributed TES-BESS system.

Heuristic Control Program

The heuristic control program is the only segment of the proposed DSM model that yields uniquely positive results in its current form. However, its contribution to the BESSs'

capacity to reduce internal imbalance via the MPC-program could be improved. Firstly, the activation price threshold could be adjusted based on the average direction of the daily imbalance. Especially if a net shortage is expected, the threshold for downward regulation could be raised to a higher price level, even slightly above zero. Alternatively the threshold could be lowered if a net surplus is expected. Moreover, additional analysis could be directed to identifying the optimal classification threshold, to reduce the large number of false negative predictions. This is especially relevant given end-constraint of the battery schedule, which seriously limit the ability of the battery to reduce imbalance, if the total daily imbalance in strongly positive or negative.

Secondly, the logistic regression model proved to be an accurate and computationally efficient method for imbalance price forecasting, which may be sufficiently effected to forecast imbalance price peaks over a longer time horizon, beyond single PTUs. Given arbitrage opportunities are likely to decrease as more players enter the (voluntary) imbalance market, and not all countries reward passive contribution, this may become a more prudent strategy.

Chapter 7

Conclusion

The aim of this thesis, i.e. the *main research question*, was the examine the potential of demand side management to reduce the imbalance costs billed to the clients of a Dutch supplier-aggregator, causes by mismatches between the day-ahead demand/supply schedule submitted to the day-ahead market, and actual demand and supply. In contrast with the common approach in the literature, the performance to the proposed model is estimated based on *actual* forecasts data. A *model predictive control* framework allowed for the iterative inclusion of more recent weather forecasts throughout the modeling horizon (*sub-question 1*). Since the forecasts of both agencies used in this thesis do not reliably get more accurate over time, a Kalman filter is implemented to ensure new forecasts actually improve the forecasting accuracy.

The demand side appliances included in the model are distributed BESSs. To accurately capture the costs of these systems, a non-linear battery degradation model is included in the objective function of the DSM program's central MILP, while variable BESS costs are included in the optimal sizing framework (*(sub-question 2)*. Moreover, a number of degradation-prone (dis) charging behaviours are prevented by static constraints relating the SoC, C-rate and daily cycles.

To take into account imbalance costs (*sub-question 3*), a binary forecasting framework based on a price threshold-heuristic is constructed. The resulting model is able to update the optimal (dis)charging schedule of the BESSs within the limited time-period available to download the data, generate new forecasts and solve the optimization problem.

An auxiliary optimization problem is solved to determine the optimal aggregate size of the distributed BESSs (*sub-question 4*). A system of 35 modules per connection (10) results in a slightly negative net cost per battery module and has an aggregate capacity of 840 kWh (compared to a total (average) daily consumption of 27.9 MW).

To test the system on a valid subset of the data, a sample of representative days are selected by hierarchical clustering using Ward's method. The clustering is based on variations in VRE supply, market conditions and forecasting accuracy (*sub-question 5*).

The absence of large negative costs per battery unit implies no substantial net reduction in imbalance costs can be achieved using this program in combination with the proposed battery type. Moreover, this result is obtained in a perfect foresight framework, which nonetheless manages to substantially reduce imbalance costs. This is in stark contrast to imbalance cost reduction achieved in the MPC-framework. Using forecast data, substantial mismatches with actual delivery result in larger imbalances, and concurrently, in higher imbalance costs. Despite the substantial research effort on DSM programs, the apparently limited ability to reduce imbalance based on real forecast data appears pose a significant challenge for continued VRE integration.

Bibliography

Afram, A., & Janabi-Sharifi, F. (2014). Theory and applications of hvac control systems–a review of model predictive control (mpc). *Building and Environment*, *72*, 343–355.

Aghaei, J., & Alizadeh, M.-I. (2013). Demand response in smart electricity grids equipped with renewable energy sources: A review. *Renewable and Sustainable Energy Reviews*, *18*, 64–72.

Aine, O. (2018). Entso-e cim implementation.

Alham, M., Elshahed, M., Ibrahim, D. K., & El Zahab, E. E. D. A. (2017). Optimal operation of power system incorporating wind energy with demand side management. *Ain Shams Engineering Journal*, *8*(1), 1–7. https://doi.org/https://doi.org/10.1016/j.asej.2015.07.004

Alipour, M., Mohammadi-Ivatloo, B., Moradi-Dalvand, M., & Zare, K. (2017). Stochastic scheduling of aggregators of plug-in electric vehicles for participation in energy and ancillary service markets. *Energy*, *118*, 1168–1179.

Aneke, M., & Wang, M. (2016). Energy storage technologies and real life applications–a state of the art review. *Applied Energy*, *179*, 350–377.

Antonanzas, J., Osorio, N., Escobar, R., Urraca, R., Martinez-de-Pison, F. J., & Antonanzas-Torres, F. (2016). Review of photovoltaic power forecasting. *Solar Energy*, *136*, 78–111.

Antoniadou-Plytaria, K., Steen, D., Carlson, O., Ghazvini, M. A. F., et al. (2020). Market-based energy management model of a building microgrid considering battery degradation. *IEEE Transactions on Smart Grid*.

Antonopoulos, I., Robu, V., Couraud, B., Kirli, D., Norbu, S., Kiprakis, A., Flynn, D., Elizondo-Gonzalez, S., & Wattam, S. (2020). Artificial intelligence and machine learning approaches to energy demand-side response: A systematic review. *Renewable and Sustainable Energy Reviews*, *130*, 109899.

Avci, M., Erkoc, M., Rahmani, A., & Asfour, S. (2013). Model predictive hvac load control in buildings using real-time electricity pricing. *Energy and Buildings*, *60*, 199–209.

Balijepalli, V. M., Pradhan, V., Khaparde, S., & Shereef, R. (2011). Review of demand response under smart grid paradigm. *ISGT2011-India*, 236–243.

Barbato, A., & Capone, A. (2014). Optimization models and methods for demand-side management of residential users: A survey. *Energies*, *7*(9), 5787–5824.

Baruah, P. J., Eyre, N., Qadrdan, M., Chaudry, M., Blainey, S., Hall, J. W., Jenkins, N., & Tran, M. (2014). Energy system impacts from heat and transport electrification. *Proceedings of the Institution of Civil Engineers-Energy*, *167*(3), 139–151.

Bianchini, G., Casini, M., Vicino, A., & Zarrilli, D. (2016). Demand-response in building heating systems: A model predictive control approach. *Applied Energy*, *168*, 159–170.

Bishop, G., Welch, G. et al. (2001). An introduction to the kalman filter. *Proc of SIGGRAPH, Course*, *8*(27599-23175), 41.

Blok, K., & Nieuwlaar, E. (2020). *Introduction to energy analysis*. Routledge.

Boßmann, T., & Staffell, I. (2015). The shape of future electricity demand: Exploring load curves in 2050s germany and britain. *Energy*, *90*, 1317–1333.

Boyd, S., & Vandenberghe, L. (2004). *Convex optimization*. Cambridge university press.

Cardoso, G., Brouhard, T., DeForest, N., Wang, D., Heleno, M., & Kotzur, L. (2018). Battery aging in multi-energy microgrid design using mixed integer linear programming. *Applied energy*, *231*, 1059–1069.

Carreiro, A. M., Jorge, H. M., & Antunes, C. H. (2017). Energy management systems aggregators: A literature survey. *Renewable and Sustainable Energy Reviews*, *73*, 1160–1172.

Castro-Gutiérrez, J., Landa-Silva, D., & Moreno-Pérez, J. (2009). Dynamic lexicographic approach for heuristic multi-objective optimization. *Proceedings of the Workshop on Intelligent Metaheuristics for Logistic Planning (CAEPIA-TTIA 2009)(Seville (Spain))*, 153–163.

Certa, A., Galante, G., Lupo, T., & Passannanti, G. (2011). Determination of pareto frontier in multi-objective maintenance optimization. *Reliability Engineering & System Safety*, *96*(7), 861–867.

Chaves-Ávila, J. P., Hakvoort, R. A., & Ramos, A. (2013). Short-term strategies for dutch wind power producers to reduce imbalance costs. *Energy Policy*, *52*, 573–582.

Chen, T., Jin, Y., Lv, H., Yang, A., Liu, M., Chen, B., Xie, Y., & Chen, Q. (2020). Applications of lithium-ion batteries in grid-scale energy storage systems. *Transactions of Tianjin University*, *26*(3), 208–217.

Chiu, W.-Y., Sun, H., & Poor, H. V. (2012). Demand-side energy storage system management in smart grid. *2012 IEEE Third International Conference on Smart Grid Communications (SmartGridComm)*, 73–78.

de Heer, H., & van der Laan, M. (2017). *Usef: Workstream on aggregator implementation models: Recommended practices and key considerations for a regulatory framework and market design on explicit demand response: Update 2017: Includes residential customer segment*. USEF.

Dengiz, T., Jochem, P., & Fichtner, W. (2019). Demand response with heuristic control strategies for modulating heat pumps. *Applied Energy*, *238*, 1346–1360.

Diekerhof, M., Monti, A., & Schwarz, S. (2018). Demand-side management—recent aspects and challenges of optimization for an efficient and robust demand-side management. *Classical and recent aspects of power system optimization* (pp. 331–360). Elsevier.

Ding, Y. M., Hong, S. H., & Li, X. H. (2014). A demand response energy management scheme for industrial facilities in smart grid. *IEEE Transactions on Industrial Informatics*, *10*(4), 2257–2269.

en Markt, A. C. (2019). Besluit derogatie dagveiling balanceringscapaciteit.

ENTSO-E. (2020). The harmonised electricity market model. *eBIX and EFET*, *2020*(1).

European Commission. (2017). Commission regulation (eu) 2017/1485 of 2 august 2017 establishing a guideline on electricity transmission system operation. *Official Journal of the European Union*, *60*, 1–120.

Evans, A., Strezov, V., & Evans, T. J. (2012). Assessment of utility energy storage options for increased renewable energy penetration. *Renewable and Sustainable Energy Reviews*, *16*(6), 4141–4147.

EZK, m. v. (2019). Klimaatakkoord.

Faisal, M., Hannan, M. A., Ker, P. J., Hussain, A., Mansor, M. B., & Blaabjerg, F. (2018). Review of energy storage system technologies in microgrid applications: Issues and challenges. *Ieee Access*, *6*, 35143–35164.

Fischer, D., & Madani, H. (2017). On heat pumps in smart grids: A review. *Renewable and Sustainable Energy Reviews*, *70*, 342–357.

Gellings, C. W. (1985). The concept of demand-side management for electric utilities. *Proceedings of the IEEE*, *73*(10), 1468–1470.

Gigoni, L., Betti, A., Crisostomi, E., Franco, A., Tucci, M., Bizzarri, F., & Mucci, D. (2017). Day-ahead hourly forecasting of power generation from photovoltaic plants. *IEEE Transactions on Sustainable Energy*, *9*(2), 831–842.

González, R. M., Gibescu, M., Cobben, S., Bongaerts, M., de Nes-Koedam, M., & Vermeiden, W. (2018). Demand response of medical freezers in a business park microgrid. *SMARTGREENS*, 120–129.

Groppi, D., Pfeifer, A., Garcia, D. A., Krajačić, G., & Duić, N. (2020). A review on energy storage and demand side management solutions in smart energy islands. *Renewable and Sustainable Energy Reviews*, *135*, 110183.

Guney, M. S., & Tepe, Y. (2017). Classification and assessment of energy storage systems. *Renewable and Sustainable Energy Reviews*, *75*, 1187–1197.

Gurobi Optimization, L. (2021). Gurobi optimizer reference manual. http://www.gurobi.com

Guyon, I., & Elisseeff, A. (2003). An introduction to variable and feature selection. *Journal of machine learning research*, *3*(Mar), 1157–1182.

Han, X., Ji, T., Zhao, Z., & Zhang, H. (2015). Economic evaluation of batteries planning in energy storage power stations for load shifting. *Renewable Energy*, *78*, 643–647.

Hekkenberg, J., M. en Notenboom. (2019). Het klimaatakkoord: Effecten en aandachtspunten. *3806*.

Henríquez, R., Wenzel, G., Olivares, D. E., & Negrete-Pincetic, M. (2017). Participation of demand response aggregators in electricity markets: Optimal portfolio management. *IEEE Transactions on Smart Grid*, *9*(5), 4861–4871.

Hesse, H. C., Schimpe, M., Kucevic, D., & Jossen, A. (2017). Lithium-ion battery storage for the grid—a review of stationary battery storage system design tailored for applications in modern power grids. *Energies*, *10*(12), 2107.

Hirth, L., Ueckerdt, F., & Edenhofer, O. (2015). Integration costs revisited–an economic framework for wind and solar variability. *Renewable Energy*, *74*, 925–939.

Hokoi, S., Matsumoto, M., & Ihara, T. (1990). Statistical time series models of solar radiation and outdoor temperature—identification of seasonal models by kalman filter. *Energy and Buildings*, *15*(3-4), 373–383.

Huber, M., Dimkova, D., & Hamacher, T. (2014). Integration of wind and solar power in europe: Assessment of flexibility requirements. *Energy*, *69*, 236–246.

Jordehi, A. R. (2019). Optimisation of demand response in electric power systems, a review. *Renewable and sustainable energy reviews*, *103*, 308–319.

Kim, D.-W., & Park, C.-S. (2017). Application of kalman filter for estimating a process disturbance in a building space. *Sustainability*, *9*(10), 1868.

Kondziella, H., & Bruckner, T. (2016). Flexibility requirements of renewable energy based electricity systems–a review of research results and methodologies. *Renewable and Sustainable Energy Reviews*, *53*, 10–22.

Koohi-Fayegh, S., & Rosen, M. A. (2020). A review of energy storage types, applications and recent developments. *Journal of Energy Storage*, *27*, 101047.

Kostková, K., Omelina, L., Kyčina, P., & Jamrich, P. (2013). An introduction to load management. *Electric Power Systems Research*, *95*, 184–191.

Kuhn, M., Johnson, K. et al. (2013). *Applied predictive modeling* (Vol. 26). Springer.

Lampropoulos, I., Kling, W., Ribeiro, P., & Berg, van den, J. (2013). History of demand side management and classification of demand response control schemes. https://doi.org/10.1109/PESMG.2013.6672715

Lampropoulos, I. (2014). Energy management of distributed resources in power systems operations.

Lampropoulos, I., Garoufalis, P., van den Bosch, P. P., & Kling, W. L. (2015). Hierarchical predictive control scheme for distributed energy storage integrated with residential demand and photovoltaic generation. *IET Generation, Transmission & Distribution*, *9*(15), 2319–2327.

Lampropoulos, I., van den Broek, M., van der Hoofd, E., Hommes, K., & van Sark, W. (2018). A system perspective to the deployment of flexibility through aggregator companies in the netherlands. *Energy Policy*, *118*, 534–551.

Lampropoulos, I., van den Broek, M., van Sark, W., van der Hoofd, E., & Hommes, K. (2017). Enabling flexibility from demand-side resources through aggregator companies. *Smart cities in the mediterranean* (pp. 333–353). Springer.

Liander. (2014). Tarieven voor aansluiting en transport elektriciteit.

Louka, P., Galanis, G., Siebert, N., Kariniotakis, G., Katsafados, P., Pytharoulis, I., & Kallos, G. (2008). Improvements in wind speed forecasts for wind power predic-

tion purposes using kalman filtering. *Journal of Wind Engineering and Industrial Aerodynamics*, *96*(12), 2348–2362.

Lu, X., Li, K., Xu, H., Wang, F., Zhou, Z., & Zhang, Y. (2020). Fundamentals and business model for resource aggregator of demand response in electricity markets. *Energy*, 117885.

Lund, P. D., Lindgren, J., Mikkola, J., & Salpakari, J. (2015). Review of energy system flexibility measures to enable high levels of variable renewable electricity. *Renewable and Sustainable Energy Reviews*, *45*, 785–807.

Luo, X., Wang, J., Dooner, M., & Clarke, J. (2015). Overview of current development in electrical energy storage technologies and the application potential in power system operation. *Applied energy*, *137*, 511–536.

Ma, J., Silva, V., Belhomme, R., Kirschen, D. S., & Ochoa, L. F. (2013). Evaluating and planning flexibility in sustainable power systems. *2013 IEEE power & energy society general meeting*, 1–11.

Maheshwari, A. (2018). Modelling, aging and optimal operation of lithium-ion batteries.

Maheshwari, A., Paterakis, N. G., Santarelli, M., & Gibescu, M. (2020). Optimizing the operation of energy storage using a non-linear lithium-ion battery degradation model. *Applied Energy*, *261*, 114360.

McLaren, J., Gagnon, P., Anderson, K., Elgqvist, E., Fu, R., & Remo, T. (2016). *Battery energy storage market: Commercial scale, lithium-ion projects in the us* (tech. rep.). National Renewable Energy Lab.(NREL), Golden, CO (United States).

Mesbah, A. (2016). Stochastic model predictive control: An overview and perspectives for future research. *IEEE Control Systems Magazine*, *36*(6), 30–44.

Mier, M., & Weissbart, C. (2020). Power markets in transition: Decarbonization, energy efficiency, and short-term demand response. *Energy Economics*, 104644.

Morales González, R., Shariat Torbaghan, S., Gibescu, M., & Cobben, S. (2016). Harnessing the flexibility of thermostatic loads in microgrids with solar power generation. *Energies*, *9*(7), 547.

Muenzel, V., de Hoog, J., Brazil, M., Vishwanath, A., & Kalyanaraman, S. (2015). A multi-factor battery cycle life prediction methodology for optimal battery management. *Proceedings of the 2015 ACM Sixth International Conference on Future Energy Systems*, 57–66.

Nahmmacher, P., Schmid, E., Hirth, L., & Knopf, B. (2016). Carpe diem: A novel approach to select representative days for long-term power system modeling. *Energy*, *112*, 430–442.

Nicolosi, M., & Fürsch, M. (2009). The impact of an increasing share of res-e on the conventional power market—the example of germany. *Zeitschrift für Energiewirtschaft*, *33*(3), 246–254.

Niesten, E., & Alkemade, F. (2016). How is value created and captured in smart grids? a review of the literature and an analysis of pilot projects. *Renewable and Sustainable Energy Reviews*, *53*, 629–638.

Notton, G., Nivet, M.-L., Voyant, C., Paoli, C., Darras, C., Motte, F., & Fouilloy, A. (2018). Intermittent and stochastic character of renewable energy sources: Consequences, cost of intermittence and benefit of forecasting. *Renewable and Sustainable Energy Reviews*, *87*, 96–105.

Okur, Ö., Voulis, N., Heijnen, P., & Lukszo, Z. (2019). Aggregator-mediated demand response: Minimizing imbalances caused by uncertainty of solar generation. *Applied Energy*, *247*, 426–437.

Oldewurtel, F., Parisio, A., Jones, C. N., Gyalistras, D., Gwerder, M., Stauch, V., Lehmann, B., & Morari, M. (2012). Use of model predictive control and weather forecasts for energy efficient building climate control. *Energy and Buildings*, *45*, 15–27.

Oldewurtel, F., Ulbig, A., Parisio, A., Andersson, G., & Morari, M. (2010). Reducing peak electricity demand in building climate control using real-time pricing and model predictive control. *49th IEEE conference on decision and control (CDC)*, 1927–1932.

Olhoff, A., & Christensen, J. M. (2019). Emissions gap report 2019.

Omar, N., Monem, M. A., Firouz, Y., Salminen, J., Smekens, J., Hegazy, O., Gaulous, H., Mulder, G., Van den Bossche, P., Coosemans, T., et al. (2014). Lithium iron phosphate based battery–assessment of the aging parameters and development of cycle life model. *Applied Energy*, *113*, 1575–1585.

Ommen, T., Markussen, W. B., & Elmegaard, B. (2014). Comparison of linear, mixed integer and non-linear programming methods in energy system dispatch modelling. *Energy*, *74*, 109–118.

Park, L., Jang, Y., Cho, S., & Kim, J. (2017). Residential demand response for renewable energy resources in smart grid systems. *IEEE Transactions on Industrial Informatics*, *13*(6), 3165–3173.

Parra, D., Norman, S. A., Walker, G. S., & Gillott, M. (2017). Optimum community energy storage for renewable energy and demand load management. *Applied energy*, *200*, 358–369.

Paterakis, N. G., Erdinç, O., & Catalão, J. P. (2017). An overview of demand response: Key-elements and international experience. *Renewable and Sustainable Energy Reviews*, *69*, 871–891.

Pelland, S., Galanis, G., & Kallos, G. (2013). Solar and photovoltaic forecasting through post-processing of the global environmental multiscale numerical weather prediction model. *Progress in photovoltaics: Research and Applications*, *21*(3), 284–296.

Pilo, F., Pisano, G., & Soma, G. G. (2009). Advanced dms to manage active distribution networks. *2009 IEEE Bucharest PowerTech*, 1–8.

Pirlot, M. (1996). General local search methods. *European journal of operational research*, *92*(3), 493–511.

Poncelet, K., Höschle, H., Delarue, E., Virag, A., & D'haeseleer, W. (2016). Selecting representative days for capturing the implications of integrating intermittent renewables in generation expansion planning problems. *IEEE Transactions on Power Systems*, *32*(3), 1936–1948.

Poplavskaya, K., & De Vries, L. (2019). Distributed energy resources and the organized balancing market: A symbiosis yet? case of three european balancing markets. *Energy policy*, *126*, 264–276.

Privara, S., Širok, J., Ferkl, L., & Cigler, J. (2011). Model predictive control of a building heating system: The first experience. *Energy and Buildings*, *43*(2-3), 564–572.

Provost, F. (2000). Machine learning from imbalanced data sets 101. *Proceedings of the AAAI'2000 workshop on imbalanced data sets*, *68*(2000), 1–3.

Rajabi, A., Li, L., Zhang, J., & Zhu, J. (2017). Aggregation of small loads for demand response programs—implementation and challenges: A review, 1–6.

Rashidizadeh-Kermani, H., Vahedipour-Dahraie, M., Shafie-khah, M., & Catalão, J. P. (2019). Stochastic programming model for scheduling demand response aggregators considering uncertain market prices and demands. *International Journal of Electrical Power & Energy Systems*, *113*, 528–538.

Renewable, I., IRENA, I. R. et al. (2017). Electricity storage and renewables: Costs and markets to 2030.

Rivera, J., Goebel, C., & Jacobsen, H.-A. (2016). Distributed convex optimization for electric vehicle aggregators. *IEEE Transactions on Smart Grid*, *8*(4), 1852–1863.

Rogosich, J. (2000). What are dynamic model?

Salah, F., Henrıquez, R., Wenzel, G., Olivares, D. E., Negrete-Pincetic, M., & Weinhardt, C. (2018). Portfolio design of a demand response aggregator with satisficing consumers. *IEEE Transactions on Smart Grid*, *10*(3), 2475–2484.

Schimpe, M., von Kuepach, M. E., Naumann, M., Hesse, H. C., Smith, K., & Jossen, A. (2018). Comprehensive modeling of temperature-dependent degradation mechanisms in lithium iron phosphate batteries. *Journal of The Electrochemical Society*, *165*(2), A181.

Schneider, S. F., Novak, P., & Kober, T. (2020). Rechargeable batteries for simultaneous demand peak shaving and price arbitrage business. *IEEE Transactions on Sustainable Energy*.

Schütz, T., Schraven, M. H., Fuchs, M., Remmen, P., & Müller, D. (2018). Comparison of clustering algorithms for the selection of typical demand days for energy system synthesis. *Renewable energy*, *129*, 570–582.

Siano, P. (2014). Demand response and smart grids—a survey. *Renewable and sustainable energy reviews*, *30*, 461–478.

Simon, D. (2001). Kalman filtering. *Embedded systems programming*, *14*(6), 72–79.

Sinsel, S. R., Riemke, R. L., & Hoffmann, V. H. (2020). Challenges and solution technologies for the integration of variable renewable energy sources—a review. *renewable energy*, *145*, 2271–2285.

Stock, J. H., & Watson, M. W. (2015). *Introduction to econometrics*.

Sundstrom, O., & Binding, C. (2011). Flexible charging optimization for electric vehicles considering distribution grid constraints. *IEEE Transactions on Smart grid*, *3*(1), 26–37.

Tanrisever, F., Derinkuyu, K., & Jongen, G. (2015). Organization and functioning of liberalized electricity markets: An overview of the dutch market. *Renewable and Sustainable Energy Reviews*, *51*, 1363–1374.

Tantithamthavorn, C., Hassan, A. E., & Matsumoto, K. (2018). The impact of class rebalancing techniques on the performance and interpretation of defect prediction models. *IEEE Transactions on Software Engineering*, *46*(11), 1200–1219.

TenneT. (2020). Imbalance pricing system. *5*, 1–16.

Terlouw, T., AlSkaif, T., Bauer, C., & van Sark, W. (2019). Multi-objective optimization of energy arbitrage in community energy storage systems using different battery technologies. *Applied Energy*, *239*, 356–372.

Tian, N., Fang, H., & Wang, Y. (2020). Real-time optimal lithium-ion battery charging based on explicit model predictive control. *IEEE Transactions on Industrial Informatics*, *17*(2), 1318–1330.

Tohidi, Y., & Gibescu, M. (2018). Stochastic optimisation for investment analysis of flow battery storage systems. *IET Renewable Power Generation*, *13*(4), 555–562.

Tohidi, Y., Gibescu, M., & Kout, W. (2018). Energy arbitrage of hydrogen-bromine flow battery between the day-ahead and imbalance electricity markets considering price uncertainty. *2018 IEEE International Energy Conference (ENERGYCON)*, 1–6.

Vardakas, J. S., Zorba, N., & Verikoukis, C. V. (2014). A survey on demand response programs in smart grids: Pricing methods and optimization algorithms. *IEEE Communications Surveys & Tutorials*, *17*(1), 152–178.

Wang, D., Coignard, J., Zeng, T., Zhang, C., & Saxena, S. (2016). Quantifying electric vehicle battery degradation from driving vs. vehicle-to-grid services. *Journal of Power Sources*, *332*, 193–203.

Wang, J., Shi, Y., & Zhou, Y. (2019). Intelligent demand response for industrial energy management considering thermostatically controlled loads and evs. *IEEE Transactions on Industrial Informatics*, *15*(6), 3432–3442.

Wang, J., Purewal, J., Liu, P., Hicks-Garner, J., Soukazian, S., Sherman, E., Sorenson, A., Vu, L., Tataria, H., & Verbrugge, M. W. (2014). Degradation of lithium ion batteries employing graphite negatives and nickel–cobalt–manganese oxide+ spinel manganese oxide positives: Part 1, aging mechanisms and life estimation. *Journal of Power Sources*, *269*, 937–948.

Ward Jr, J. H. (1963). Hierarchical grouping to optimize an objective function. *Journal of the American statistical association*, *58*(301), 236–244.

Wickert, M., & Siddappa, C. (2018). Exploring the extended kalman filter for gps positioning using simulated user and satellite track data. *Proc. 17th Python in Science Conference*, 84–90.

Xu, B., Oudalov, A., Ulbig, A., Andersson, G., & Kirschen, D. S. (2016). Modeling of lithium-ion battery degradation for cell life assessment. *IEEE Transactions on Smart Grid*, *9*(2), 1131–1140.

Xu, Z., Callaway, D. S., Hu, Z., & Song, Y. (2016). Hierarchical coordination of heterogeneous flexible loads. *IEEE Transactions on Power Systems*, *31*(6), 4206–4216.

Zakeri, B., & Syri, S. (2015). Electrical energy storage systems: A comparative life cycle cost analysis. *Renewable and sustainable energy reviews*, *42*, 569–596.

Zhou, Y., Wang, C., Wu, J., Wang, J., Cheng, M., & Li, G. (2017). Optimal scheduling of aggregated thermostatically controlled loads with renewable generation in the intraday electricity market. *Applied energy*, *188*, 456–465.

Appendix A

Solar PV Generation

Table A.1: Best performing regression model for each producer

client	model	d	RMSE	nRMSE	Rsq	Betas	p_values
prod1	GHI,GHIsq,GHITemp	4	5.500	2.750	0.953	[0.19, 0.0, -0.0]	[0.05, 0.14, 0.16]
		12	5.652	2.826	0.951	[0.19, 0.0, -0.0]	[0.0, 0.15, 0.05]
		14	5.687	2.844	0.950	[0.2, 0.0, -0.0]	[0.0, 0.15, 0.07]
		10	5.755	2.878	0.950	[0.19, 0.0, -0.0]	[0.0, 0.01, 0.05]
prod2	GHI,GHIsq,GHITemp	6	6.821	2.966	0.906	[1.25, -0.01, 0.06]	[0.0, 0.05, 0.26]
		4	7.004	3.045	0.909	[1.26, -0.01, 0.05]	[0.03, 0.14, 0.34]
	GHI,Temp,GHITemp	6	7.012	3.049	0.902	[1.14, 0.26, 0.02]	[0.0, 0.24, 0.52]
	GHI,GHIsq,Temp	6	7.044	3.063	0.905	[1.45, -0.01, 0.11]	[0.0, 0.1, 0.52]
prod3	GHI,GHIsq,GHITemp	6	7.235	3.146	0.905	[1.24, -0.01, 0.07]	[0.0, 0.08, 0.21]
		4	7.400	3.217	0.909	[1.25, -0.01, 0.06]	[0.03, 0.17, 0.33]
	GHI,Temp,GHITemp	6	7.433	3.232	0.901	[1.14, 0.25, 0.03]	[0.0, 0.3, 0.41]
	GHI,GHITemp	6	7.474	3.249	0.900	[1.17, 0.03]	[0.0, 0.38]
prod4	GHI,GHIsq,GHITemp	4	49.510	2.476	0.963	[1.9, 0.0, -0.02]	[0.0, 0.0, 0.31]
	GHI,GHIsq,Temp	4	50.715	2.536	0.962	[1.71, 0.0, -0.26]	[0.0, 0.0, 0.49]
	GHI,GHIsq	4	50.887	2.544	0.962	[1.68, 0.0]	[0.0, 0.0]
	GHI,GHIsq,GHITemp	6	51.958	2.598	0.963	[1.9, 0.0, -0.02]	[0.0, 0.0, 0.14]

Table A.2: Best performing regression model for each producer

client	model	d	RMSE	nRMSE	Rsq	Betas	p_values
pros1	GHI,GHIsq,GHITemp	8	5.413	2.035	0.945	[0.33, 0.0, -0.0]	[0.0, 0.03, 0.11]
		4	5.445	2.047	0.944	[0.32, 0.0, -0.0]	[0.0, 0.16, 0.16]
		26	5.451	2.049	0.949	[0.32, 0.0, -0.0]	[0.0, 0.0, 0.15]
		14	5.454	2.050	0.949	[0.32, 0.0, -0.0]	[0.0, 0.0, 0.19]
pros2	GHI,GHIsq,GHITemp	4	8.351	6.232	0.695	[0.11, 0.0, -0.0]	[0.14, 0.15, 0.09]
	GHI,GHITemp	4	8.549	6.380	0.680	[0.11, 0.0]	[0.2, 0.14]
	GHI,Temp,GHITemp	4	8.553	6.383	0.680	[0.12, -0.06, 0.0]	[0.2, 0.39, 0.14]
	GHI,GHIsq,GHITemp	6	8.963	6.689	0.666	[0.08, 0.0, 0.01]	[0.21, 0.09, 0.02]
pros3	GHI,GHIsq	4	9.345	9.345	0.532	[0.15, 0.0]	[0.05, 0.05]
	GHI,GHIsq,Temp	4	9.375	9.375	0.533	[0.15, -0.0, 0.03]	[0.08, 0.05, 0.53]
	GHI,GHIsq,GHITemp	4	9.442	9.442	0.581	[0.07, -0.0, 0.0]	[0.07, 0.07, 0.17]
	GHI,Temp	4	9.747	9.747	0.506	[0.17, -0.01]	[0.0, 0.38]
pros4	GHI,GHIsq,GHITemp	4	29.584	8.218	0.694	[0.06, 0.0, 0.03]	[0.12, 0.14, 0.12]
	GHI,Temp,GHITemp	4	31.068	8.630	0.679	[0.15, 0.02, 0.04]	[0.12, 0.34, 0.17]
	GHI,GHIsq	4	31.143	8.651	0.646	[0.51, 0.0]	[0.0, 0.09]
	GHI,GHITemp	4	31.211	8.670	0.678	[0.16, 0.04]	[0.12, 0.15]
pros5	GHI,GHIsq,GHITemp	14	5.355	3.570	0.946	[0.19, 0.0, -0.0]	[0.0, 0.0, 0.29]
		12	5.375	3.583	0.946	[0.18, 0.0, -0.0]	[0.0, 0.01, 0.31]
		20	5.389	3.592	0.946	[0.19, 0.0, -0.0]	[0.0, 0.0, 0.17]
		22	5.394	3.596	0.945	[0.19, 0.0, -0.0]	[0.0, 0.0, 0.19]
pros6	GHI,GHIsq,Temp	14	3.786	2.227	0.943	[0.24, 0.0, -0.04]	[0.0, 0.1, 0.27]
		16	3.788	2.228	0.944	[0.24, 0.0, -0.04]	[0.0, 0.09, 0.25]
	GHI,GHIsq,GHITemp	8	3.788	2.228	0.942	[0.25, 0.0, -0.0]	[0.0, 0.19, 0.23]
	GHI,GHIsq,Temp	4	3.794	2.232	0.944	[0.24, 0.0, -0.06]	[0.0, 0.13, 0.37]
pros7	GHI,GHIsq,GHITemp	4	14.291	7.940	0.513	[0.15, -0.01, 0.11]	[0.14, 0.23, 0.04]
		6	14.689	8.160	0.472	[0.18, -0.01, 0.18]	[0.1, 0.2, 0.15]
	GHI,GHIsq	4	14.691	8.162	0.453	[0.59, -0.0]	[0.0, 0.24]
	GHI,GHIsq,Temp	4	14.761	8.201	0.453	[0.56, -0.0, 0.23]	[0.0, 0.27, 0.42]
pros8	GHI,GHIsq,GHITemp	8	2.280	2.452	0.942	[0.14, 0.0, -0.0]	[0.0, 0.09, 0.18]
	GHI,GHIsq,Temp	8	2.288	2.460	0.941	[0.13, 0.0, -0.03]	[0.0, 0.14, 0.34]
	GHI,GHIsq,GHITemp	4	2.290	2.463	0.942	[0.13, 0.0, -0.0]	[0.0, 0.15, 0.2]
	GHI,GHIsq,Temp	10	2.294	2.466	0.942	[0.13, 0.0, -0.03]	[0.0, 0.09, 0.34]

Appendix B

Kalman Filter

Table B.1: Error metrics of ARIMA(p,d,q) models with p=[3,5],d=[0,1],q[1,2] (left) and AIC's of ARMA(p,q) models p=[0,5],q=[0,2], applied to a backward looking rolling windows between 5 and 25 days.

window (d)	(p,d,q)	MSE	RMSE	MAE	Order (p,d,q)	AIC
15	(5, 0, 1)	1.708e+04	97.478	84.427	(2, 0, 2)	3594.35
	(4, 0, 1)	1.704e+04	97.553	84.488	(3, 0, 1)	3594.51
	(5, 0, 2)	1.706e+04	97.564	84.553	(3, 0, 2)	3594.93
16	(4, 0, 1)	1.700e+04	97.596	84.709	(4, 0, 2)	3595.36
	(4, 0, 2)	1.671e+04	97.603	84.573	(5, 0, 2)	3595.55
	(5, 0, 1)	1.706e+04	97.642	84.706	(2, 0, 1)	3595.80
	(3, 0, 2)	1.672e+04	97.659	84.212	(4, 0, 1)	3596.06
14	(4, 0, 1)	1.706e+04	97.660	84.493	(5, 0, 1)	3596.56
17	(4, 0, 2)	1.709e+04	97.706	84.684	(4, 0, 0)	3597.11
14	(4, 0, 2)	1.710e+04	97.779	84.729	(5, 0, 0)	3597.72
	(5, 0, 1)	1.716e+04	97.843	84.704	(3, 0, 0)	3603.46
11	(5, 0, 1)	1.683e+04	97.961	84.837	(2, 0, 0)	3618.25
15	(4, 0, 2)	1.713e+04	97.974	84.908	(1, 0, 2)	3633.14
17	(4, 0, 1)	1.740e+04	98.029	84.915	(1, 0, 1)	3653.49
19	(3, 0, 2)	1.685e+04	98.047	84.336	(1, 0, 0)	3712.85
24	(4, 0, 2)	1.736e+04	98.056	84.502	(0, 0, 2)	3793.78
13	(4, 0, 2)	1.702e+04	98.099	84.974	(0, 0, 1)	3934.10
24	(5, 1, 2)	1.746e+04	98.220	85.411	(0, 0, 0)	4264.31
11	(4, 0, 1)	1.691e+04	98.248	85.043		
10	(5, 0, 2)	1.690e+04	98.254	85.346		
13	(4, 0, 1)	1.713e+04	98.264	85.122		
10	(5, 0, 1)	1.676e+04	98.314	85.327		
13	(5, 0, 1)	1.719e+04	98.409	85.261		
17	(5, 0, 1)	1.769e+04	98.484	85.307		
18	(4, 0, 1)	1.781e+04	98.541	85.470		
10	(4, 0, 2)	1.655e+04	98.652	85.782		

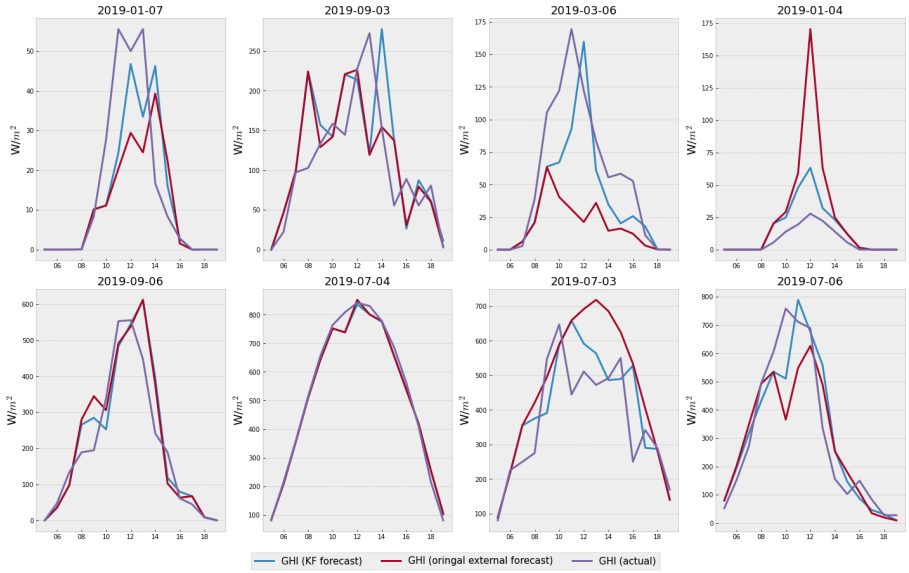

Figure B.1: 1-hour ahead forecast before and after applying the Kalman Filter

Appendix C

Imbalance Market Forecasting

Table C.1: Selected Features upward and downward regulation

	rank	upward regulation
27	1	slope_downward
31	1	3_upward_res
26	1	d6_downward
32	1	4_upward_res
33	1	5_upward_res
34	1	6_upward_res
20	1	6_downward
42	1	0_downward_res
16	1	2_downward
29	1	1_upward_res
14	1	0_downward
44	1	2_downward_res
43	1	1_downward_res
11	1	d5_upward
76	1	6_price_high
48	1	6_downward_res
47	1	5_downward_res
5	1	5_upward
12	1	d6_upward
6	1	6_upward
30	1	2_upward_res
7	1	d1_upward
46	1	4_downward_res
104	1	6_price_low
45	1	3_downward_res
13	18	slope_upward
9	36	d3_upward

	rank	downward regulation
30	1	2_upward_res
32	1	4_upward_res
31	1	3_upward_res
88	1	4_price_mid
29	1	1_upward_res
27	1	slope_downward
26	1	d6_downward
42	1	0_downward_res
43	1	1_downward_res
44	1	2_downward_res
20	1	6_downward
45	1	3_downward_res
33	1	5_upward_res
47	1	5_downward_res
46	1	4_downward_res
104	1	6_price_low
75	1	5_price_high
76	1	6_price_high
4	1	4_upward
6	1	6_upward
48	1	6_downward_res
34	1	6_upward_res
77	1	d1_price_high
82	1	d6_price_high
12	1	d6_upward
99	2	1_price_low

Table C.2: Selected Features upward and downward price threshold

Table C.3: Logit Model: Upward Regulation

Model:	Logit	Pseudo R-squared:	0.454
Dependent Variable:	reg_up	AIC:	145249.0070
Date:	2021-03-07 11:41	BIC:	145422.4015
No. Observations:	198724	Log-Likelihood:	-72608.
Df Model:	16	LL-Null:	-1.3287e+05
Df Residuals:	198707	LLR p-value:	0.0000
Converged:	1.0000	Scale:	1.0000
No. Iterations:	8.0000		

	Coef.	Std.Err.	z	P> |z|	[0.025	0.975]
6_price_low	-0.0400	0.0005	-83.6742	0.0000	-0.0409	-0.0391
1_upward_res	-0.1067	0.0034	-31.5472	0.0000	-0.1133	-0.1001
d6_downward	-0.0859	0.0032	-26.7915	0.0000	-0.0922	-0.0796
0_downward	0.0330	0.0009	35.2695	0.0000	0.0312	0.0348
d1_upward	-0.0161	0.0023	-7.1373	0.0000	-0.0206	-0.0117
6_upward	0.1230	0.0029	42.0143	0.0000	0.1173	0.1288
6_price_high	0.0205	0.0004	50.7044	0.0000	0.0197	0.0213
3_downward_res	-0.1452	0.0086	-16.9063	0.0000	-0.1620	-0.1284
5_upward	-0.1075	0.0029	-37.5726	0.0000	-0.1131	-0.1019
2_downward	-0.0283	0.0017	-16.9030	0.0000	-0.0316	-0.0250
d3_upward	-0.0117	0.0034	-3.4810	0.0005	-0.0183	-0.0051
6_downward	-0.0321	0.0010	-30.8935	0.0000	-0.0341	-0.0300
slope_upward	0.0526	0.0071	7.4096	0.0000	0.0387	0.0665
reg_up_LAG	0.5581	0.0165	33.7671	0.0000	0.5257	0.5905
reg_down_LAG	-0.9209	0.0184	-50.1517	0.0000	-0.9569	-0.8849
reg_up_2LAG	-0.5567	0.0155	-35.9270	0.0000	-0.5870	-0.5263
reg_down_2LAG	-0.5834	0.0153	-38.1265	0.0000	-0.6134	-0.5534

Table C.4: Logit Model: Downward Regulation

Model:	Logit	Pseudo R-squared:	0.479
Dependent Variable:	reg_down	AIC:	140816.1332
Date:	2021-03-07 17:02	BIC:	140989.5276
No. Observations:	198724	Log-Likelihood:	-70391.
Df Model:	16	LL-Null:	-1.3513e+05
Df Residuals:	198707	LLR p-value:	0.0000
Converged:	1.0000	Scale:	1.0000
No. Iterations:	9.0000		

	Coef.	Std.Err.	z	P> |z|	[0.025	0.975]
1_price_low	0.0060	0.0005	13.3530	0.0000	0.0051	0.0069
d1_price_high	-0.0321	0.0018	-17.7693	0.0000	-0.0357	-0.0286
0_downward_res	0.1497	0.0075	19.8869	0.0000	0.1349	0.1644
3_upward_res	0.1281	0.0046	28.0753	0.0000	0.1192	0.1370
6_price_low	0.0390	0.0004	88.2156	0.0000	0.0382	0.0399
6_downward	0.0242	0.0002	100.7681	0.0000	0.0237	0.0246
d6_downward	0.0643	0.0017	38.6537	0.0000	0.0610	0.0675
4_upward	0.0791	0.0012	65.2331	0.0000	0.0767	0.0815
slope_downward	0.0730	0.0019	38.5627	0.0000	0.0693	0.0767
6_upward	-0.0879	0.0015	-59.1056	0.0000	-0.0908	-0.0850
d6_price_high	-0.0524	0.0012	-42.9514	0.0000	-0.0548	-0.0500
5_price_high	-0.0428	0.0007	-65.0674	0.0000	-0.0441	-0.0416
4_price_mid	-0.0224	0.0005	-47.4433	0.0000	-0.0233	-0.0215
reg_up_LAG	-0.4445	0.0199	-22.2946	0.0000	-0.4836	-0.4054
reg_down_LAG	0.7264	0.0182	39.8690	0.0000	0.6907	0.7621
reg_up_2LAG	-0.1292	0.0183	-7.0601	0.0000	-0.1650	-0.0933
reg_down_2LAG	-0.2461	0.0176	-13.9890	0.0000	-0.2806	-0.2116

Table C.5: Logit Model: Predict Surpassing of Upward Threshold

Model:	Logit	Pseudo R-squared:	0.516
Dependent Variable:	threshold_up	AIC:	29817.3577
Date:	2021-03-07 17:28	BIC:	30064.0412
No. Observations:	68626	Log-Likelihood:	-14882.
Df Model:	26	LL-Null:	-30727.
Df Residuals:	68599	LLR p-value:	0.0000
Converged:	1.0000	Scale:	1.0000
No. Iterations:	9.0000		

	Coef.	Std.Err.	z	P> |z|	[0.025	0.975]
d6_upward	0.0929	0.0026	35.9004	0.0000	0.0878	0.0980
3_price_mid	-0.1475	0.0015	-96.1205	0.0000	-0.1505	-0.1445
6_price_low	0.0505	0.0026	19.4172	0.0000	0.0454	0.0556
5_price_high	0.0577	0.0019	29.8991	0.0000	0.0539	0.0614
0-6	-0.8482	0.0431	-19.6875	0.0000	-0.9327	-0.7638
m-j	-1.0994	0.0476	-23.0820	0.0000	-1.1927	-1.0060
0_emergency	4.3652	1.1429	3.8195	0.0001	2.1252	6.6052
d6_downward	-0.0821	0.0092	-8.9442	0.0000	-0.1001	-0.0641
1_price_high	0.0072	0.0020	3.6476	0.0003	0.0033	0.0110
s-o	-0.8971	0.0482	-18.6175	0.0000	-0.9915	-0.8026
j-f	-0.0796	0.0540	-1.4737	0.1406	-0.1855	0.0263
d6_price_high	0.0650	0.0019	33.7765	0.0000	0.0612	0.0688
6-12	0.0338	0.0393	0.8583	0.3907	-0.0433	0.1108
d2_price_low	0.0294	0.0063	4.6923	0.0000	0.0171	0.0417
4_emergency	-0.4115	0.8800	-0.4676	0.6401	-2.1363	1.3133
12-18	-0.2052	0.0344	-5.9710	0.0000	-0.2725	-0.1378
j-a	-1.2080	0.0479	-25.2428	0.0000	-1.3018	-1.1142
1_emergency	-2.2535	1.4369	-1.5684	0.1168	-5.0697	0.5627
0_price_high	0.0018	0.0017	1.0535	0.2921	-0.0015	0.0051
1_upward_res	-0.0369	0.0086	-4.2895	0.0000	-0.0538	-0.0201
2_upward	0.0232	0.0033	7.0317	0.0000	0.0168	0.0297
3_price_high	0.0098	0.0021	4.6152	0.0000	0.0056	0.0140
3_upward	-0.0040	0.0064	-0.6172	0.5371	-0.0165	0.0086
4_price_high	0.0090	0.0026	3.4689	0.0005	0.0039	0.0142
4_upward	-0.0253	0.0037	-6.9286	0.0000	-0.0325	-0.0182
d4_downward	-0.0513	0.0079	-6.5142	0.0000	-0.0667	-0.0359
d6_price_mid	-0.3946	0.3201	-1.2326	0.2177	-1.0220	0.2328

Table C.6: Logit Model: Predict Surpassing of Downward Threshold

Model:	Logit	Pseudo R-squared:	0.408
Dependent Variable:	threshold_down	AIC:	26515.2276
Date:	2021-03-07 17:50	BIC:	26727.0609
No. Observations:	73876	Log-Likelihood:	-13235.
Df Model:	22	LL-Null:	-22369.
Df Residuals:	73853	LLR p-value:	0.0000
Converged:	1.0000	Scale:	1.0000
No. Iterations:	8.0000		

	Coef.	Std.Err.	z	P> |z|	[0.025	0.975]
3_upward	0.0433	0.0130	3.3360	0.0008	0.0178	0.0687
6_downward	0.0017	0.0008	1.9966	0.0459	0.0000	0.0034
s-o	-0.5332	0.0498	-10.7159	0.0000	-0.6308	-0.4357
6_price_high	-0.0135	0.0040	-3.4094	0.0007	-0.0213	-0.0057
12-18	-0.2091	0.0331	-6.3165	0.0000	-0.2740	-0.1442
3_price_low	-0.0050	0.0023	-2.1972	0.0280	-0.0094	-0.0005
d2_upward	-0.0196	0.0071	-2.7815	0.0054	-0.0335	-0.0058
3_upward_res	0.0389	0.0099	3.9169	0.0001	0.0195	0.0584
0_price_low	-0.0136	0.0022	-6.1569	0.0000	-0.0179	-0.0092
d6_downward	0.0951	0.0030	31.6323	0.0000	0.0892	0.1010
6_price_low	-0.0413	0.0015	-28.3156	0.0000	-0.0441	-0.0384
1_price_low	-0.0243	0.0028	-8.7959	0.0000	-0.0297	-0.0189
2_upward	-0.0223	0.0095	-2.3513	0.0187	-0.0410	-0.0037
6_upward	-0.0295	0.0062	-4.7674	0.0000	-0.0417	-0.0174
m-j	-0.3018	0.0505	-5.9784	0.0000	-0.4008	-0.2029
j-f	0.0834	0.0444	1.8764	0.0606	-0.0037	0.1704
0_downward	-0.0120	0.0024	-5.0867	0.0000	-0.0166	-0.0074
1_downward	0.0189	0.0029	6.5630	0.0000	0.0132	0.0245
1_price_mid	1.2658	0.4098	3.0888	0.0020	0.4626	2.0690
2_price_low	-0.0121	0.0026	-4.6439	0.0000	-0.0172	-0.0070
3_price_mid	-1.3251	0.4098	-3.2334	0.0012	-2.1282	-0.5219
4_price_high	0.0033	0.0032	1.0347	0.3008	-0.0030	0.0096
d5_price_low	0.0147	0.0024	6.2136	0.0000	0.0101	0.0194

Appendix D

Select Representative Days

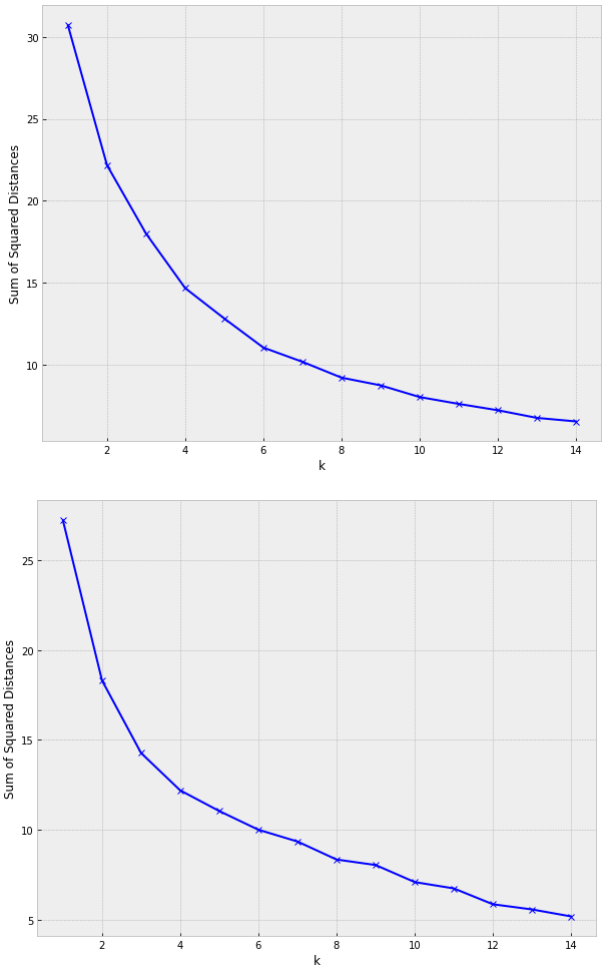

Figure D.1: The elbow plots obtained from k-means clustering of BR and KNMI data offer a heuristic to determine the optimal amount of clusters. The plot show the decrease in the Sum of Squared distances of the data points in the cluster as the number of clusters increase. The inflection point ("elbow") of the plot indicates the optimal number of clusters

Appendix E

Results

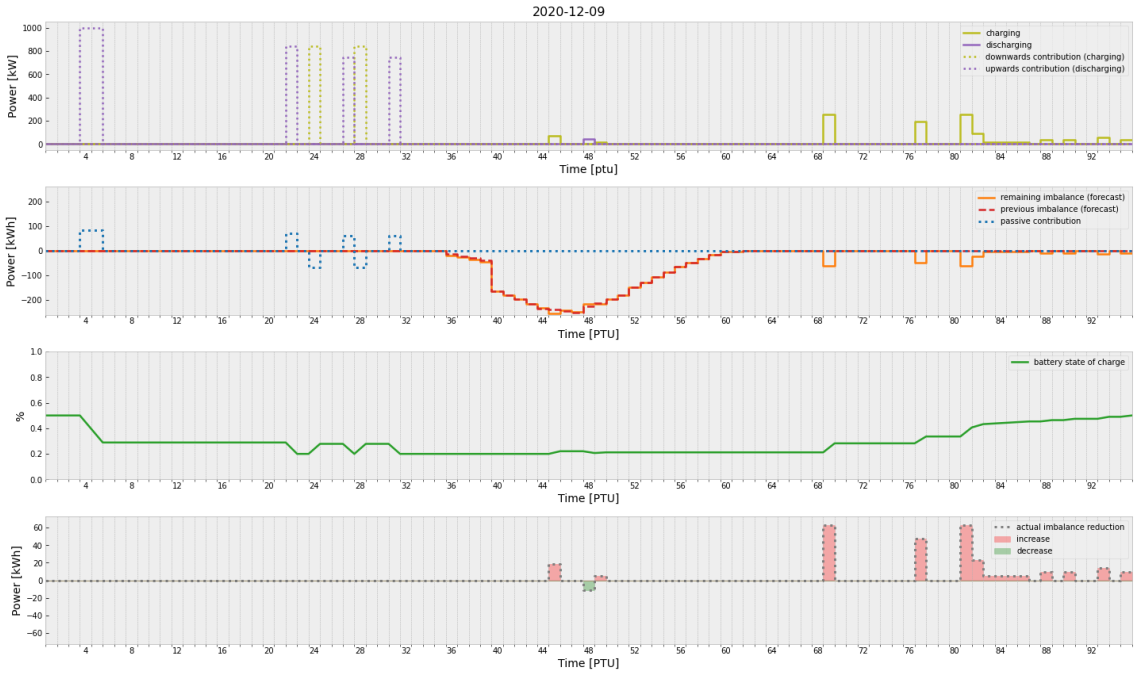

Figure E.1: model run 9 December 2020 (BR-cluster 0)

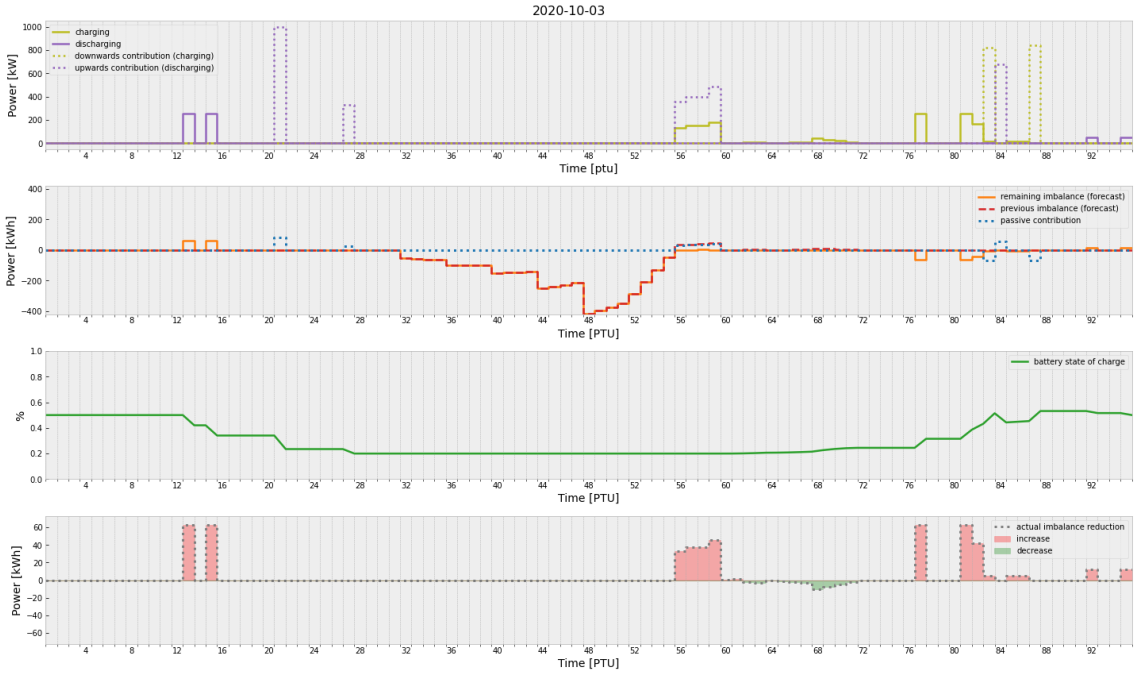

Figure E.2: model run 3 Oktober 2020 (BR-cluster 0)

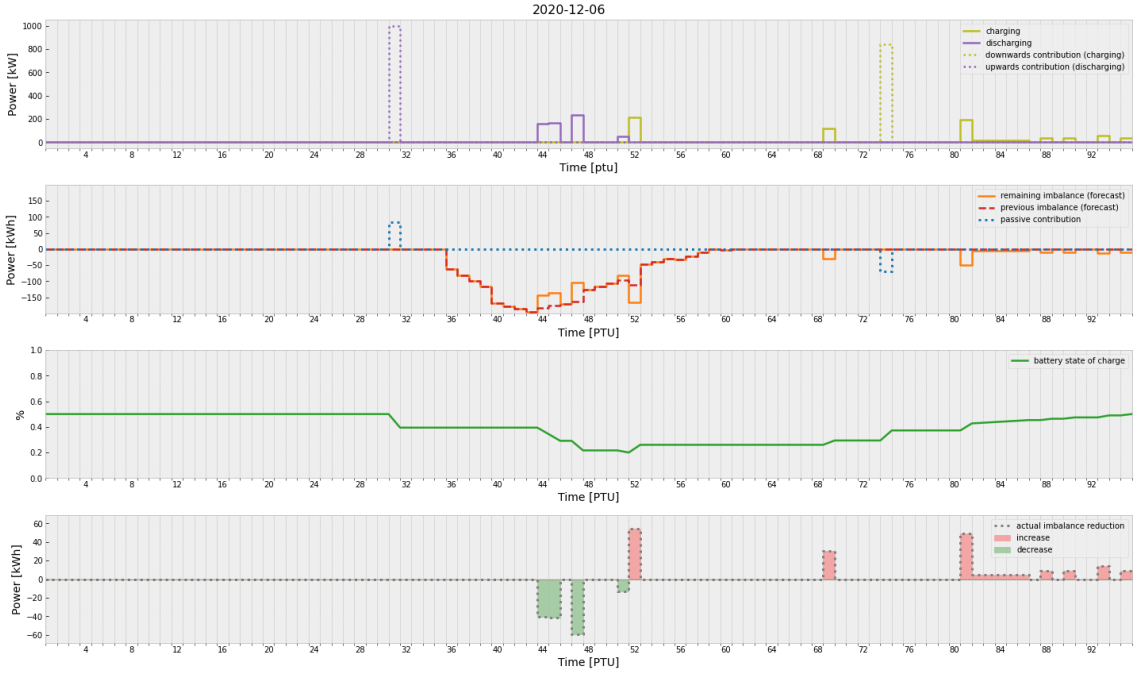

Figure E.5: model run 6 December 2020 (BR-cluster 2)

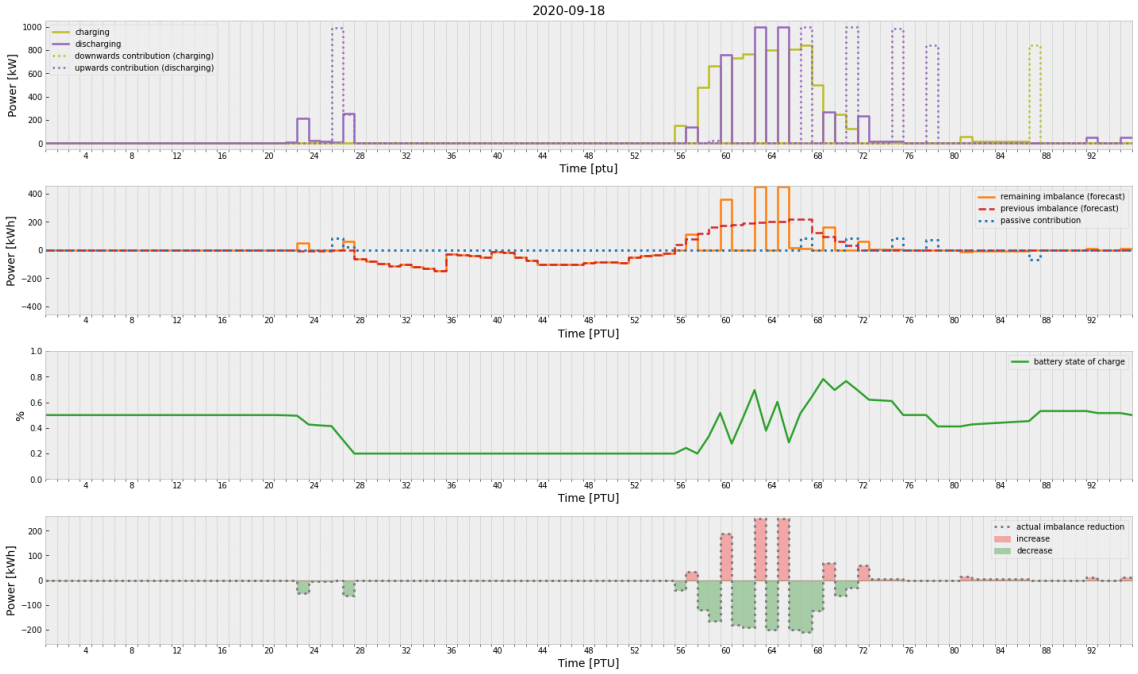

Figure E.3: model run 18 September 2020 (BR-cluster 1)

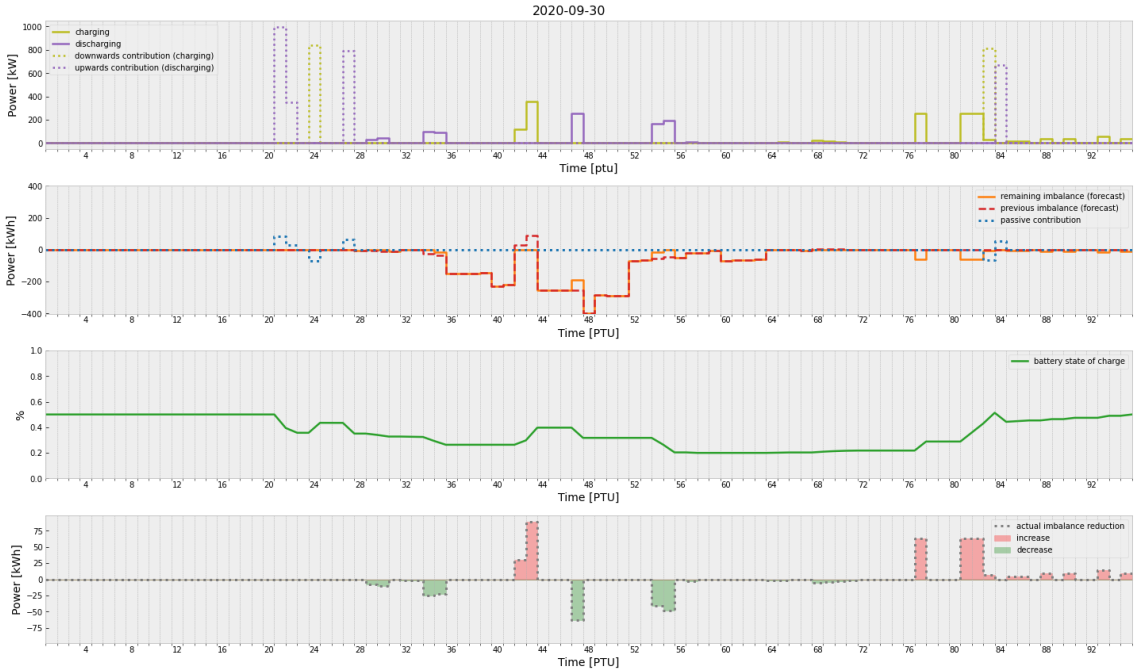

Figure E.4: model run 30 September 2020 (BR-cluster 1)

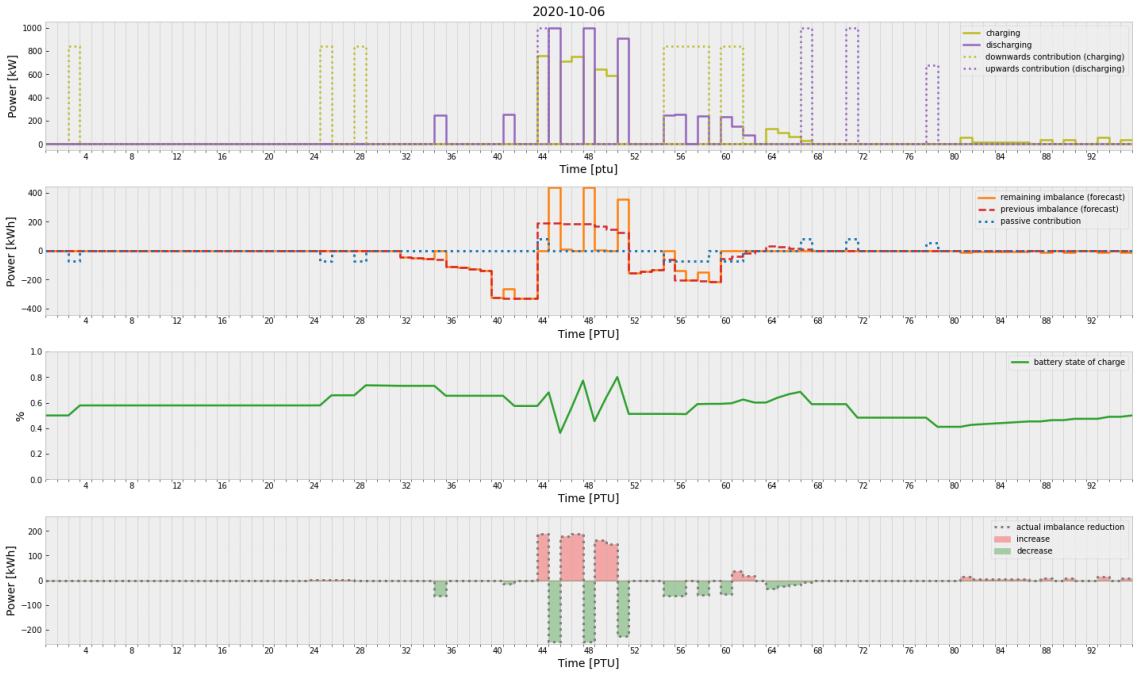

Figure E.6: model run 6 Oktober 2020 (BR-cluster 2)